ARKIV FÖR FYSIK

UTGIVET AV

KUNGL. SVENSKA VETENSKAPSAKADEMIEN

Band 6 Nr 49

ÅKE NILSSON

A precision determination of the K excitation potential of some $3d$ elements

---

STOCKHOLM

ALMQVIST & WIKSELLS BOKTRYCKERI AB

LONDON

H. K. LEWIS & CO., LTD

136, GOWER STREET

1953

PARIS

LIBRAIRIE C. KLINCKSIECK

11 RUE DE LILLE

Uppsala

1953

Digitized by the Internet Archive
in 2026

https://archive.org/details/IA41548912_0013

A PRECISION DETERMINATION OF THE *K* EXCITATION POTENTIAL OF SOME 3*d* ELEMENTS

INAUGURAL DISSERTATION

BY

ÅKE NILSSON

FIL. LIC., KALM.

BY DUE PERMISSION OF THE PHILOSOPHICAL FACULTY OF THE UNIVERSITY OF UPPSALA, TO BE PUBLICLY DISCUSSED IN THE LECTURE HALL OF THE INSTITUTE OF PHYSICS, ON MAY 23RD, 1953, AT 10 A. M., FOR THE DEGREE OF DOCTOR OF PHILOSOPHY

UPPSALA 1953

ALMQVIST & WIKSELLS BOKTRYCKERI AB

R. UNIV.
BIBLIOTHEEK
LEIDEN

ARKIV FÖR FYSIK Band 6 nr 49

Communicated 11 March 1953 by Axel E. Lindh and Gunnar Hägg

A precision determination of the K excitation potential of some $3d$ elements

By Åke Nilsson

With 41 figures in the text

Contents

Acknowledgements 514
Introduction 514

Chapter I. The X-ray tube 515
A. The contamination of the target 515
B. Construction 517

Chapter II. Spectrometer arrangements 526
A. The concave crystal spectrometer 526
B. The crystals and the crystal holder 527
C. The Geiger counter 527
D. The pumps and evacuation system 530
E. The high voltage equipment 532

Chapter III. The intensity of the spectrometer 534

Chapter IV. Recordings with the spectrometer 535
A. Adjustment 535
B. Procedure 537

Chapter V. Measurements of the high voltage 540
A. The potentiometer circuit 540
B. The potentiometer resistances 540
C. The *emf* of the Nife cell 542
D. Voltage corrections applied 542
E. The work function 544

Chapter VI. The K excitation curves 553
A. Chromium 553
B. Oxidation influence upon the curves 558
C. Titanium 559
D. Iron 563
E. Cobalt 566
F. Nickel 568
G. Copper 569

Chapter VII. Comparison of excitation curves and absorption edges 575
A. Electronic excitation 575
B. The K absorption edge 577
C. The resolution of the structure 579

Chapter VIII. Determination of h/e 581
A. Comparison between the two X-ray methods 581
B. The results 581
C. Error discussion 583

Chapter IX. The structure of the excitation curves and the electron theory of metals 584
A. Theoretical outline 584
B. Discussion of the structure 587

Summary 590
References 591

Acknowledgements

The following investigation was carried out at the Physical Laboratory of Uppsala University. After a period of preliminary work research was started in 1948. Some results were to hand as early as 1949–50, but since the apparatus was improved at a later stage, the majority of the results here published was obtained in the year 1952.

I should like to express my sincere gratitude to the head of the Physical Laboratory, Prof. AXEL E. LINDH, for the constant interest with which he has followed my investigations, for valuable suggestions and friendly encouragement.

For some years I have had the pleasure of co-operating with Prof. PER OHLIN and the present investigation is intimately connected with certain questions arising from his earlier work. I wish to thank him for criticism and advice and for the inspiration he has given me both as a teacher and a friend.

I wish to record my gratitude to all my fellow workers at the Physical Laboratory for good advice and interesting discussions. I am indebted to Mr. REGINALD STEDMAN, B.A., for the translation of the Swedish manuscript, and to Mr. JOHN ILIFFE, B.A., for assistance with the English text.

Finally I thank my family in Eslöv whose quiet support and patience have meant so much to me during the course of this investigation.

Uppsala, April, 1953.

Introduction

The present investigation deals with the determination of characteristic X-ray intensities as functions of the voltage of the X-ray tube, in order to find the excitation potentials of certain X-ray lines.

The excitation potential of an X-ray line is the lowest accelerating voltage of the X-ray tube for which the line in question appears. Characteristic radiation is emitted when excited atoms reorganise. The excitation of an energy level is therefore the primary atomic event, to which the measurements correspond.

An X-ray level may be excited by an electron or a photon of sufficient energy. The excitation potential and the frequency of the absorption edge are equivalent quantities, referring to the same amount of energy, eV and $h\nu$ respectively. This fact may be utilised for determination of the constant h/e.

The method of investigating the voltage dependence of X-ray intensities in order to find the position of atomic energy levels was early applied to the soft

X-ray region. [Cf. SIEGBAHN 1931, p. 434.] The radiation from the anticathode impinged directly on a metal surface, and the photo-current from this surface was determined as a function of the X-ray tube voltage. An investigation on these lines carried out by SKINNER [1932, 1933] introduced many of the problems recurring in the present investigation, such as target contamination and the work function correction.

A considerable improvement in technique is made possible by the construction of high intensity spectrometers with sensitive detectors such as the ionisation chamber, the Geiger counter and the photomultiplier. Use of monochromatic radiation greatly simplifies the problems involved. However, very few investigations of excitation potentials have been reported in the last two decades.

PARRATT [1936] made beautiful determinations of excitation potentials for satellite lines in the K spectrum, using a double crystal spectrometer and ionisation chamber.

Later, BEARDEN & SCHWARZ [1941], determined excitation potentials for Ni, Co, W and some other metals, and by numerical comparison with corresponding absorption edges, arrived at a figure for h/e.

The present research was undertaken in connection with precision determinations of h/e from the short wavelength limit of the continuous X-ray spectrum and investigations of the fine structure in the neighbourhood of this limit [OHLIN 1941, 1942, NILSSON & OHLIN 1946]. The original purpose was to endeavour to make a new determination of h/e, and at the same time to obtain data relevant to the problems associated with the work function correction. It was soon clear that a high degree of resolution could be achieved in determinations of excitation potential, and the unexpected detail richness of the curves obtained brought into the picture problems belonging to the sphere of solid state physics. The purity of the target — an essential factor in determinations of this kind — became one of the main experimental objects of attention.

Some questions of nomenclature may be made clear:

1) The curves obtained are consistently called excitation curves, as distinct from absorption curves, though the latter are also in a sense excitation curves. 2) The term "excitation potential" can be given a wider meaning than a single threshold value for a spectral line: it can refer to transitions to the bottom of each unoccupied energy band for which these transitions are connected with an abrupt increase in the recorded intensity. 3) By analogy with absorption curves, the word "edge" is also applied to the excitation curves, where there is no risk of misunderstanding.

Chapter I. The X-ray tube

A. The contamination of the target

One of the most troublesome problems in the present investigation was the contamination of the target while in operation. It is well known that a certain amount of vapourisation of the cathode cannot be avoided. Tungsten lines appear sooner or later in the spectrum from an X-ray tube with tungsten cathode. In order to minimise such difficulties, OHLIN constructed a tube with a large distance between the cathode and target for determinations of h/e. A magnetic lens was incorporated for the purpose of regulating the size and position of the focal spot. This tube was tested in connection with measurements of the Ohlin structure at the quantum

limit of continuous spectra, and is described in the paper by NILSSON and OHLIN [1946]. The cathode used on that occasion was of unipotential oxide-coated type, which obviates the deterioration in the voltage resolution caused by the voltage drop across a tungsten cathode.

The first attempts to obtain excitation curves were made with this X-ray tube. Fairly reproducible curves were obtained with a powder anticathode; some K excitation curves were taken for calcium's $K\alpha_1$ line with calcium oxide as anticathode. But similar experiments with chromium and titanium were entirely unsuccessful. This proved to be due to the rapid formation of a contaminating layer on the focal spot. Organic molecules with abundant carbon from vacuum seals and pumps are distintegrated by the electron beam, leading to the deposition of a layer of free carbon on the target. Oxides and sulphides are also formed by oxygen and sulphur in the tube's residual gases. Since electrons accelerated by a voltage as low as that used here do not penetrate far in solids, the X-radiation is emitted from a very shallow surface layer. The characteristic radiation of the target metal is therefore increasingly repressed as the contaminating layer becomes thicker. With a powder anticathode, on the other hand, the target continually recovers from contamination as grains of the powder are loosened by the electron bombardment, exposing fresh surfaces of the powder. A powder anticathode, however, must be unsatisfactory for measurements where even small temporary variations of intensity may distort the results.

Instead of using a powder anticathode special precautions were taken to obtain an exceptionally clean vacuum, in order to eliminate contamination of the focal spot, at least during the time necessary for the determination of an excitation curve. This attempt was eventually successful, at first with red-hot anticathodes, and later even with cold. In metal X-ray tubes it is not possible to abolish all oxidation, as the degassing of the walls can never be perfect. In such tubes, under given vacuum conditions, there is for each element a maximum time for the determination of an excitation curve before oxide formation produces too large a distortion of the measurements. This maximum time was found to vary with different anticathodes from about ½ hr. for the easily oxidised elements to over 2 hrs. for metals such as chromium and nickel. A moderate increase in the target temperature effected a considerable reduction of oxidation, and it was in fact necessary to use higher target temperatures for cobalt and iron. (See the descriptions of the individual excitation curves in Chapter VI.)

The necessity for complete purity of the target surface is, as mentioned above, connected with the rapid absorption of an electron beam by solids. It is possible to estimate the retardation of the electrons quantitatively either by the Thomson-Whiddington law [see for instance TERRILL 1923], or with the help of an expression formulated by WILLIAMS [1930–31]. According to such calculations a carbon contamination of 100 Å retards a 10 kV electron beam by about 25 eV and a tungsten layer of the same thickness by about 200 eV. The 10 kV electron beam is totally absorbed by a metal target of the elements used in this investigation in a layer of, or less than, ½ micron.

The deposition of carbon on surfaces bombarded with electrons has been treated in detail in connection with the electron microscope [KÖNIG 1948 and references there].

Another important type of target contamination is the oxidation occurring during the evaporation from the metal furnace used. This oxidation is dependent on the degassing, on the degree of vacuum, and on the rate of evaporation. There is a greater

risk of oxide contamination of the evaporated layer if evaporation is relatively slow [STAHL 1949, LEVINSTEIN 1949]. During the Cr $K\alpha_1$ measurements, an attempt was made to obtain excitation curves for chromium films, 100 Å thick, evaporated on to a Be layer. The excitation potentials for these films corresponded to the K absorption edge of Cr_2O_3. This result showed that the chromium layer was considerably oxidised.

The ordinary well known conditions for obtaining a pure vacuum must be strictly considered if the resolving power of the high voltage set employed is to be fully utilised. A summary of such important vacuum factors is given below:

(1) The evacuating system should have a high pumping rate and low limiting vacuum. (2) Backstreaming of oil vapour from the diffusion pump or other parts of the apparatus must be effectively prevented. (3) Vacuum connections should be of large bore. Surfaces liable to appreciable rise in temperature under operating conditions should not be enclosed in spaces with narrow openings. (4) All parts of the apparatus exposed to higher temperatures under operating conditions should be effectively degassed beforehand, preferably at a temperature above the operational temperature. (5) Metal surfaces heated under operational conditions should not contain metals with high vapour pressures. Brass should be avoided in parts not effectively water-cooled, and likewise soft solders. (6) The inner surface of the X-ray tube should not include organic sealing substances liable to give off vapour at operating temperatures. All indispensable organic sealing substances should adjoin well-cooled surfaces, and should be isolated from the high vacuum space by long diffusion paths. Rubber seals and Glyptal laquer belong to this category. Picein seals should be totally avoided. (7) The effect of cathode evaporation or sputtering should be reduced to a minimum by having a large distance between the cathode and target, by screening non-emitting parts of the heater filament, and in the case of oxide cathodes, by applying a thin layer of oxide as well as careful formation and degassing. (8) A furnace for the renewal of the target surface with an evaporation film under vacuum should be mounted inside the X-ray tube. (9) The electron beam should be well concentrated, so that stray bombardment of badly cooled surfaces does not take place. (Good electron-optical symmetry and central beams.) (10) Provision should be made to deviate the electron beam from the anticathode after renewal of its surface, so that it is not under bombardment while other preparations are being made for intensity measurements.

B. Construction

The X-ray tube previously mentioned was reconstructed in complete conformity with these principles, and its final form is shown in Figs. 2–8. The parts liable to be bombarded with electrons were made of copper, and the other inner surfaces were of porcelain or brass. All vacuum seals were either rubber rings or Glyptal lacquer. The rubber rings were treated with warm potassium hydroxide solution [after YARWOOD]. Glyptal lacquer was dried in an oven at 120° C, after which its vapour pressure is comparable with that of brass [JNANANANDA].

The removable *target* was a cylinder of copper fitting tightly into the water-cooled copper holder, to which it was fastened by screws through the basal flange. Figs. 4 and 7. The target in Fig. 7 a was used for excitation curves at high temperatures. A molybdenum pin was screwed into the short copper base, its head being slotted to take the inset anticathode plate. The temperature of this plate depended on

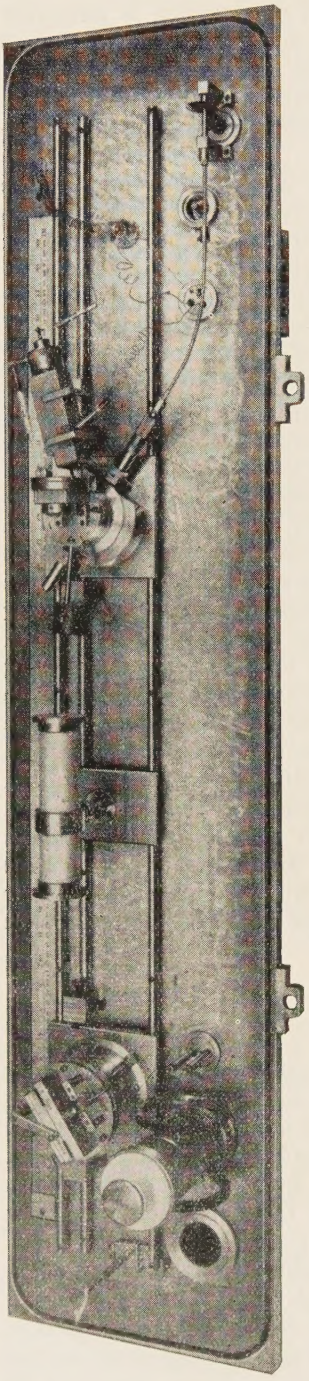

Fig. 1. View of the spectrometer table.

To the left the upper part of the X-ray tube, and the crystal holder; in the centre a screen against scattered radiation; to the right the slit and Geiger counter on their mounting, and a lamp to illuminate the micrometer scale.

the diameter of the pin and the intensity of bombardment, and could be regulated over a wide range. The principal type of target used is shown in Fig. 7 b. It was made of copper, and was used in conjunction with the metal evaporation furnace. The radiating surface was at an angle of 71.6° to the axis. There must be a certain temperature gradient in the copper cylinder, and a rough estimate gave the temperature at the focal spot as about 100° above room temperature with an emission current of 20 mA. For some metals it was desirable to increase the temperature some hundreds of degrees. Since the metals in question were all relatively poor conductors of heat, this higher temperature was obtained by using a plate of the metal, fitted tightly into the slot in the end of the copper cylinder.

The target was observable under bombardment through a window in the lid of the spectrometer, by means of two aluminium mirrors and a telescope. Incandescent temperatures were measured with an optical pyrometer, which was corrected for the reflections at the two aluminium mirrors. The aperture at S in Fig. 4 had to be kept open when the target was observed visually, and a pyrex-glass tube was then fitted over the copper cylinder to isolate the tube and spectrometer vacua from one another.

The evaporating furnace and its mounting are shown in Fig. 8. The mounting was attached to the cooling jacket, and bored with a hole of sufficient diameter to allow the electron beam to pass unobstructed through the centre when the X-ray tube was in normal operation. The furnace was made of molybdenum, which can be machined without difficulty. Tungsten would have been better with regard to its lower vapour pressure, but attempts to make a tungsten furnace had to be abandoned because of the metal's hardness and brittleness. The vapour pressure of molybdenum is sufficiently low at 1500° C not to affect evaporation of the target metal [LAW 1948]. (A provisional tungsten furnace was made for the evaporation of titanium,

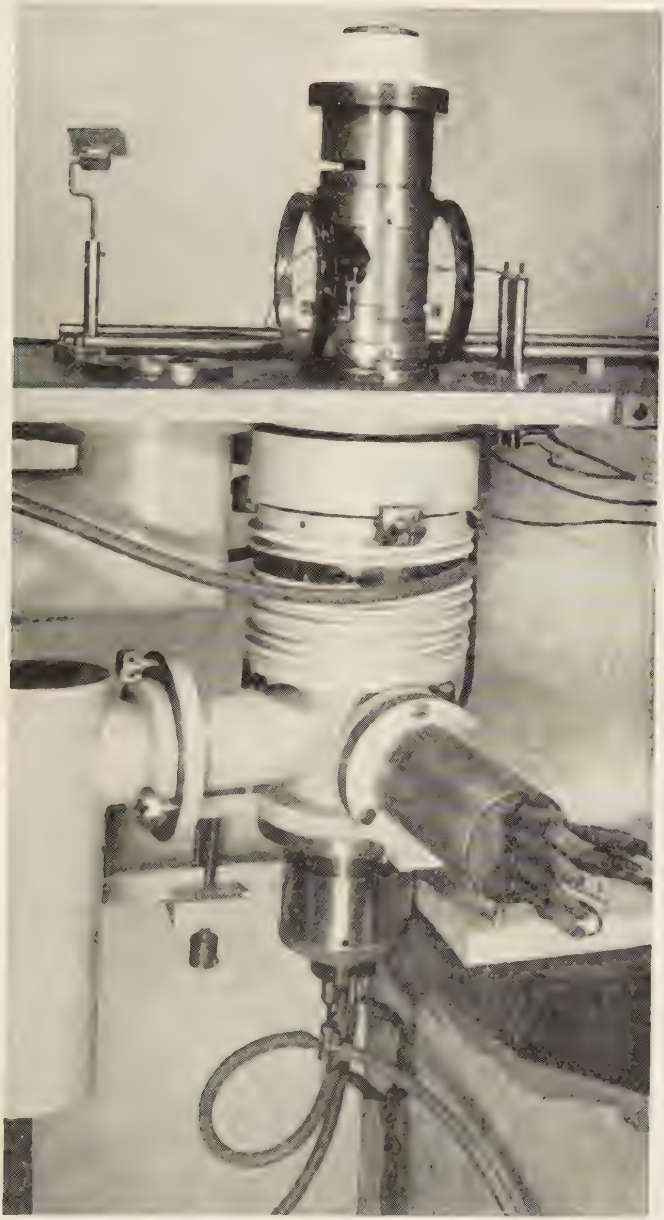

Fig. 2. View of the X-ray tube.

The radiation emerges from the horizontal slit near the top. Between this slit and the spectrometer table are the deflector coils and the circular opening through which the anticathode can be observed with the help of mirrrors when the tube is in operation. The iron case of the focusing coil is visible below the spectrometer table, the cathode and ionisation gauge lower down. To the left are the evacuation tubes to the spectrometer and X-ray tube, the latter fitted with a liquid-air trap.

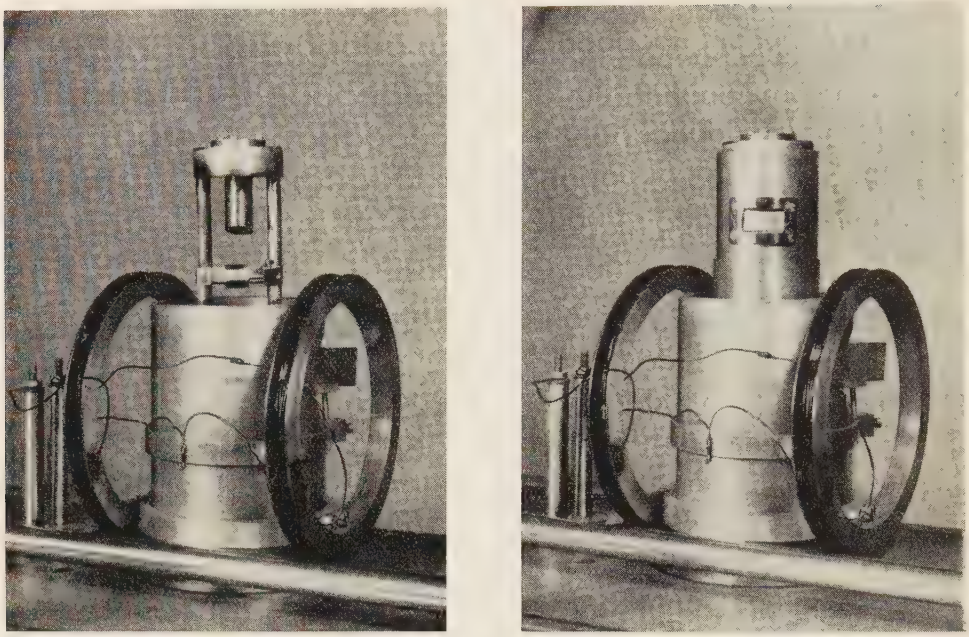

Fig. 3. The X-ray tube dismounted for changing of the target.

The earthed outer cover is removed in the right-hand figure, revealing the anticathode housing. This too is removed in the left-hand figure, showing the target and evaporation furnace.

which requires a temperature of 1800° C.) The furnace was heated by means of the electron beam, which was deflected from its normal central course for this purpose. The thick walls of the furnace ensured a uniform temperature distribution and a reproducible evaporation rate. At a given voltage, this rate could be determined in terms of the electron current. The furnace was calibrated in this respect by measuring the $K\alpha_1$ intensity of the evaporated element with copper or beryllium as target base. The intensity increases as evaporation proceeds until the layer deposited on the anticathode is so thick that the electrons penetrating the entire layer are retarded to such an extent that they can no longer emit the $K\alpha_1$ frequency, neither in the

---

Fig. 4. Section of the upper part of the X-ray tube.

A – porcelain insulator for centring the copper tube *E*.
B – exchangeable target. Fig. 7.
C – window covered with thin metal foil (Al or Ni).
D – evaporation furnace and mounting. Figs. 3 and 8.
E – anticathode housing of copper.
F – cooling tubes to the anticathode, in the figure turned 90° from their proper position.
G – coils for deflecting the electron beam.
H – spectrometer table.
I – focusing coil in soft iron case.
K – adjustment screw for the focusing coil.
L – brass plate supporting the anticathode system.
M – copper anode with a 6 mm aperture and an outer ring of evacuation holes. *L* and *M* are short-circuited.
N – water-cooling.
O – porcelain insulator.
P – inlet for cooling water to the anticathode.
Q – porcelain insulator.
R – grooves for rubber rings.
S – rotatable copper cylinder for closing the inner mirror window.
T – collar for the removable part of the outer cover.

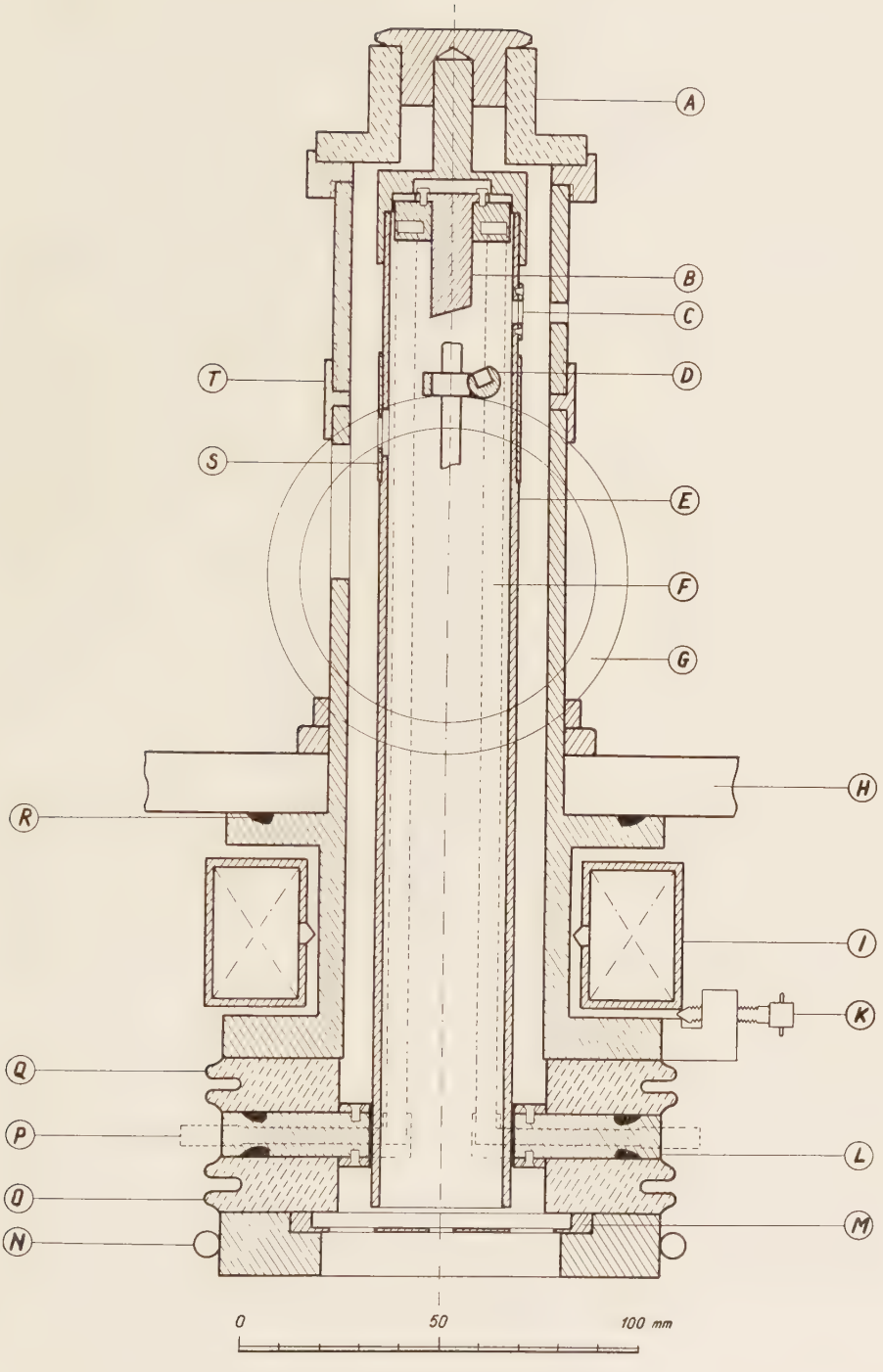
A
B
C
T
D
S
E
F
G
H
R
I
K
Q
P
L
O
M
N
0
50
100 mm

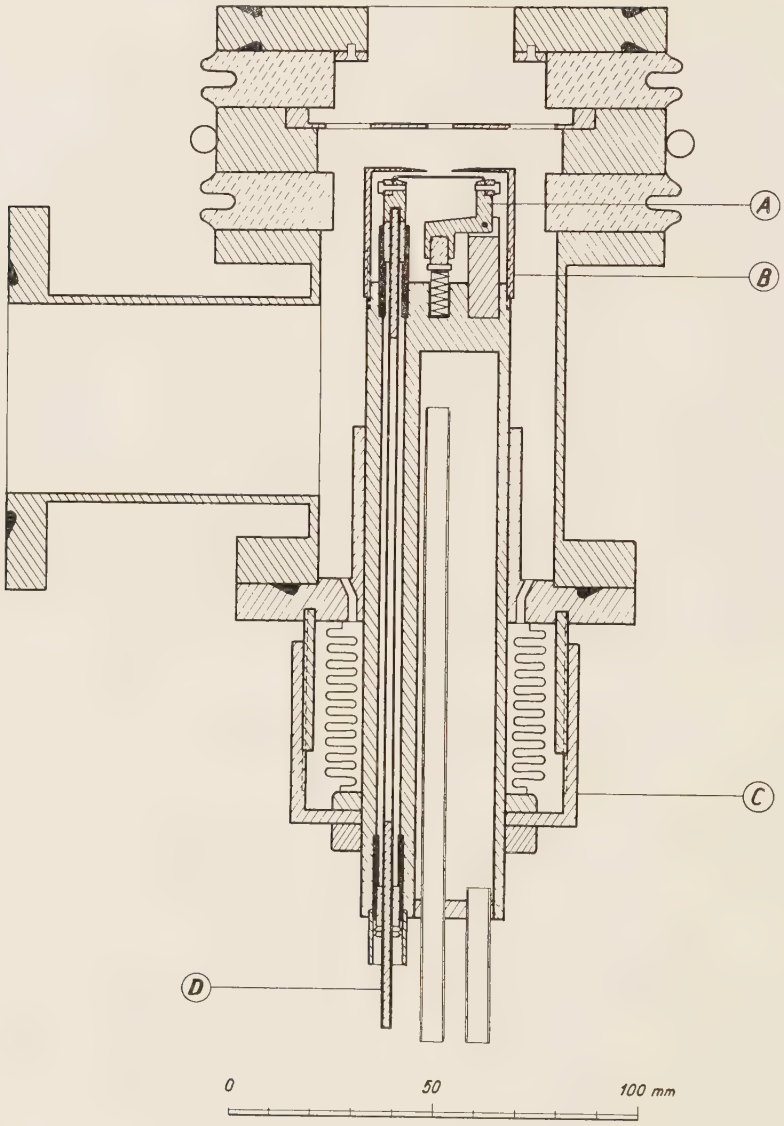

Fig. 5. Section of the lower part of the X-ray tube with the tungsten cathode.

A – pivoted cathode support, fitted with a spring to stretch the filament.
B – earthed cathode shield with 6 mm circular aperture.
C – threaded cylinder for adjusting the height of the cathode.
D – insulated steel rod, the outer end water-cooled when the tube is in operation.

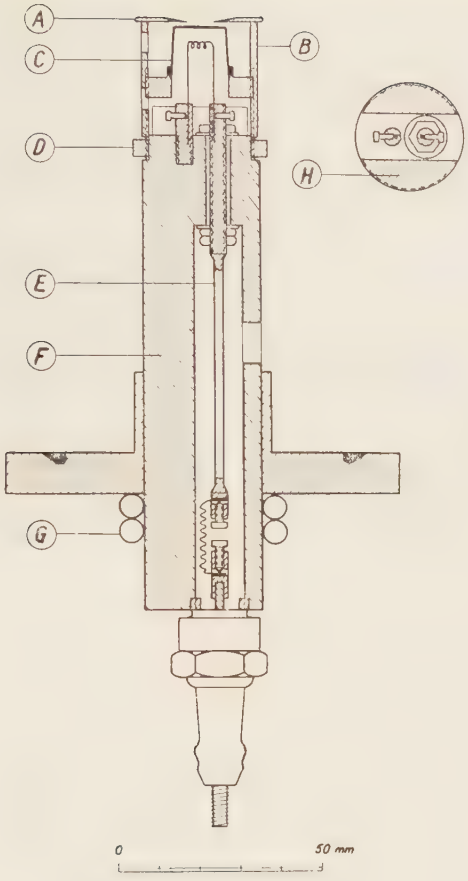

Fig. 6. Oxide-coated cathode.

A – nickel plate with 6 mm circular aperture, the height adjustable by means of the threaded brass cylinder *B*.
C – platinum cap for the oxide coating, with a flanged iron base adjustable vertically.
D – lock nut.
E – steel rod with insulating sheath. Longitudinal expansion is taken up by the free lower end, and thus does not move the insulated filament support.
F – solid copper rod.
G – water cooling.
H – filament base, horizontal section.

continuous spectrum nor in the characteristic. Evaporation rates giving this minimum layer in 2–5 minutes were preferred.

Special difficulties were encountered in evaporating nickel. Nickel readily forms an alloy with molybdenum, and its vapour pressure is then lowered considerably. The lowest melting point for a Mo-Ni alloy is a theoretical upper temperature limit for the evaporation furnace. But this temperature gave too low an evaporation rate. Attempts to separate the nickel from the molybdenum by graphite were unsuccessful because of carbide formation. The carbides formed a skin over the nickel surface [cf. SKINNER & JOHNSTON 1937]. Success was finally achieved by inserting a tungsten

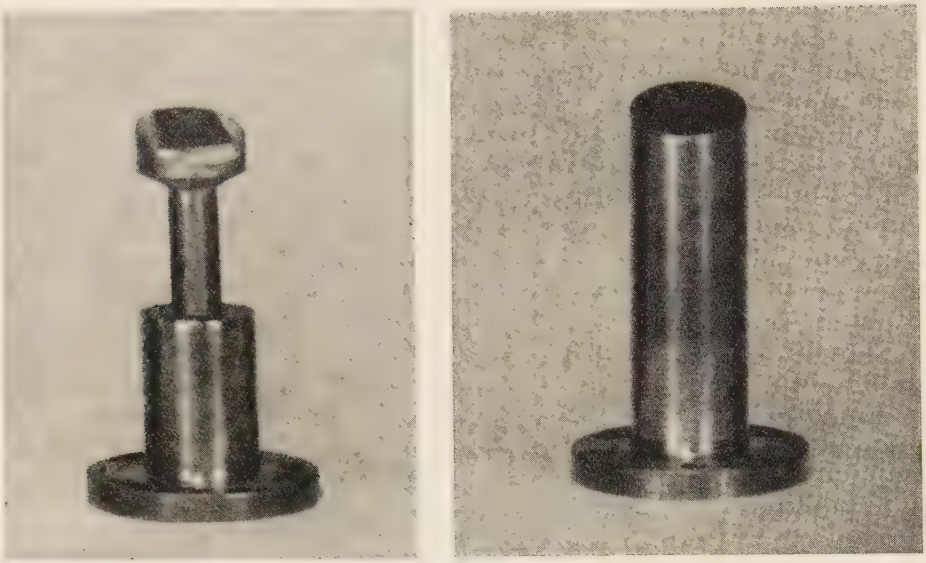

a b

Fig. 7. Two types of target.

a. Molybdenum pin screwed into a copper base, with a wide slot for the target plate.
b. Solid copper target with a polished end surface to take the evaporation deposit.

crucible in place of the graphite, whereupon temperatures giving a good rate of evaporation were attained. A tungsten crucible with an evaporation plate is shown to the right of Fig. 8.

The experience gained with nickel was utilised in dealing with iron and cobalt. The evaporation temperature for these three elements was the melting point or just under (about 1500° C). Chromium and copper, neither of which wets a molybdenum surface, were both evaporated directly from the molybdenum furnace, at about 1100° C in each case. Titanium was evaporated just above its melting point (1720° C). The vapour pressures at the evaporation temperatures used were some hundredths of a mm Hg [LAW 1948].

Each time the spectrometer had been opened, the furnace had to be carefully degassed. This was performed at a temperature 100–200° lower than the evaporation temperature. The rate of evaporation is then decreased by about a power of ten. After degassing, a film three to four times the minimum thickness (see above) was evaporated on to the anticathode before the intensity measurements were commenced.

The cathode. Both oxide-coated cathodes and tungsten cathodes were used, the latter for the main determinations, the former to investigate the effect of the work function on the excitation potential.

The tungsten cathode is shown in Fig. 5. The filament was straight, with a free length of 22 mm and a diameter of 0.35 mm. It was kept taut by means of a spring arrangement, and was screened from the interelectrode electric field so that only a small central part emitted. The size of the emitting part could be estimated from the size of the focal spot, which was a comparatively sharp, enlarged image of the emitting wire. The length of the focal spot was about 6 mm, and the magnification

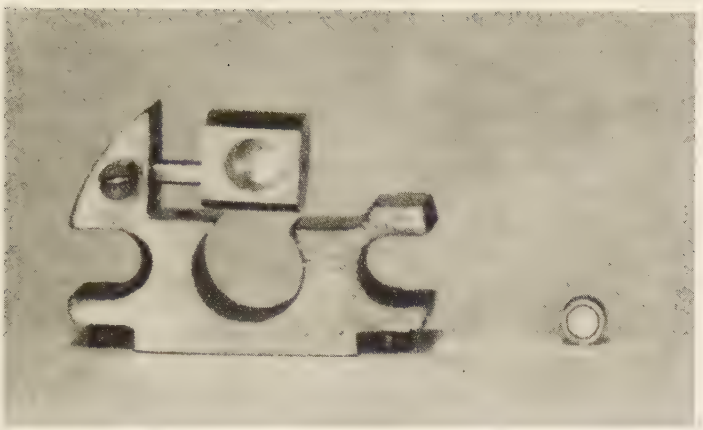

Fig. 8. Evaporation furnace of molybdenum with a copper mounting.
To the right a small wolfram crucible used when evaporationg iron, cobalt and nickel.

produced by the magnetic lens (I, Fig. 4) about 2, so the emitting length of the filament was about 3 mm, a seventh of the filament's total length. The heater voltage was 1.7–2.1 V, which means that the voltage drop across the emitting part of the wire must have been about 0.3 V. In view of this slight drop, the tungsten may be described as a cathode nearly unipotential.

The heater circuit is given in Fig. 13. The heater current was obtained from a lead accumulator, B6. Since this current was 10 A and the determination of a curve took several hours, the accumulator voltage fell slightly during the interval. A corresponding drop in emission was avoided by inserting the battery B5 (low internal resistance) in parallel with filament and the rheostat R7. The fixed resistor R8 was chosen so that a very small current was taken from B5. The B5 battery potential was thus kept constant, and consquently the heater current as well. The arrangement was convenient in operation, and variations in the electron emission did not exceed 0.1 %.

The construction of the oxide cathode is indicated in Fig. 6. The base metal used was originally nickel, but later platinum. The oxide-paste was obtained from *Schönander*, Stockholm, and contained roughly equal amounts of barium and strontium, with a slight addition of calcium. When degassing and formation were carried out carefully, emission was steady (though not to the same degree as with the tungsten cathode). The shortening of the oxide cathode's life due to the admission of air into the spectrometer was a serious disadvantage, however. The emission from the oxide cathode was very sensitive to variations in the residual gases, and was markedly affected by the degassing procedure prior to measurements. The oxide cathode is strictly unipotential, but this property is not balanced by the disadvantages mentioned. Yet another disadvantage is the fact that the work function for an oxide cathode is not known with the same exactitude as that for tungsten, about which more will be said in a later chapter.

The electron beam was employed for three purposes: it was used for degassing the X-ray tube, for heating the evaporation furnace, and for the production of X-rays. It was controlled by means of two electron lenses and a deflector coil.

The cathode and anode plate in combination can be described as an electrostatic acceleration lens. Centring should be precise, in order to avoid unnecessary spreading. Increasing the distance between the cathode and anode diminishes the angular aperture of the beam and increases the electron current to the anode. With the tungsten cathode a larger distance gave better focusing. At 20 mA emission, the current loss was about 1 mA with the distance actually used.

The encased coil I in Fig. 4 was a convergent electron-optical lens focusing an image of the emitting section of the cathode on the target when the current through it was correctly adjusted. A horizontal linear image could be obtained with the tungsten cathode. Magnetic lenses have a focal length proportional to V/i^2 — where V is the beam voltage and i the coil current — so a certain amount of blurring occurs when V varies. This effect must be taken into account when large voltage ranges are involved. When emission and voltage are constant, the X-ray intensity produced varies with i, and has a maximum for a particular value of i. This value of the coil current was taken as the operating current.

The deflector double-coil is shown in Figs 1–4. It was used to deflect the electron beam: (1) against the target housing for degassing, (2) against the furnace for evaporating metals, (3) from the normal focal position to protect a clean target, and (4) to broaden the focus, in order to even out the temperature and the radiating target surface. The latter effect was achieved by sending an alternating current through the coil, causing an oscillation of the beam. Such oscillation of the electron beam did not effect the X-ray intensity when the focus was central and the slit and crystal correctly adjusted.

Window C in Fig. 4, for X-rays, was covered with a thin metal foil. This was of 0.5 μ aluminium except when the heat from the furnace might have affected this metal. In such cases a 1–2 μ etched nickel foil was used.

Degassing was checked by two vacuum gauges — an ionisation instrument connected to the X-ray tube (Fig. 2) and a Pirani manometer between the mechanical pump and the booster pump. Both gauges were highly sensitive to degassing pressures. Degassing was satisfactory if neither gauge showed any pressure increase when the electron beam was swung over from the target to the target housing or the furnace.

Chapter II. Spectrometer arrangements

A. The concave crystal spectrometer

The high-vacuum spectrometer used for this investigation was constructed by OHLIN for the determination of Planck's constant from the short wavelength limit of the continuous X-ray spectra. This spectrometer was one employing a bent crystal [JOHANN 1931] and has already been described in detail [OHLIN, Diss. 1941]. Parts of the apparatus that have been used unaltered will therefore be described but briefly here. The changes necessitated by the special requirements of the present investigation apply chiefly to the previously described X-ray tube, the Geiger counter, and the vacuum system.

The body of the spectrometer was of wrought iron which has a very low porosity, imparting good vacuum properties to the walls of the chamber. The base was made from an I-section beam, and the lid from a segment of a boiler tube. Both were reinforced with welded flanges and plates. The ground, plane upper surface of the

I-beam was the spectrometer table. Holes were bored in it for evacuating, for the X-ray tube, and for mechanical attachments. Fig. 1. The spectrometer was made vacuum tight by means of rubber rings.

The main parts of the spectrometer were the X-ray tube, the crystal, and the detector, consisting of slit and Geiger counter.

The position of the X-ray tube was fixed, at a short distance from the crystal. The tube could be turned to give radiation in the desired direction.

The tables for crystal holder and for the detector could be moved longitudinally along steel rods and locked in any desired position. The crystal table was provided with a circular scale, and could be rotated to give the required angle of reflection. The slit and target were fixed at the same level above the spectrometer table, while the level of the crystal could be varied.

The slit consisted of two steel edges, one of which was adjustable. By means of a lever arrangement the slit could be turned to a position exactly parallel with the X-ray line investigated.

The slit, the Geiger counter, and a counterweight formed a single unit. It was possible to turn this unit about a vertical axis through the slit, and to move it in a straight line in a direction chosen. This was accomplished by a construction involving a cone and micrometer slide. Fig. 10. The slide was arranged to give a motion along the tangent to the Rowland circle for determining the position and intensity distribution of an X-ray line. Satisfactory reproducibility of the slide position had been obtained by a ball-bearing arrangement that rendered the motion almost frictionless. The position was adjusted by means of a micrometer screw, manipulated externally through a rotatable vacuum connection. The scale of the micrometer screw could be read through a window in the lid of the spectrometer.

B. The crystals and the crystal holder

The crystals were bent in steel holders with precision ground cylindrical surfaces of 1000 mm radius. The holders were so designed that stresses in the bending pieces were reduced to a minimum [HAGLUND 1941]. The dimension of the crystals were $15 \times 25 \times 0.5$ mm.

The Ti $K\alpha_1$ line was recorded with quartz $10\bar{1}1$ [d_1 = 3335.74 X.U., BROGREN & FRISKOPP 1948], and the other lines with topaz 101 [d_1 = 1352.86 X.U., SILFVERBERG 1944]. Both crystals give high intensity in the first order reflection [INGELSTAM 1939].

The quartz crystal was supplied by *l'Optique Scientifique* and the topaz by *Steeg & Reuter*.

The opening of crystal holder was 2×12 mm for quartz and 1.5×12 mm for topaz. The entire reflecting surface of the crystal could be utilised. The radii of the crystal surfaces were within 1 % of that of the bending pieces.

Scattered radiation was screened by a knife-edge stop in front of the crystal.

C. The Geiger counter

The wavelengths of the X-ray lines investigated were between 1.5 and 2.7 Å. The usual Geiger counters with argon or krypton have low efficiency in this range. Xenon has the L_{III} absorption edge at 2.6 Å, and in the range immediately below

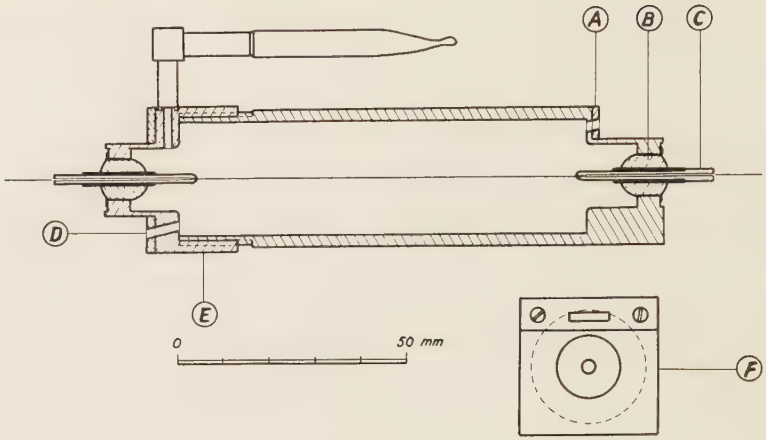

Fig 9. Section of the Geiger counter.

A – front window.
B – glass seal.
C – brass rod, drilled to take the central anode wire.
D – the rear window.
E – removable threaded end piece.
F – the counter seen from the front.

this value xenon's linear absorption coefficient is 4 or 5 times as large as krypton's and 6 to 8 times as large as argon's. Counters are seldom filled with xenon, however, partly because of the low mobility of xenon ions and partly because of the difficulties to get the counters to function. It is customary to increase the efficiency of the argon counters by raising the pressure, but this necessitates an undesirable increase in the starting potential.

Xenon-filled counters were used for the present investigation. The ionisation potentials of xenon and ethyl alcohol are too close for alcohol to be used as quenching agent [BROGREN 1949]. But ethyl ether may be used. The ionisation potential of xenon is 12.08 V and of ethyl ether 9.72 V [MORRISON & NICHOLSON 1952].

A diagram of the Geiger counter is given in Fig. 9. The X-ray beam passed through the tube diagonally in order to utilise the longest possible absorption path.

The ends of the anode wire in a Geiger counter are usually surrounded by tubular quartz insulators, which prevent a continuous discharge in the narrower parts of the tube. But such insulators give rise to insensitive volumes. Quartz tubes can be avoided if the anode is connected with end wires of a suitable larger diameter. In the Geiger counter used, the anode wire entered the tube through axial holes in brass rods of 2 mm diameter (C), soldered to commercial glass-metal seals. The ends of the brass envelope were bored with large diameter holes, barely allowing sufficient space for the two windows A and D. By this arrangement the brass sleeves could be drawn back towards the end of the main volume, without affecting the length of the plateau. The field achieved is such that no dead spaces occur, which is of great importance for the efficiency of the counter, since the greater part of the incident X-radiation is absorbed close to the window A.

The end piece E was removable to facilitate internal cleaning when refilling the tube. It was threaded on to the main section. The window D was provided for easy adjustment of the Geiger counter in the spectrometer.

The dimensions of the main volume were 25 × 90 mm. The radius of the end holes

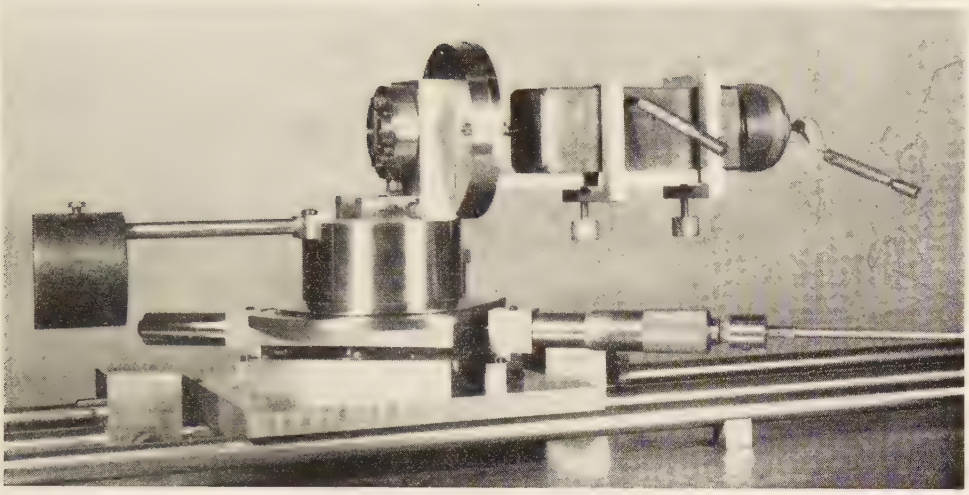

Fig. 10. The Geiger counter on its carriage.

The slit may be seen in front of the counter. The counter, slit and counterweight are mounted as a unit which may be moved along the tangent to the Rowland circle by means of the micrometer screw visible lower down in the photograph.

was 7 mm. The windows, 9×2 mm, were covered with 20 μ cellophane. The anode was made of 0.15 mm molybdenum wire.

The counter was finally sealed with Glyptal lacquer, which was dried at 80° C since the cellophane windows did not tolerate higher temperatures. Special grooves were cut around the windows to prevent Glyptal lacquer coming into contact with the gas inside the tube. Since Glyptal absorbs ethyl ether to some extent, its presence would shorten the life of the counter. The end piece E was also sealed with Glyptal lacquer, painted around the outer end of the thread.

The counter was filled with xenon at 75–90 mm, and 10 mm ether. The $K\alpha_1$ lines investigated were absorbed 80 to 100 % (except Ti $K\alpha_1$ which lies on the wrong side of the L_{III} edge of xenon).

Fig. 11 shows an example of a plateau curve. The length of the plateau was about 350 V. It will be seen that the slope is very slight; it varied between 0.01 and 0.025 % per volt for four counters used. The slope of the plateau is principally due to spurious counts and dead space. The small slope of the counters used indicates that these drawbacks were insignificant in the present case.

Since the components in the xenon-ether counter give heavier ions than those of an argon-ether tube, the dead-time of the former must be expected to be longer. The mean value of the dead-time measured on four occasions with newly filled tubes was $(9.7 \pm 0.8)\ 10^{-4}$ seconds.

The life-time of the xenon-ether tube is comparable with that of the argon-alcohol tube, provided ether-absorbing substances are eliminated. When the counter died, it had to be taken apart for cleaning of the cathode and changing of the wire. Refilling of uncleaned counters is not advisable, since the discharges lead to formation of heavy hydrocarbons which are deposited on the walls of the tube [cf. FARMER & BROWN 1948]. An interesting corroboration of this was given by a double-counter

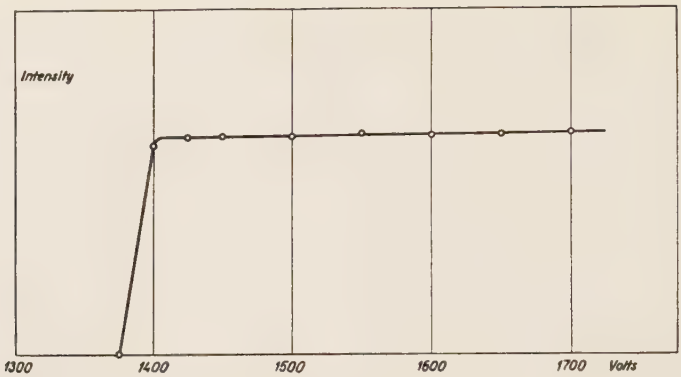

Fig. 11. The plateau curve of the Geiger counter filled with 75 mm xenon and 12 mm ethyl ether

used for the first determinations. The counter consisted of two single tubes coupled together with parallel anodes and with the gas in common. The incident radiation was perpendicular to the anode wires. When the tube subjected to the most intense radiation died, the other tube still had a perfectly good plateau, despite the fact that the gas mixture was common to them both.

A quenching circuit of Neher-Pickering type was used [NEHER & PICKERING 1938], and the pulses were recorded by a scale-of-64 and a Cenco mechanical high-impedance counter. The resolving time of the scaler was some microseconds. The scaler and the quenching circuit were supplied by the *Atomic Instrument Company* (Models 101-A and 203).

The mounting of the Geiger counter in the spectrometer is shown in Fig. 10.

D. The pumps and evacuation system

The high vacuum was obtained with a three-stage oil diffusion pump, preceded by a mechanical pump and booster diffusion pump. The high-vacuum pump contained octoil-S and the booster pump silicone oil (DC 703). The final vacuum was 10^{-6} mm Hg, the booster pump by itself giving 2.10^{-5} mm.

Both the diffusion pumps were kept constantly under vacuum. The spectrometer was evacuated to a few thousandths of a mm Hg by the mechanical pump, by-passing the diffusion pumps. The final pump was used only with high vacua (pressure less than 10^{-4} mm Hg).

Backstreaming of oil vapour from diffusion pumps is a well known fact [cf. PARRATT & JOSSEM 1952]. It was absolutely essential that this phenomenon was completely prevented in the present investigation, to which end the system of traps shown in Fig. 12 was introduced. These traps lowered the pumping rate to some extent, but this was not inconvenient as the main factor determining the time of evacuation was the slow degassing of the spectrometer.

The final pump is G in Fig. 12. The water-cooled copper baffles at F were a sufficient barrier to oil vapour to prevent visible deposition of oil on the surface above them. The final obstruction to backstreaming oil vapour was the liquid air trap E, the lower end of which was surrounded by charcoal.

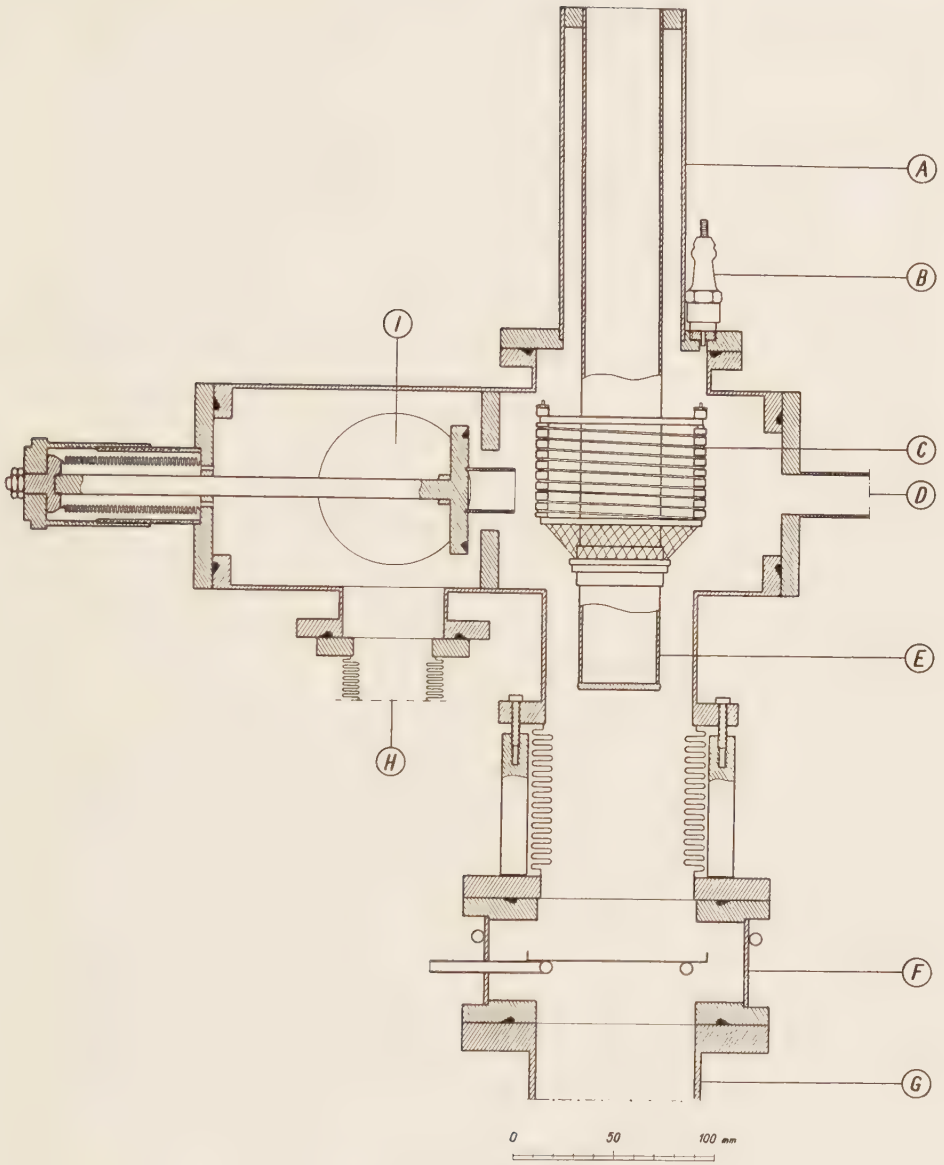

Fig. 12. Diagram of the high-vacuum system.

A – outer jacket of the liquid-air cooled charcoal trap. — A copper cooling cylinder is attached during the degassing of the charcoal.

B – sparking plug connection to the heating coil of the charcoal trap.

C – the charcoal trap. A heating coil of Kanthal[1] wire forms the outer wall, a wide-meshed metal net the bottom, while a sheet of mica insulates the charcoal from the nickel silver tube *E*.

D – connection to an ionisation gauge.

E – nickel silver liquid air trap.

F – top of the diffusion pump *G*, with water-cooled baffles for the condensation of oil vapour.

G – 3-stage oil diffusion pump (VMF-260, Distillation Products, Inc.).

H and *I* – connections to the X-ray tube and the spectrometer respectively.

[1] An alloy consisting of iron, chromium, aluminium and cobalt, manufactured by AB. Kanthal, Hallstahammar, Sweden.

Degassed charcoal is a powerful gas absorbent even at room temperature, and at the temperature of liquid oxygen it is an ideal pump with an almost infinite pumping rate.

The charcoal was degassed at no more than 200° C, as it was not desirable to heat nearby rubber joints to a higher temperature. The degassing was not found to be ineffective, however. The final pump was not in operation during degassing of the charcoal, because of the inferior vacuum conditions prevailing, and the booster pump with its more resistive oil pumped by itself.

The spectrometer and X-ray tube were evacuated simultaneously via the two connections I and H in Fig. 12. There was a second liquid air trap in the connection to the X-ray tube, to prevent organic vapours from the spectrometer from reaching the X-ray tube. The above system of traps provided a vacuum completely free from organic vapours. This was demonstrated by the fact that a water-cooled chromium target showed no colour change of the focal spot after a test run of ten hours.

The vacuum system also included two vacuum-meter tubes: one for the Pirani gauge, type *SER*, VM4, range $1 \cdot 10^{-4}$ mm Hg, measuring the forevacuum, and one for the ionisation gauge, type *Standard* 4101–D, attached directly to the X-ray tube. The latter had been removed from its glass envelope and mounted in a brass chamber with a large opening into the X-ray tube (Fig. 2).

In making the preparations for an excitation curve, the apparatus was evacuated as follows: —

(1) The mechanical pump evacuated the spectrometer from atmospheric pressure down to the pump's limiting vacuum.

(2) The spectrometer was shut off from the rest of the vacuum system and left for 12–18 hrs., to remove occluded gases from its inner surfaces.

The booster pump was started, and the current through the heating coil of the charcoal trap switched on. The charcoal had to be kept at 200° for 6–10 hours.

(3) The degassed spectrometer was evacuated with the booster pump. The high-vacuum pump was started and the heating current of the charcoal trap switched off.

(4) When the ionisation gauge indicated 10^{-5} mm Hg, the charcoal trap was filled with liquid oxygen.

(5) After some hours of pumping with the high-vacuum pump, the X-ray tube was put into operation.

(6) The application of the cathode heating current and the anode voltage of the X-ray tube was accompanied by an increase in pressure, especially when the spectrometer had been opened prior to evacuation. When the degassing of the various parts of the X-ray tube was complete (see the description of the X-ray tube), the cooling trap of the X-ray tube was filled with liquid oxygen. The actual measurements then commenced.

E. The high voltage equipment

The circuit diagram of the high-voltage set is shown in Fig. 13. The primary voltage of the Greinacher rectifying circuit was stabilised with an a.c. voltage stabiliser (*Philips* GM 444), and was regulated with an autotransformer and rheostats. The high-voltage transformer delivered 10 kV with a primary voltage of 220.

The rectified voltage was filtered in a smoothing circuit according to OHLIN [1941]. A pulse in the rectified high-voltage passes via the condenser C3 to the triode

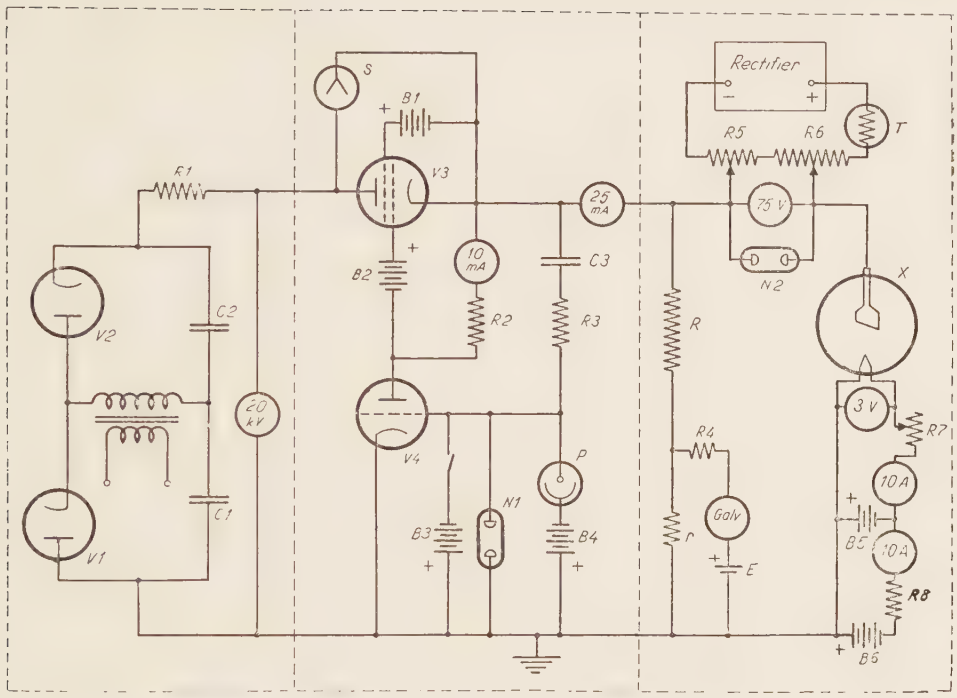

Fig. 13. Circuit diagram.

The section to the left is the Greinacher rectifying circuit, in the middle the smoothing circuit, and to the right the precision potentiometer, the rectifier for additional voltages, the filament heating circuit and the X-ray tube.

*V*1, *V*2 – Philips rectifier valves DA 7/700.
*V*3 – Philips amplifier valve 4650.
*V*4 – Marconi transmitting valve MT-4.
P – Cetron photocell 1 *V* AB.
T – Philips current regulator 1928.
*N*1, *N*2 – Philips neon lamps 4378.

*B*1, *B*2, *B*4 – dry batteries, 150–200 volts.
*B*3 – grid battery, 8–16 volts.
*B*5 – lead accumulator, 12V, 120 amp. hrs.
*B*6 – lead accumulator, 30V, 160 amp. hrs.

*R*1 – 50 kΩ.
*R*2 – 100 kΩ.
*R*3 – 0.5 MΩ.
*R*4 – 1 MΩ + 0.1 MΩ + 5 kΩ, disconnectible.
*R*5 – 10 Ω.
*R*6 – 2500 Ω.

*C*1, *C*2 – 2.3 μF.
*C*3 – 0.1 μF.
X – X-ray tube.
S – electrostatic voltmeter.

r – Wolff precision resistor box.
R – manganin-wire resistors:

Four Siemens-Halske prec. resistors of 1/2 MΩ, max. 10 mA.
Eight Siemens » » of 1/4 MΩ, max. 3 mA.
One Pye precision resistor of 1 MΩ, max. 2 mA.

E – Nife cell, 15 amp. hrs.
Galv – Moll galvanometer, Kipp & Zonen, type O (Period undamped 1.3 secs.).
Voltmeter, 0–75 *V* – Roller-Smith precision instument, type NPD.
Rectifier – rectifier circuit with high tension insulation, 600 V/200 mA (Schönander, Stockholm).

V4, where it is inverted and amplified, and reaches the grid of the pentode V3 with a phase and amplitude such that the original voltage pulse is compensated by the change in the anode voltage of the pentode.

Leakage in the condenser C3 is compensated by the photocell P, which acts as a counter-leak. This counter-leak was automatically controlled by the galvanometer in the potentiometer circuit, the photocell being illuminated by a band of light reflected from the galvanometer mirror. The galvanometer was adjusted so that this light band covered the border of the photocell in the zero position [VON FRIESEN 1935].

The following relation between variations in the input voltage (dV_1) and the output voltage (dV) may be derived from the value of the resistor R2 and data for the valves in the circuit [OHLIN 1941]: $dV = (dV_1/4000) - 6dI$, where I is the output current in amps. The ripple of the smoothed output was measured with a cathode ray oscillograph. It had the form of a somewhat distorted sine wave. The peak-to-peak voltage at $V = 6$ kV and $I = 0.02$ A was 0.08 V, approximately equal to the value obtained from the formula.

The variable additional voltage was obtained from a rectifying circuit floating at the basic high voltage. The primary voltage for this circuit was taken from the a.c. stabiliser mentioned above. The output voltage was regulated by means of a potentiometer coupling with coarse and fine adjustments. The smoothing section eliminated ripple entirely, within the limits of measurement.

Chapter III. The intensity of the spectrometer

The recorded intensity in the spectrometer depended on (1) the current density in focus, (2) the form of the focal spot, (3) the distance between target and crystal, (4) the reflection intensity of the crystal plane, (5) the size of the reflecting surface, (6) the slit width and (7) the efficiency of the detector.

The current density in focus. This was regulated by the cathode emission as the size of the focal spot was almost constant. A current of 20–25 mA was generally used. This value of the current was near the available maximum because of the short emitting section of the filament. With a wider diaphragm in front of the filament the available emission could have been increased but this would decrease the homogeneity of the electron beam.

The form of the focal spot. The focus of the X-ray tube should have such a form and position that the entire crystal opening is filled with radiation. The entering X-rays must strike the different parts of the crystal in such directions that reflection is possible according to the Bragg law. The beams capable of reflection have an intersection point (real or virtual) on the Rowland cricle. It is a wellknown condition for high intensity that the focal spot fills the entire extension between the two chords from the intersection point mentioned to the ends of the crystal opening. This condition is automatically fulfilled in the actual X-ray tube as the intensity is adjusted to the optimum value by regulation of the current in the magnetic focusing lens. The length of the focus was 6 mm (Chapter I). The height was determined by the oscillating motion of the electron beam. The alternating current in the deflection coils was regulated to give the focus a width on the target of 3 mm, corresponding to a vertical height of 1 mm. Thus the vertical projection of the focal spot had dimensions agreeing well with the projection of the crystal opening.

The distance between the target and crystal. Acc. to JOHANN the intensity will increase if the target is brought towards the crystal. At the same time a larger focal spot can be used, which is often advantageous. A tendency has therefore occurred to make the target-crystal distance short. In the actual case this distance was 10–15 cm.

Lately BROGREN, however, has critizised this tendency on theoretical grounds and he has obtained preliminary experimental support for his ideas [to be published]. The opinion of BROGREN is that the target should have a position near the above mentioned intersection point. A radiating surface element near this point would fill the entire crystal opening with radiation able to be reflected. If the surface element is moved towards the crystal only a very small angular width is reflected according to the diffraction theory of Darwin, Ewald and Prins [COMPTON and ALLISON 1935, SIEGBAHN 1931].

The reflection intensity of the crystal plane. See INGELSTAM [1939].

The size of the reflecting surface. The bent crystals could be used without limiting the opening to prevent occurrence of "ghosts". Unfortunately the height of the crystal opening was small (1.5-2 mm) and could have been increased in order to gain intensity. The intensity gain with increased reflecting surface is obtained at the price of spectral resolution [cf. SANDSTRÖM 1935]. An excitation curve, however, refers to a volt scale and to voltage resolution and spectral focusing defects only cause a decrease of the ratio of the characteristic intensity to the continuous background. This independence of the excitation curve in relation to focusing defects is founded on the following suppositions: (1) that the asymmetry of the spectral line is independent of the excitation voltage (and thus the excitation curve at the long wavelength side similar to that at the short wavelength side) and (2) that the continuous background has a constant slope. The first supposition is fulfilled as long as the voltage is not high enough to cause double ionization by direct electron impact. The second condition will be considered in Capter IV.

The slit width. The slit width was chosen equal to the width at half-maximum intensity of the spectral lines. Because of the form of the spectral lines that is the optimal slit width. A smaller slit would only change the ratio between characteristic and continuous radiation to a negligible degree. In an artificial way this ratio could, however, be considerably increased by using target metal in the form of thin layers on beryllium base. See Chapter VI (A).

The detector. The detector should have an efficiency of 100 %. This is almost realized with the present xenon-ether counters. See Chapter II (C).

Chapter IV. Recordings with the spectrometer

A. Adjustment

The electron beam was brought to bear on the centre of the target by means of the adjusting screws on the focusing lens. The tungsten cathode was turned to a position in which the elongated focal spot was put in the horizontal plane and at right angles to the target-crystal direction. Fluorescent material was applied to the target for this purpose.

The crystal was adjusted so that its cylindrical reflecting surface was parallel to the axis of rotation of the crystal table. The crystal was then moved horizontally

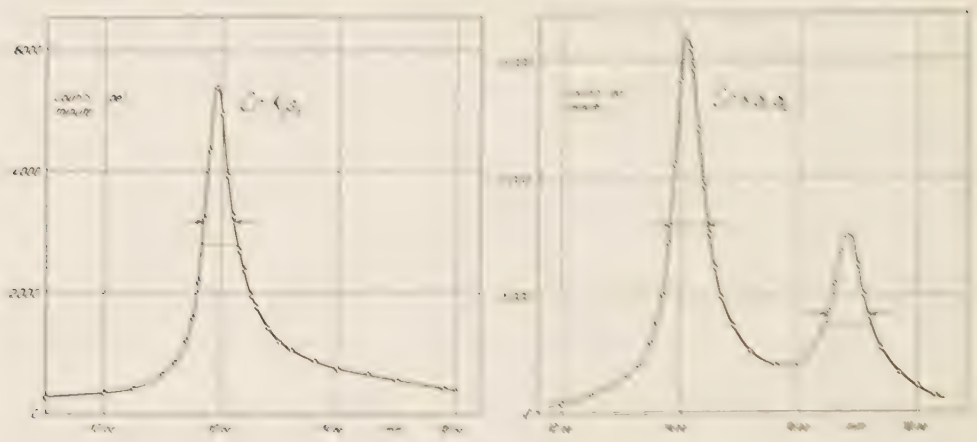

Fig. 14. The intensity distribution of the Cr lines, plotted against the readings of the micrometer screw.

until this axis coincided with the surface of the crystal. The end sections, if not as accurately bent as the rest, could be screened by the knife edge so that sharp spectral lines were obtained. Further details regarding the adjustment of a concave crystal spectrometer may be obtained from the appropriate literature [e.g. SANDSTRÖM 1935].

The crystal was moved along the spectrometer track (Fig. 1) until the incident beam could fill the whole of the reflecting surface. The slit was adjusted on to the Rowland circle and arranged to be moved along the tangent. Then the slit opening was made parallel to the X ray line. The latter adjustment was carried out with the aid of a photographic plate. The distances on the plate between the X ray line and the opposite ends of the slit were measured with a comparator. The largest distance difference tolerated was 0.005 mm. This maximum allowance corresponds to between 1 and 4 % of the slit width used for the recordings of the excitation curves. The length of the slit was 8 mm.

The Geiger counter being mounted and its position adjusted, a profile curve of the X ray line in question was plotted. The slit width was about 0.07 mm during these

Table 1.

Element and X-ray line	Full width of the X-ray line at half maximum intensity		Slit width		
			Actual	Along the tangent	
	mm	volts	mm	mm	volts
Ti $K\alpha_1$	0.352	3.6	0.140	0.341	3.5
Cr $K\alpha_1$	0.640	2.2	0.340	0.640	2.2
Cr $K\beta_1$	0.628	3.1	0.400	0.520	2.6
Fe $K\alpha_1$	0.500	3.1	0.330	0.490	3.1
Co $K\alpha_1$	0.348	2.7	0.210	0.318	2.5
Ni $K\alpha_1$	0.292	2.8	0.170	0.278	2.6
Cu $K\alpha_1$	0.240	2.8	0.136	0.239	2.8

determinations. Fig. 14 shows the intensity distribution of the chromium lines considered, plotted against the reading of the micrometer screw.

The width and position of the slit were adjusted in accordance with the profile curve. Line breadths and slit widths are given in Table 1. The half maximum breadth in Fig. 14 is marked by a horizontal line, and the adjusted positions of the slit edges with arrows.

B. Procedure

The vacuum requirements and evacuation procedure have already been treated in the description of the evacuation system and X ray tube. A check had to be made to ensure that degassing was complete before proceeding with measurements. When conditions in the X-ray tube had become stationary as regards temperature, heating current and emission, the Geiger counter was set in operation. The optimum focusing current and the invariability of the intensity with the oscillation current were tested before each series of determinations.

Before commencing with evaporation on to the target, the intensity of the X-ray beam was measured for the additional voltages $v = 0$ and 75 V. The potentiometer circuit was visually adjusted for an excitation potential in the v range between 15 and 25 V. The first series of determinations were made with an evaporated layer on a target base of a foreign metal (Be or Cu). Evaporation was performed in 5 minute stages, and the attainment of the thinnest layer functioning as a thick target was determined by measuring the intensity increase at 0 and 75 V between each evaporation period. Only one measurement was required with a target base of different atomic number, since the furnace conditions were completely reproducible. A layer four or five times as thick as the minimum layer was evaporated on to the target, to make quite sure of a pure target, and particular attention was paid to the vacuum gauges during the final stages of evaporation, to see that the pressure did not rise (cf. Chapter I.).

It was important to know for each element and temperature the longest bombardment time compatible with no appreciable oxidation of the target surface. This time was first estimated by visual examination of the target, and later, when signs of oxidation had been identified in sensitive parts of the excitation curves, with the help of these curves.

The maximum times thus determined for normal targets were not sufficiently long to permit uninterrupted measurements of the complete K excitation curve. The curve therefore had to be divided up into two, three or four sections, the target surface being renewed between the different sections. It was later possible to combine these sections to a complete curve. Since minor displacements might possibly occur between the different sections, the ends of these sections should overlap. The intensity at a certain voltage point was calculated from the time for 50×64 or 100×64 pulses, this time being converted to counts per minute with the dead time of the Geiger counter taken as 3.0 sec. per 3200 counts. Between one and five such determinations were made for each voltage value. The total number of pulses per point depended on (1) the time available for the curve section concerned, (2) the risk of external electric disturbances, and (3) the statistical resolution required. The number of pulses given in Tables 20–22 and the standard deviation indicated in the figures, is an average value for the entire curve. The voltage interval between the points was 1, 1·2 or 1·4 volt, according to the circumstances. The cobalt curve of Fig. 34 provides a

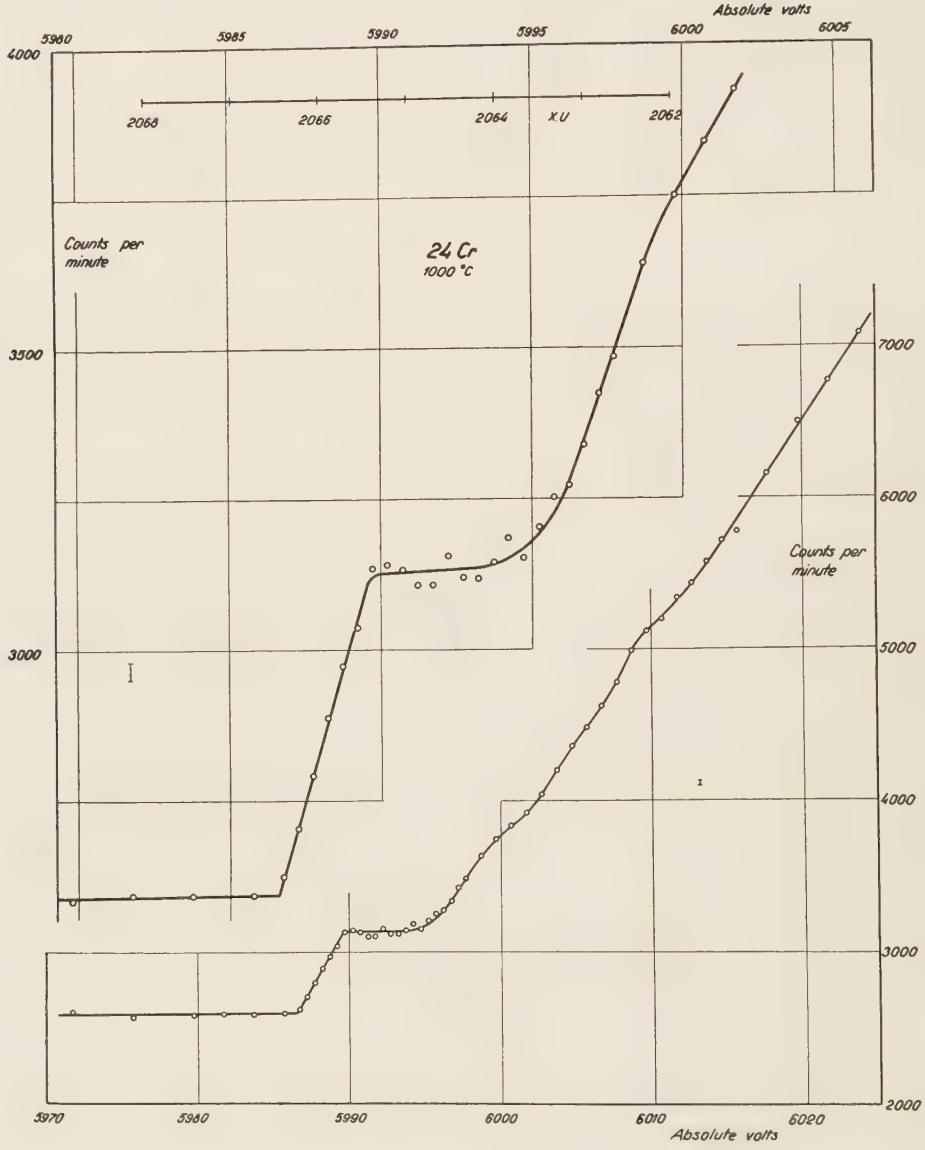

Fig. 15. Excitation curve of Cr $K\alpha_1$. Mean of Nos. 14 and 15, Table 7.

The upper curve shows an enlarged section of the lower one. The voltage scale includes the work function correction.

The separate X.U. scale in this and the following figures is calculated from the absolute-volt scale, with $h/e = 1.3793 \cdot 10^{-17}$ erg. sec/e.s.u.

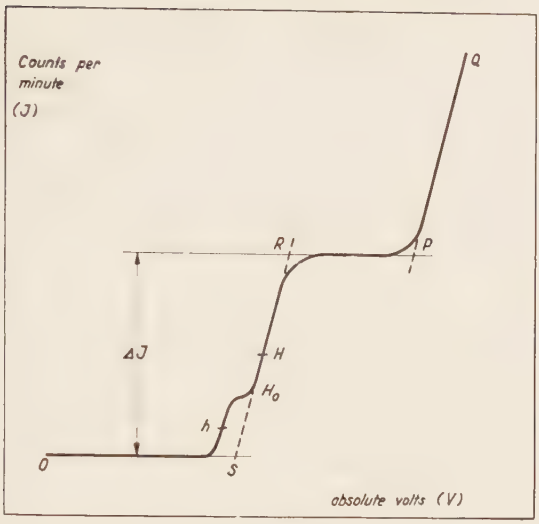

Fig. 16. The general appearance of the excitation curves, and the notation used.

diagrammatic illustration of the procedure in determining an excitation curve in two sections.

The occasional displacement in the intensity level which was mentioned above might conceivably be explained by (1) changes in the target or the window foil during evaporation, (2) slow change of the efficiency of the Geiger counter, or (3) gradually increasing contamination of the target. The effect of (2) was eliminated by taking series with decreasing voltages as well as with increasing voltages. A check was made on (3) by means of one or two "standard points" on horizontal parts of the curve, which were measured before and after a series of determinations. When displacement of a section was observed, the curve was regarded as suspect.

Fig. 15 shows a chromium curve taken at a temperature of 1000 1100° C. There is a clearly marked plateau before the definite increase in intensity.

The wavelength scale included with the curves is calculated from the relation $hc/\lambda = eV$, with $c = 299790$ km/sec. [Bearden & Watts 1951], $h/e = 1.3793.10^{-17}$ erg. sec./e.s.u. [Bearden & Watts 1951], and the conversion factor for kX units to Ångström units = 1.00202 [Bragg 1947].

An interesting structural detail was discovered at the foot of the excitation curve for normal target temperatures. Its disappearance at the higher temperatures may be due to insufficient resolution — but there are presumably other more fundamental causes as well (See Chapter VI). The essential features of the excitation curves are illustrated diagrammatically by Fig. 16. The voltages and intensities given in the tables refer to this model and the notation used there. The model is most appropriate for chromium and titanium; for other metals, the respective figures give an idea of how close the resemblance is.

The sections OS, RP and PQ have usually been drawn as straight lines. Strictly speaking, this is true only for the intensity in the section OS. Both RP and PQ probably have a fine structure which the number of pulses counted was too low to reveal. See Fig. 39, however.

Apart from the zero level of the Geiger counter (80 counts/min.), the background is due to the continuous radiation. The intensity distribution of this radiation from a thick target was investigated by KULENKAMPFF [1922]. He showed that when the voltage applied to the X-ray tube is constant, the continuous intensity is a linear function of the frequency (apart from an interval near the short wavelength limit). Estimation based on Kulenkampff's results shows that the background of the excitation curves for the elements considered increases about 0.1 % per volt.

The standard deviation (the square root of number of pulses per point) shown in the figures, refers to the intensity where it is drawn.

Chapter V. Measurement of the high voltage

A. The potentiometer circuit

This circuit is shown to the right in Fig. 13. The smoothed high voltage measured by the precision potentiometer is

$$V_{R+r} = E \cdot \frac{R+r}{r}.$$

The resistances R and r are described under Fig. 13. They had a low temperature coefficient (of the order of 10^{-5} deg.$^{-1}$), being made of manganin wire. The temperature coefficient of the Nife cell is about ten times as high, but at constant temperature its *emf* E is very stable, because of the low self-discharge of the alkali accumulator.

The resistances in the potentiometer circuit were measured with a Wolff precision bridge. The *emf* of the Nife cell was measured by comparison with a standard cell, using a Wolff potentiometer.

The laboratory temperature was kept constant with the aid of thermostats. The temperature variation of the Nife cell was not allowed to exceed 0.2° during a series of determinations.

The additional voltage v was measured with a Roller-Smith voltmeter, which was calibrated with a bridge against a standard cell.

Certain corrections ΔV had to be applied to the calculated voltage V_{R+r}. If the corrected voltage is denoted by V_0, the following expression is obtained for V, the voltage corresponding to the electron energy at the target:—

$$V = V_0 + v, \text{ where } V_0 = V_{R+r} + \Delta V.$$

The voltages are expressed in absolute volts, unless otherwise stated. The Wolff bridge was graduated in international ohms, so resistances are given in that unit.

B. The potentiometer resistances

The Wolff bridge had a guaranteed accuracy of 0.01 % at 20° C.

Readings were made for several consecutive bridge positions in the neighbourhood of the galvanometer zero. The same series was then measured with reversed bridge current, after which the resistance value was determined graphically.

Table 2. Measurements of the precision resistance R.

Date	R (int. ohm)	R_{mean}
13.3.48	3 968 620	
4.7.49	3 968 790	
16.3.50	3 968 520	
14.8.50	3 968 840	3 968 690
24.8.50	3 719 960	
27.2.51	3 719 690	3 719 820
13.4.51	4 964 780	
28.8.52	4 964 940	4 964 860
28.8.52	4 960 930	
23.10.52	4 960 790	4 960 860

Table 3. The potentiometer resistances.

	Nos.	r (int. ohm)	R (int. ohm)
Ti $K\alpha_1$	1–10	1 288.30	4 960 860
Cr $K\alpha_1$	1	845.78	3 968 690
	2– 6	840.78	3 968 690
	7– 8	870.78	3 968 690
	9–19	815.78	3 719 820
	20	1 083.33	4 964 860
	21–23	1 066.33	4 960 860
Cr $K\beta_1$	24	1 072.35	4 964 860
	25	1 082.34	4 964 860
Fe $K\alpha_1$	1–5	897.76	4 960 860
Co $K\alpha_1$	1–5	828.76	4 964 860
Ni $K\alpha_1$	1	767.78	4 964 860
	2–4	765.78	4 960 860
Cu $K\alpha_1$	1–5	713.79	4 964 860

The large resistance R was divided up into 1/2 MΩ sections for measurement. The 1000 : 10 ratio of the Wolff bridge was used for this measurement, whereas the 1000 : 1000 ratio was used for the resistance r. It was therefore necessary to determine the relationship between these two ratios. The 1000 : 10 ratio gave a higher value than the 1000 : 1000, the factor involved being 1.00018 ± 0.00004. Table 2 summarises the measurements of R. The values given have been corrected with the above factor. Table 3 gives details of the potentiometer resistances used for the various determinations.

Table 4 a.

Cell No.	LN 363 896	LN 363 923	L 215 790	Mean	
Date of certificate	13.5.47	13.5.47	30.7.47		
Certified int. volts	1.01896	1.01892	1.01826	Int. volts	Abs. volts
April 1948			1.01822	1.01822	1.01856
Nov. 1948	1.01821	1.01822	1.01823	1.01822	1.01856
April 1949	1.01823	1.01824	1.01824	1.01824	1.01858

Table 4 b.

Cell No.	L 265 648	L 265 694	M 163 417	M 164 214	Mean
Date of certificate	23.8.50	23.8.50	31.7.50	1.9.50	
Certified abs. volts	1.01856	1.01857	1.01864	1.01858	(abs. volts)
April 1951	1.01862	1.01857	1.01854	1.01850	1.01856
Nov. 1951	1.01866	1.01859	1.01855	1.01849	1.01857
March 1952	(1.01870)	1.01860	1.01856	1.01851	1.01856
June 1952	(1.01874)	1.01861	1.01856	1.01850	1.01856
Sept. 1952		1.01862	1.01855	1.01849	1.01855

Table 4 a and b. Comparison between the Pye 58946 cell and various new Weston elements at the Institute of Physics. The tables give the *emf* at 20° C of Pye 58946 in the same unit system as the corresponding certificate. In the mean column of Table a, the conversion factor between absolute and international volts is 1.00033. [DUMOND & COHEN 1948.] LN = Leeds & Northrup Co. L = Cambridge Instrument Co. M = Muirhead and Co.

C. The *emf* of the Nife cell

The Nife cell was compared before and after each series of determinations with Weston cell L-215790, which served as secondary standard cell. The primary standard was the Pye 58946 cell, manufactured in 1936 and with a certified *emf* at 20° C of 1.0182 int. volts. This cell was frequently compared with new Weston cells; the results of the comparisons are given in Tables 4 a and b. The same cell was used by OHLIN in 1940 [cf. OHLIN 1941], and since then the *emf* has remained constant within the limits of measurement. A twin cell, Pye 58947, has remained equally invariable, the largest measured difference between the two being 2.10^{-5} V. The potential assigned to the Pye 58946 cell in all calculations was 1.01856 absolute volts.

The mean value of E for each series of determinations is given in the tables of the excitation potentials. It was not possible to avoid a slight increase in the temperature of the Nife cell, which meant a decrease in its *emf*, but the difference between the initial and final values was less than $5 \cdot 10^{-5}$ V, except in a few cases.

D. Voltage corrections applied

1. The cathode potential

The cathode potential was zero for the oxide cathode. Most of the determinations were made with the tungsten cathode, however. Only a short central section of the tungsten filament emitted electrons, and the mean potential v_c of this section was

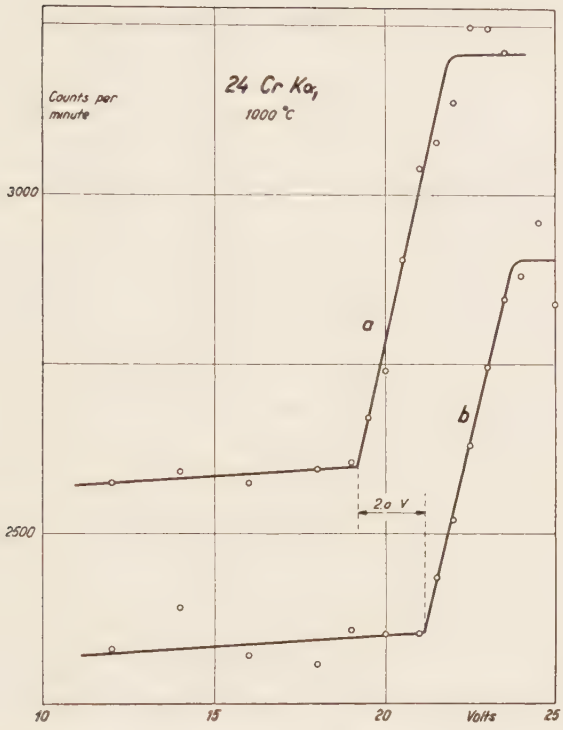

Fig. 17. Voltage displacement resulting from a change in the sign of the cathode potential. a – negative filament, b – positive filament.

Table 5. The potential v_c of the tungsten cathode.

	Ti	Cr	Cu
Point determined (Fig. 16)	*h*	*S*	*S*
Filament voltage v_f	1.99	1.71	1.76
v_f negative (v volts)	20.1	19.1	35.7
v_f positive (v volts)	22.3	21.1	37.8
Voltage displacement	2.2	2.0	2.1
Cathode potential v_c (v_f neg.)	−1.1	−1.0	-1.0_5

determined by reversing the potential of the unearthed end of the filament. The displacement of the curve due to this reversal should be $2v_c$. Table 5 and Fig. 17. The filament was normally negative with respect to earth.

2. The temperature effect of the manganin resistors

The current through the resistors R was of the order of 10^{-5} A during measurements with the Wolff bridge. But for the excitation determinations the current was 1–2 mA.

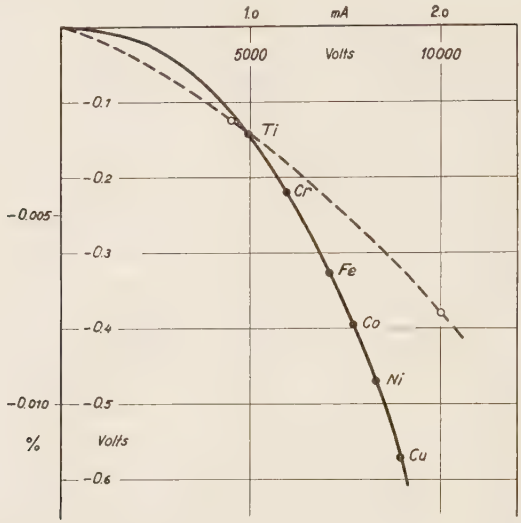

Fig. 18. Voltage corrections for the temperature effect in the resistance R (4 964 860 Ω). ○ – observed values of $\Delta R/R$. ● – voltage corrections (v_R).

The resistance correction for the consequent temperature change was determined in the following manner. Currents of 0.9 and 2.0 mA were sent through the resistors, and the resistance then measured several times at 5 min. intervals. Extrapolation to time zero gave the values of $\Delta R/R$ in Fig. 18. The corresponding voltage corrections are given by the unbroken line.

3. Mean thermal energy of the emitted electrons

When electrons leave the surface of the cathode, they have an initial thermal energy distribution which approximately obeys Maxwell's distribution law [see, for instance, HERRMANN & WAGENER 1943]. The mean energy in the direction normal to the emitting surface, v_M, is calculated from the formula $v_M = kT$, where k is Boltzmanns constant ($= 0.86 \cdot 10^{-4}$ eV/deg.) and T the absolute temperature. T may be taken as 2400° K for the tungsten cathode, and 1200° K for the oxide cathode. The corresponding values of v_M are 0.2 and 0.1 eV.

A summary of the corrections described above is given for Ti and Cr in Table 6 a.

E. The work function

1. Introduction

The work function of a metal signifies the energy required to lift an electron from the Fermi level in the conduction band to a point just outside the metal's surface. The work function is due to image forces and the electrostatic double layer at the surface.

If two metals at the same temperature are electrically connected, the number of electrons passing from one metal to the other in unit time, as well as their velocity

Table 6 a. Voltage corrections for Ti and Cr with the work function omitted.

	Nos.	Cathode	$\lvert v_c \rvert$	v_R	v_M	ΔV^*
Ti	1–4, 8–9	W	1.1	−0.1	0.2	+1.2
	5–7, 10	oxide	0	−0.1	0.1	0
Cr	4– 6	W	2.2	−0.4	0.2	+2.0
	13–18	W	1.0	−0.4	0.2	+0.8
	19	W	1.1	−0.4	0.2	+0.9
	20, 22–25	W	1.1	−0.2	0.2	+1.1
	21	W	1.2	−0.2	0.2	+1.2
	1–3, 7–12	oxide	0	−0.4	0.1	−0.3

Table 6 b. Voltage corrections for 22 Ti–29 Cu. Tungsten cathode. Work function included.

	Nos.	$\lvert v_c \rvert$	v_R	v_M	v_φ	ΔV
Ti	1–4, 8–9	1.1	−0.1	0.2	4.5	+5.7
Cr	22–25	1.1	−0.2	0.2	4.5	+5.6
	21	1.2	−0.2	0.2	4.5	+5.7
Fe	1–4	1.1	−0.3	0.2	4.5	+5.5
	5	1.0	−0.3	0.2	4.5	+5.4
Co	1–5	1.1	−0.4	0.2	4.5	+5.4
Ni	1–4	1.1	−0.5	0.2	4.5	+5.3
Cu	1, 4, 5	1.0	−0.6	0.2	4.5	+5.1
	2, 3	1.1	−0.6	0.2	4.5	+5.2

Table 6 a and b. The voltage corrections.

v_c = cathode potential. The filament voltage v_f was between −1.70 and −2.10 volts, with the exception of Nos. 4–6, Cr, where $v_f = -3.6$ volts.

v_R = voltage correction for the temperature effect in the resistance R (Fig. 18).

v_M = mean thermal energy of the emitted electrons.

v_φ = work function correction.

$\Delta V = \lvert v_c \rvert - \lvert v_R \rvert + v_M + v_\varphi$ = the total correction to be applied to V_{R+r}.

ΔV^* = the total correction to be applied to V_{R+r} with the work function correction omitted.

$V_{R+r} + \Delta V = V_0$.

$V_{R+r} + \Delta V^* = V_0^*$.

distribution, must be equal in opposite directions. This means that the Fermi levels of the two metals are shifted to the same potential. An external potential difference — the Volta potential — therefore arises, as may be confirmed experimentally.

If we suppose that the two metals are the cathode and anticathode of an X-ray tube, whose applied voltage we for the moment put equal to zero, it follows from what has been said above (1) that only electrons with thermal energy greater than the cathode's work function can leave its surface and reach the interelectrode vacuum, and (2) that if such an electron happens to reach the target, it delivers up the same maximum energy as if it had happened to return to the cathode — i.e. an energy equal to the cathode's work function.

But if the cathode and anticathode are now separated by an electromotive force, the energy corresponding to this force will be added to the work function energy. The total kinetic energy of an electron striking the target is therefore the sum of the potential difference between the Fermi levels and the cathode's work function. As the potential difference between the Fermi levels is the quantity measured by a voltmeter, the work function must be a further necessary correction.

OHLIN [1941], in his determination of h/e by an X-ray method, obtained results which cast doubt on the necessity for the work function correction. OHLIN determined the minimum anode-cathode voltage V which could produce X-radiation of wavelength λ. The relation $hc/\lambda = eV$ implies that for a constant wavelength, h/e should be proportional to the voltage V. OHLIN carried out his determinations in the range 3000–5000 V, where the work function would mean a correction of about 0.1 %. This correction is much larger than the obtained reproducibility (± 0.02 %). When OHLIN corrected his voltage values V with the work function, a definite drift appeared in the results. Without the correction, the individual results had a normal statistical distribution about a mean. For this reason, and on account of the precision with which he had made all measurements, he drew the understandable conclusion that the theory was incorrect on this point, and rejected the correction.

OHLIN's results gave rise to a discussion which may be described as still unsettled [PANOFSKY, GREEN & DUMOND 1942, OHLIN 1942, DUMOND 1947 and 1948, DUMOND & COHEN 1948, BEARDEN & SCHWARZ 1950, BEARDEN, JOHNSON & WATTS 1951]. Two papers are of special interest:— OHLIN [1942 b] and BEARDEN, JOHNSON & WATTS [1951]. Both contain a comparison of voltage determinations for the high frequency limit of the continuous X-ray spectrum with oxide and tungsten cathodes. OHLIN found that the values obtained with tungsten target and tungsten filament closely agreed with those obtained with oxide cathodes and different target substances. BEARDEN, JOHNSON & WATTS, however, observed a difference of 3 V, corresponding to the difference in work function between the two cathodes used. This difference is 0.03 % of their total voltage (10 kV), and the probable error given is ± 0.003 %.

2. Measurements and discussion

Since it is possible to determine h/e from measurements of excitation potentials, the problem of the work function correction also appears in the present investigation. The phenomena concerned are, however, different, involving different excitation processes, and consequently a rule for one may not be valid for the other. It was therefore necessary to make a new enquiry into the question of the work function correction in the case of K excitation, regardless of previously published

Table 7. Cr K α_1. Temperature: 1 000°–1 100° C.

	No.	E_{mean}	V_{R+r}	V_0^*	S	H	R	P
Oxide-coated cathode	1	1.26660	5 944.6	5 944.3	5 985.6	5 987.0	5 988.3	5 994.9
	2	1.26017	5 949.6	5 949.3	5 985.2	5 986.7	5 988.1	5 993.9
	3	1.26016	5 949.5	5 949.2	5 985.1	5 986.6	5 988.1	5 993.9
				Mean, abs. volts	5 985.3	5 986.8	5 988.2	5 994.2
Tungsten cathode	4	1.25913	5 944.7	5 946.7	5 982.3	5 983.7	5 985.1	5 991.4
	5	1.25913	5 944.7	5 946.7	5 982.3	5 983.7	5 985.0	5 991.2
	6	1.25853	5 941.8	5 943.8	5 982.7	—	—	—
	13	1.30733	5 962.5	5 963.3	5 982.4	5 983.8	5 985.2	—
	14	1.30727	5 962.2	5 963.0	5 982.0	5 983.6	5 985.2	5 990.4
	15	1.30733	5 962.5	5 963.3	5 982.1	5 983.4	5 984.7	5 990.8
				Mean, abs. volts	5 982.3	5 983.6	5 985.0	5 991.0
				$V_{\text{oxide}} - V_W$	3.0	3.2	3.2	3.2

Anticathode: Chromium plate, supported on a molybdenum pin (Fig. 7 a).

The work function correction is omitted in this table.

Table 8. Cr K α_1.

	No.	E_{mean}	V_{R+r}	V_0^*	S	H	R	P
Oxide-coated cathode	7	1.30969	5 970.4	5 970.1	5 985.8	5 987.5	5 989.1	5 995.5
	8	1.30965	5 970.2	5 969.9	5 985.9	5 987.4	5 988.9	5 995.3
	9	1.30707	5 961.3	5 961.0	5 985.5	5 986.8	5 988.0	5 994.2
	10	1.30716	5 961.7	5 961.4	5 985.8	5 987.2	5 988.5	5 995.2
	11	1.30727	5 962.2	5 961.9	5 985.8	5 987.2	5 988.7	5 995.1
	12	1.30731	5 962.4	5 962.1	5 985.8	5 987.3	5 988.7	5 995.4
				Mean, abs. volts	5 985.8	5 987.2	5 988.7	5 995.1
Tungsten cathode	16	1.30735	5 962.6	5 963.4	5 983.5	5 984.8	5 986.1	5 992.6
	17	1.30735	5 962.6	5 963.4	5 983.4	5 984.9	5 986.4	5 992.8
	18	1.30707	5 961.3	5 962.1	5 982.8	5 984.5	5 986.2	5 991.8
	19	1.30662	5 959.3	5 960.2	5 982.9	5 984.4	5 985.9	5 993.1
	20	1.29837	5 951.7	5 952.8	5 983.6	5 985.1	5 986.6	5 993.4
	21	1.28189	5 965.0	5 966.2	5 983.3	5 984.9	5 986.4	5 992.5
	22	1.28187	5 964.9	5 966.0	5 983.5	5 985.0	5 986.4	5 992.5
				Mean, abs. volts	5 983.3	5 984.8	5 986.3	5 992.7
				$V_{\text{oxide}} - V_W$	2.5	2.4	2.4	2.4

Anticathode: Nos. 7–12, 16–19. Chromium-electroplated copper.
Nos. 20–22, Chromium, evaporation deposit on copper.

The work function correction is omitted in this table.

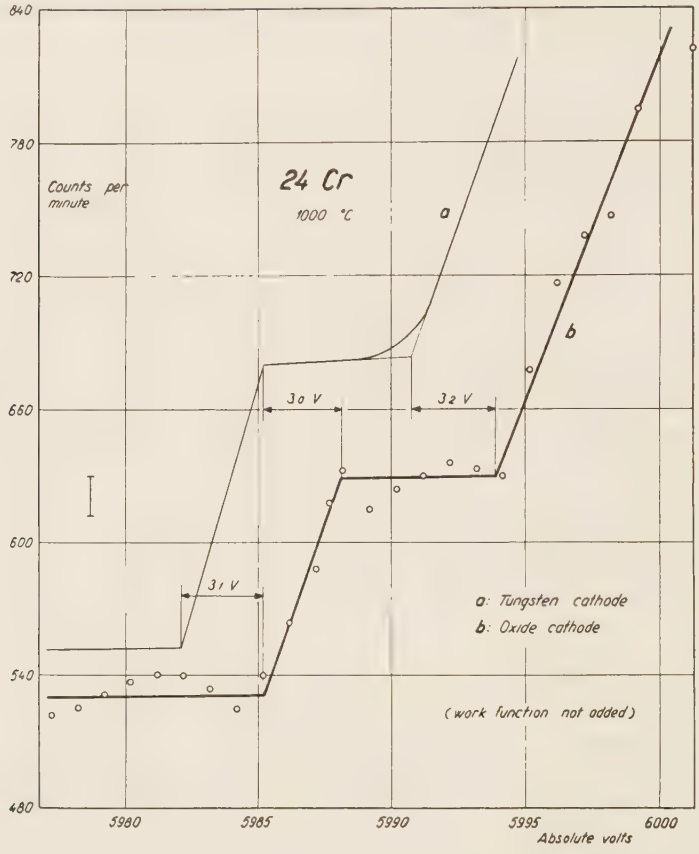

Fig. 19. Cr $K\alpha_1$ excitation curves, the work function correction omitted. Anticathode at red heat.

The intensity scale refers to the oxide cathode curve (No. 2, Table 7). The tungsten cathode curve is the one shown in Fig. 15.

measurements. One of the curves obtained was so near the quantum limit for the continuous radiation, that it was possible to make a direct comparison between the two types of curves.

The K excitation potential of chromium was determined in 1949–50 with both oxide cathode and tungsten cathode. The results of these determinations are given in Tables 7 8 and Figs. 19–20 (together with some later results). Similar determinations were made in 1952 for a titanium target. The results are given in Tables 12–13. A graphical summary of the results for both chromium and titanium is given in Fig. 21.

The chromium curves were obtained for both incandescent and cooled targets. The results for cooled targets require a considerably cleaner vacuum to be reproducible than do the targets at red-heat. The surface of a chromium target at red-heat may be said to renew itself, in view of the high vapour pressure of the metal at such temperatures.

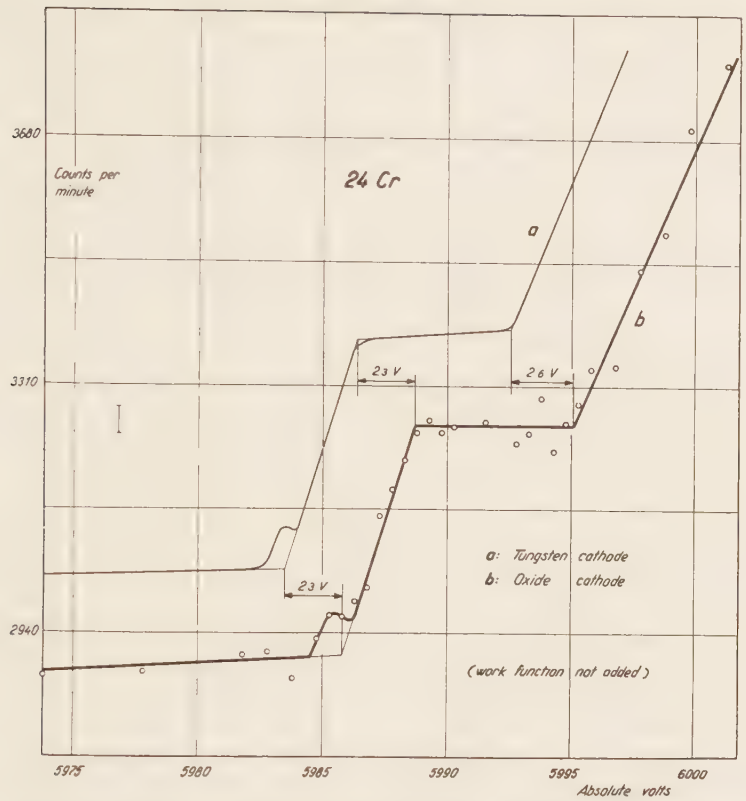

Fig. 20. Cr $K\alpha_1$ excitation curves, the work function correction omitted. Water-cooled anticathode.

The intensity scale refers to the oxide cathode curve (No. 11, Table 8). The tungsten cathode curve is the one shown in Fig. 22.

The coating of the oxide cathode was a mixture of barium, strontium and calcium oxides. Barium chloride, strontium nitrate and calcium chloride in the molecular proportions 5 : 5 : 1 were emulsified in a mixture of amyl acetate and Zapon lacquer, and applied to the cathode with a glass rod. The oxides were formed at 1000–1100° C, the subsequent operating temperature being 950 1000° C. The base metal was platinum, except for chromium curves Nos. 1–3 and 7–8, for which it was nickel.

The oxide layer of normal thickness was bright white in colour. It proved to be difficult to degas such layers sufficiently for water-cooled anticathodes not to be contaminated in operation, and thinner oxide films were therefore used with such anticathodes. For this purpose, the emulsion of the salts previously mentioned was further diluted with amyl acetate, and the layer applied to the cathode was so thin that the metal underneath was clearly discernible. The contamination of the target was reduced by this means, and reproducible curves obtained, even with cooled targets. As may be seen from Fig. 21, the voltage displacement for these cathodes was not quite regular, and curves for a cooled titanium target were therefore determined later with a normal oxide coating on the cathode. Rapid determination in combination

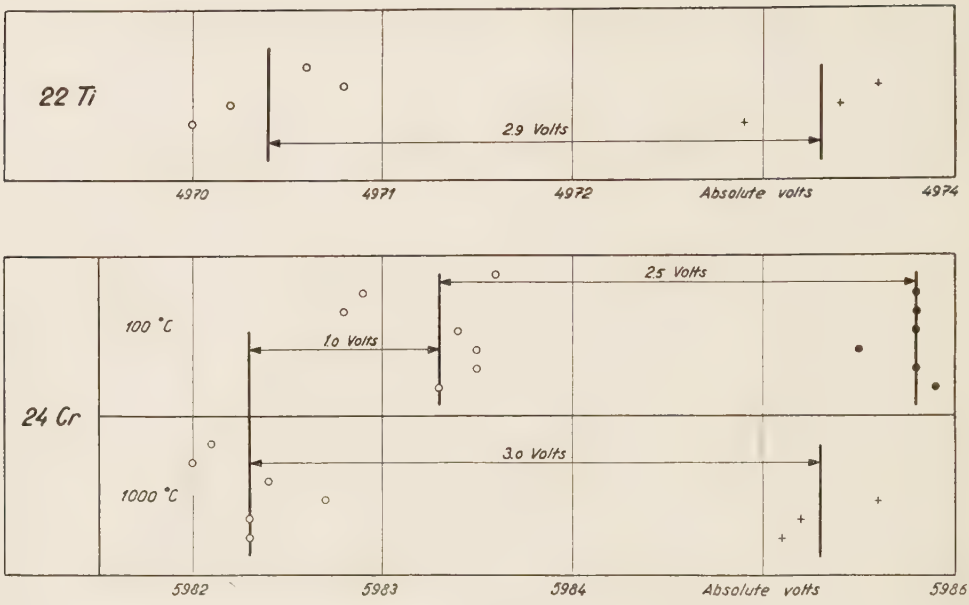

Fig. 21. The distribution of the determined potentials of 22 Ti, point *P*, and 24 Cr, point *S*, the work function correction being omitted.

○ – tungsten cathode. + – normal oxide cathode. ● – thin oxide films.

with titanium evaporation made this possible. (Chromium curves Nos. 1 19 were obtained without evaporation.) On account of the large structure at the foot of the primary edge S of the titanium curves, the excitation potential given for Ti in Fig. 21 refers to the secondary edge P.

Fig. 21 gives a good idea of the spread of the measured values due to random variations. When the same resistances R and r were used for the whole series of measurements, the spreading was mainly due to the error of the Wolff potentiometer (± 0.01 %), and of the galvanometer zero reading (± 0.3 V). Fig. 21 shows that the measured values lie within a range of 1 V, which is a measure of the reproducibility attainable. Voltage differences occurring when either the cathode or target were changed, without other alterations, may therefore be assigned a maximum uncertainty of ± 1 V. The values obtained with oxide and tungsten cathodes differ by a clear voltage margin. Fig. 21 and Tables 7, 8 and 13 show that the average values for the different targets were displaced 2.9–3.2 V with normal oxide cahtodes, and 2.4–2.5 V with the extremely thin oxide coatings.

Tungsten's work function is 4.5 V. An applied electrostatic field diminishes the work function by an amount which is proportional to the square root of the field intensity at the surface. This effect is only a matter of millivolts for the fields used here, however, and is therefore negligible. Thermoelectric potentials at the cathode can be estimated to be of the same order of magnitude.

The work function of an oxide cathode is more complicated. The definition is analogous to that given for a metal, i.e., the work function is the amount of energy required to transfer an electron from the Fermi level of the base metal to a point in the vacuum

just outside the surface of the oxide layer. The work function depends on the composition of the oxide, on the base metal, on the thickness of the oxide layer, and on the activation of the cathode. During the activation a boundary layer of metal oxides is formed, an interface which plays an important part in the emissive properties of the cathode. The passage of a current gives rise to a potential drop across the interface and the oxide layer. For further details about oxide cathodes, reference may be made to relevant literature [HERRMANN & WAGENER 1943 and 1944, FRIEDENSTEIN et al. 1946–47, EISENSTEIN 1948].

The work functions for the individual oxides on a nickel base are given as 1.9 V (CaO), 1.4 V (SrO), and 1.1 V (BaO). The value given for extremely thin layers of SrO on a nickel base is 2.0 V, which is 0.6 V higher than that for the normal oxide layer [EISENSTEIN 1948]. LIEBOLD used a similar oxide mixture as in the present investigation, and obtained a value of 1.4 V for both nickel and platinum bases. HUBER gave 1.4–1.6 V for mixtures of SrO and BaO in different proportions on a nickel base. Regarding LIEBOLD's and HUBER's results, see FRIEDENSTEIN et al. [1946–47].

Electron and X-ray diffraction measurements have shown that the more volatile components of the oxide mixture disappear from the surface of the oxide layer. A BaO SrO cathode coating was found to consist of SrO to a depth of 300–2000 atom layers [HUBER & WAGENER 1942], so it may be presumed that SrO predominated in the oxide coating used by the present author. There is thus good reason to assume that the work function for the oxide cathodes in question was 1.4 ± 0.2 V. The difference between this value and the work function of tungsten is 3.1 V, which agrees with the observed voltage displacements for Ti and Cr targets. Moreover, the voltage displacement between the normal oxide coating and extremely thin oxide coating is of the same magnitude and sign as the difference between the work function values for normal and thin SrO coatings.

The results obtained constitute a proof that a correction should be applied, depending on the cathode and of the same order of magnitude as the thermionic work function. The proper correction is a quantity called the calorimetric work function. The difference between the calorimetric and thermionic work function is negligible for our purpose. [Cf. PANOFSKY, GREEN & DUMOND 1942.]

3. Continuous and characteristic radiation

The electronic processes involved in the emission of brehmsstrahlung and in the excitation of X-ray levels may be different with regard to the work function correction. A decision can be reached by comparing the "electronic" energy difference between two energy levels in an atom with the spectroscopically determined difference. These differences should either be the same or differ by an amount equivalent to the work function of the cathode. If they are equal, it is shown that the work function should be treated in the same way in relation to continuous and characteristic radiation.

The curve in Fig. 25 enables us to make such a comparison. One level considered is the $M_{II, III}$ level of chromium, corresponding to the maximum intensity of the $K\beta_1$ line. The $K\beta_1$ line arises from the $(K - M_{II, III})$ transition, and its shape and position have been determined by BEARDEN & SHAW [1935]. The shape may be given in terms of the width at half-maximum and the asymmetry. BEARDEN & SHAW give the width as 3.0 V, and the asymmetry as 1.53 for the $(1 + 1)$ position of the

Table 9. Cr $K\alpha_1$, $K\alpha_2$ and $K\beta_1$.

	No.	E_{mean}	V_{R+r}	V_0	h	S	H	R	P
Cr $K\alpha_1$	21	1.28189	5 965.0	5 970.7	5 987.4	5 987.8	5 989.4	5 990.9	5 997.0
	22	1.28187	5 964.9	5 970.5	5 987.4	5 988.0	5 989.5	5 990.9	5 997.0
			Mean, abs. volts		5 987.4	5 987.9	5 989.4	5 990.9	5 997.0
Cr $K\alpha_2$	23	1.28187	5 964.9	5 970.5	—	5 988.1	5 989.6	5 991.0	5 996.7
Cr $K\beta_1$	24	1.28669	5 958.5	5 964.1	—	5 988.2	5 989.7	5 991.2	5 995.8

Anticathode: Nos. 21–23. Chromium, evaporation deposit on copper.
No. 24. Chromium, evaporation deposit on beryllium.

Cathode: Tungsten filament.

Table 10. The quantum limit (V_L) of the continuous spectrum at the Cr $K\beta_1$ line.

No.	E_{mean}	V_{R+r}	V_0^*	V_0	V_L^*	V_L	$(h/e)^* \cdot 10^{17}$	$h/e \cdot 10^{17}$
25 a	1.28669	5 903.5	5 904.6	5 909.1	5 941.1	5 945.6	1.3782	1.3792
25 b	1.28669	5 903.5	5 904.6	5 909.1	5 941.6	5 946.1	1.3783	1.3794
						Mean	1.3783	1.3793

Cr $K\beta_1$ = 2 080.60 X.U. [BEARDEN and SHAW 1935.]
λ_{slit} = 2 080.67 X.U. (Correction for asymmetry of $K\beta_1$. Fig. 14.)
Slit width = 2.6 volts.
Units in the table: voltages in absolute volts.
h/e in ergsec./e.s.u.

* signifies that the work function correction is omitted.

crystals in the double crystal spectrometer. The present author's corresponding values for the $K\alpha_2$ line (Fig. 14) are 3.1 and 1.5, so there should be no risk of discrepancy in the position of the maximum intensity.

The other level considered corresponds to the main edge of the K absorption curve obtained by SANNER [1941]. Sanner measured the inflection point of the absorption edge. His results show that it occurs at 1/3 the height of the main edge.

The difference between the above-mentioned levels may be calculated from SANNER's K absorption edge (2065.95 ± 0.15) X.U., and BEARDEN & SHAW's Cr $K\beta_1$ value (2080.60 ± 0.05) X.U., using the expression $h/e \cdot (c/\lambda_K - c/\lambda_{\beta_1})$.

The energy difference obtained is (42.2 ± 0.6) eV (independent of inaccuracy in the h/e value, arising from uncertainty as to the necessity for the work function correction).

The same energy level difference can be calculated from electronic determinations as the energy between the K excitation potential and the short wavelength limit of the continuous spectrum for a wavelength corresponding to the peak of the $K\beta_1$ line. The excitation potential value must be commensurable with the inflection

point of the K absorption edge, which means that the value taken should be 5989.2 abs. volts (Table 9). The quantum limit determined has to be corrected for the 0.2 V difference between the centre of the slit and the peak of the line: 5945.9 + 0.2 = 5946.1 abs. volts (Table 10). The required voltage difference is thus 43.1 V, with an approximate error of ± 1 V, which is in full agreement with the value obtained spectroscopically.

Since the $K\beta_1$ and $K\alpha_1$ lines have the same excitation potential, it is possible to obtain a more exact value from the $K\alpha_1$ determination (Table 11). The voltage difference obtained in this way is 42.7 V.

A new value for the Cr $M_{II, III}$ edge has recently been published [GYORGY & HARVEY 1952]. The voltage value for this edge is equal to the difference between the $M_{II, III}$ level and the Fermi level. This difference has a more exact definition than the difference calculated from the K absorption edge. As we shall see later, the Fermi level corresponds to the point h in Fig. 16. The voltage difference $h_{Cr} - V_L = 5987.4 - 5946.1 = 41.3$ V (Tables 9 and 10). The direct spectroscopic value is 41.6 ± 0.3 V.

4. Conclusions

We may thus conclude (1) that the nature of the cathode surface effects the energy of the electron, (2) that this effect coincides with the work function of the cathode within the limits of experimental error, and (3) that the maximum available kinetic energy of electrons is the same in determinations of the excitation potential as in determinations of the limit of continuous radiation.

The excitation potentials in the tables have been corrected for the work function of the cathode. A summary of all corrections applied is given for the greater part of the curves obtained with a tungsten cathode in Table 6 b. Where no correction has been made for the work function, the value is marked with an asterisk.

Chapter VI. The *K* excitation curves

A. Chromium

General properties

The chromium targets were of three types: (1) ground chromium plate 1 mm thick, (2) electrolytic deposits on a copper-nickel base, and (3) chromium films evaporated on to a copper base. Analytically pure chromium was used for (1) and (3), fused according to Goldschmidt.

Chromium melts at 1860° C, but the vapour pressure is high even in the solid state. The evaporation temperature was 1100–1200° C, and the molybdenum furnace was used.

Chromium is not readily oxidised under electron bombardment. The experience of the present author was quite different from that of GYORGY & HARVEY [1952] in this respect; — they evaporated chromium continuously on to the target when making determinations.

Chromium crystallises in body-centred cubic crystals, and is stable in this form up to more than 1600° C.

The K absorption edges for Cr and Cr_2O_3 have been determined by SANNER [1941]. The main edge of Cr_2O_3 is 10.5 V higher than the edge of the pure element.

Information about the physical and chemical properties of the metals concerned have been taken from ESPE & KNOLL [1936], VAN ARKEL [1939], LAW [1948] and SZABÓ & LAKATOS [1952].

Tables and Curves

The earlier K excitation curves were obtained without an evaporation furnace. Only Nos. 20–24 are with evaporation films. There was very seldom any trace of contamination in focus after the introduction of liquid-air traps.

Table 11. Summary of Cr Kα_1, tungsten cathode. Work function correction included.

Nos.	Anticathode temperature	*S*	*H*	*R*	*P*
4–15	1 000° C	5 986.8	5 988.1	5 989.5	5 995.5
16–20	100° C	5 987.7	5 989.2	5 990.7	5 997.2
21–22	100° C	5 987.9	5 989.4	5 990.9	5 997.0
Mean Nos. 16–22		5 987.8	5 989.3	5 990.8	5 997.1
$V_{100°} - V_{1000°}$		1.0	1.2	1.3	1.6

There is a better statistical resolution in Nos. 21–22 than in the earlier curves, and more attention has been paid to the *h* structure. The results are given in Table 9. A summary of the chromium determinations with tungsten cathode is given in Table 11. Voltage differences and intensity characteristics are given in Tables 20 a and b, the latter including a comparison between the three lines determined in chromium's K spectrum.

Figs. 15, 22–26 and 30 show the different curves obtained for chromium. See also Figs. 17, 19 and 20.

100° C and 1 000° C

The curves for incandescent targets (1000–1100° C) differ from those for targets at about 100° C in the following respects: (1) the *h* structure is absent, (2) ΔI is larger, (3) the plateau *RP* is shorter (Table 20 a), and (4) the curve as a whole is displaced towards lower energies. Compare Figs. 15, 17 and 19 with Figs. 20 and 22.

The reasons that the *h* structure disappears at higher temperatures may be purely experimental: too low a statistical resolution, and too large voltage intervals between the points plotted. But the broadening of the Fermi level as the temperature rises may also account for a smoothing out of the excitation curve near the excitation limit. According to SKINNER [1946], we may take the breadth of the Fermi level as $6kT$. This corresponds to the energy difference between the levels 5 % and 95 % occupied (cf. Chapter IX), and gives us widths of 0.19 V and 0.66 V at 100° C and 1000° C respectively. A structure 0.5 V wide is consequently smoothed out at the higher temperature.

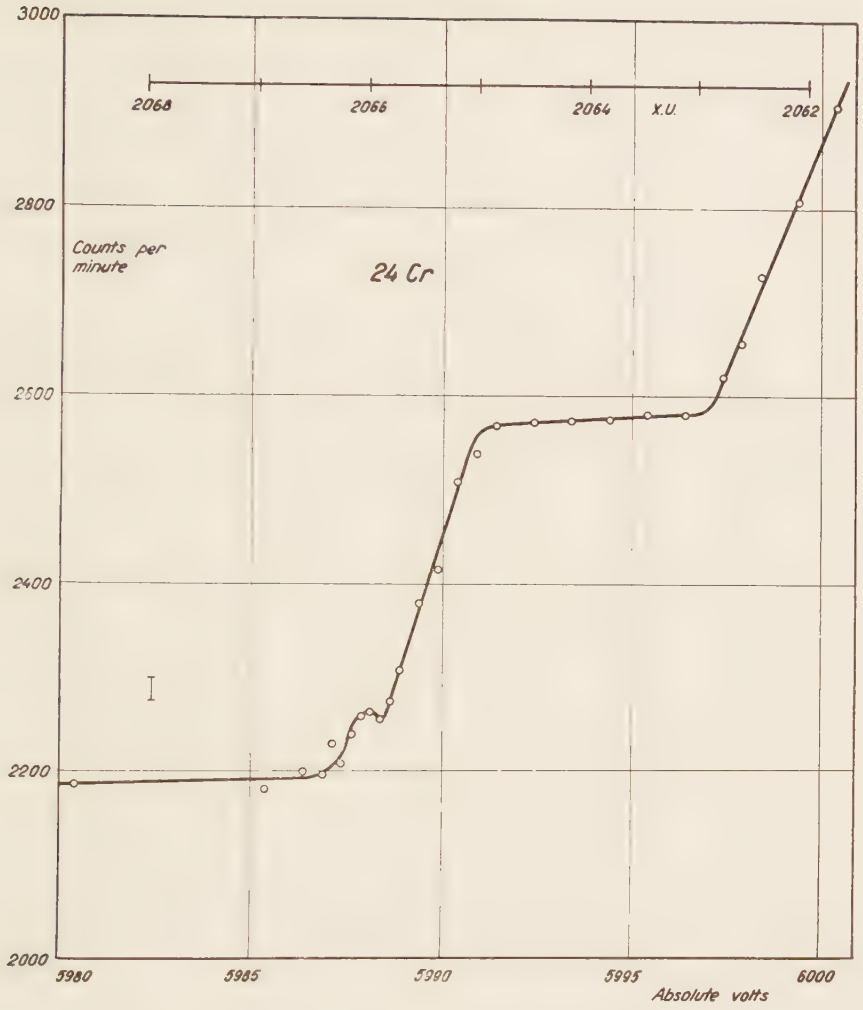

Fig. 22. Cr $K\alpha_1$. Evaporation deposit on copper. No. 22, Table 9.

Generally, a smoothing out of the structural details may be expected at higher temperatures, by analogy with what happens in the case of the absorption edges [HANAWALT 1931]. Where the excitation curve has been drawn with a sharp corner, this should be regarded as a more or less rough approximation.

The displacement towards lower energies at higher temperatures is clearly evident in Fig. 21 and Table 11. Displacements might be expected as a consequence of changes in the lattice constant — e.g. owing to thermal expansion, or transition to another crystal system. KURYLENKO [1939] observed a similar displacement with temperature of iron's K absorption edge. He made his measurements for a target at 960° C, thus above the transition temperature to γ-Fe. [See also CAUCHOIS 1952.]

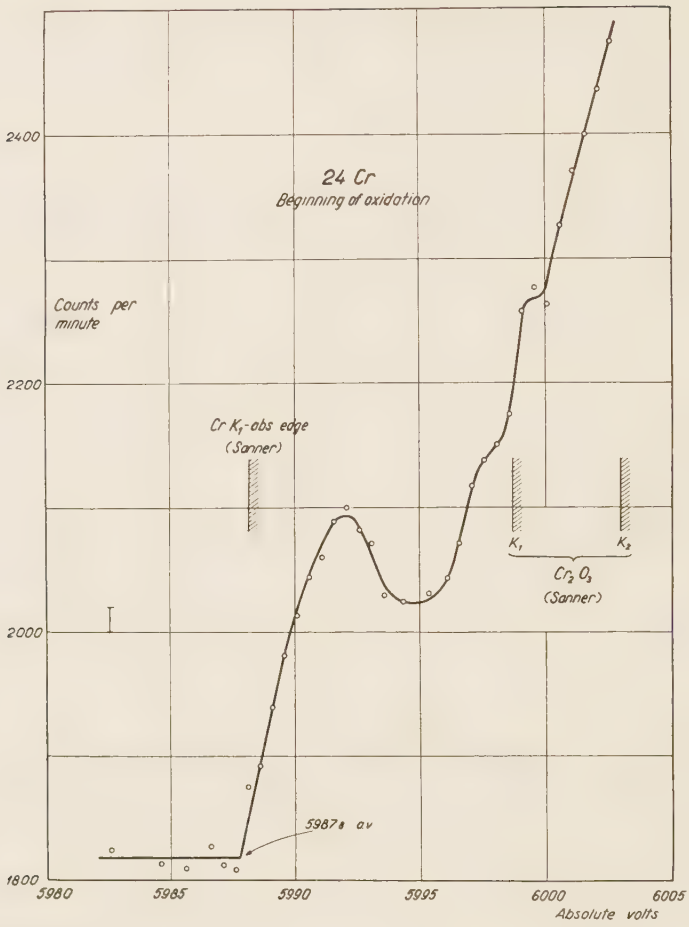

Fig. 23. Cr $K\alpha_1$ excitation curve with the chromium-plated copper anticathode slightly contaminated.

K α_1 and K α_2

Series Nos. 22 and 23 were obtained in immediate succession, and Fig. 24 shows their agreement as to position and shape. It will be seen from Table 20 b that ΔI for $K\alpha_1$ and $K\alpha_2$ are in the ratio 1 : 0.48.

K β_1

The intensity of the Cr $K\beta_1$ line is only about 20 % of that of the $K\alpha_1$ line. Near the excitation potential it scarcely rises above the continuous background. Figs. 25, 26 and Table 20 b.

With a thick target the slope of the background is so steep that the structure of the $K\beta_1$ curve disappears. However, the use of a thin target makes it possible to obtain a level background. The thin target was prepared by evaporating chromium on to a beryllium base. This method has been used previously for similar purposes [cf.

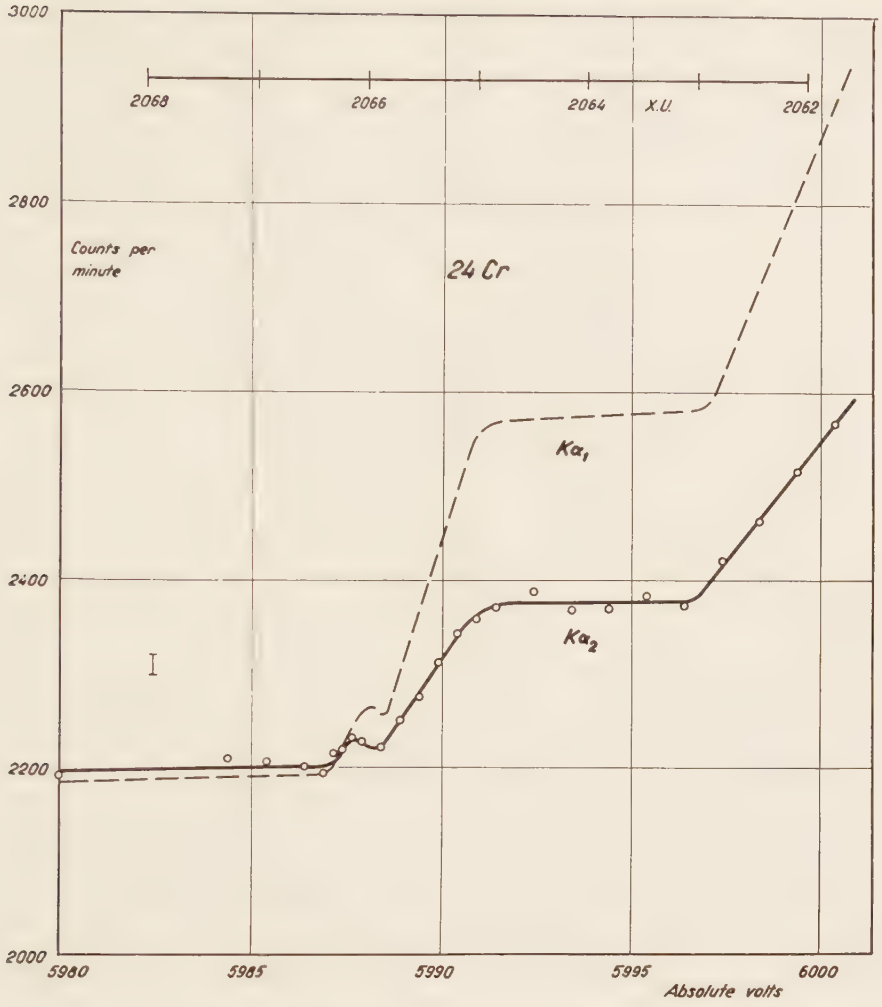

Fig. 24. Cr $K\alpha_2$. Evaporation deposit on copper. No. 23, Table 9. The dotted line is the $K\alpha_1$ curve of Fig. 22.

Coster & van Zuylen 1932]. An attempt was made to evaporate beryllium directly on to a copper base, but the metal is very brittle, and showed a tendency to flake at thicknesses of about 1 micron. The target base finally used consisted of 0.2-0.3 microns beryllium on copper, with 0.3 microns aluminium as an intermediate layer. This target was durable. Its continuous spectrum is shown in Fig. 25, curve (a). The thickness of the evaporated chromium layer was of the order of 500 Å.[1]

The continuous background with the thin Cr film had an intensity about 40% of the thick Cr target's, and levelled out just before the excitation potential of Cr $K\beta_1$ to an almost horizontal distribution.

[1] Docent E. Ingelstam, Stockholm, determined the thickness interferometrically, and I would like to take this opportunity of thanking him.

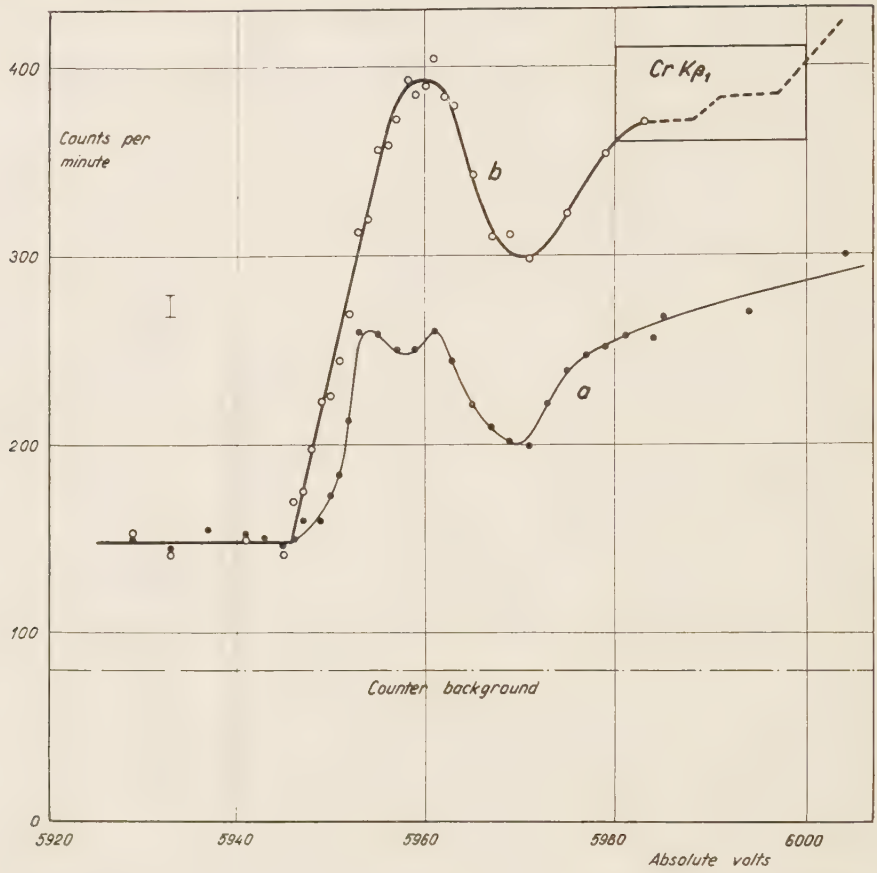

Fig. 25. The continuous X-ray spectrum at the Cr $K\beta_1$ excitation curve (dotted).

The rectangle in the upper right corner corresponds to the square marked in Fig. 26.
a. Isochromat for the pure beryllium anticathode.
b. Isochromat for the same beryllium anticathode with a thin evaporation deposit of chromium.

B. Oxidation influence upon the curves

Contamination of the focal spot because of oxidation could be detected in the excitation curves even when there was scarcely any visible discolouration of the target. Certain structural details were very sensitive to contamination. A broad intensity minimum appeared in the RP ridge of the titanium and chromium curves (Fig. 23). At the same time, changes occurred in the neighbourhood of the oxide absorption edges (the positions of these according to Sanner are indicated in Fig. 23). Nevertheless, the position of the main edge in the voltage scale did not change even when the focal spot was discoloured to such a degree that the oxidation depression of the *RP* ridge might touch the level of the background.

The elements 26 Fe to 29 Cu behaved otherwise. The immediate effect of the first signs of oxidation was a marked diminution of intensity just above *R*, with a simul-

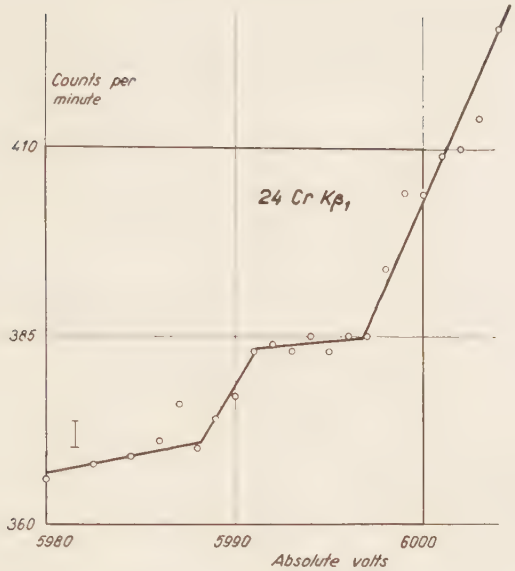

Fig. 26. Cr $K\beta_1$. Thin evaporation deposit on beryllium. The curve corresponds to the mean of six series of readings. No. 24, Table 9.

taneous appearance of intensity peaks near *P*. Fig. 37 shows two copper curves, one (a) for slight oxidation, the other (b) with so extensive oxidation of the focal spot that the pure copper radiation is completely suppressed. The displacement of curve (a) relative to curve (b) is about 3 V, which agrees with the difference between the K absorption curves for Cu and CuO given by BARNES [1933].

Whereas the *RP* ridge of chromium and copper tends to sink, the opposite effect is observed with Fe-Cu, apart from the depression at *R*. The difference seems to be connected with the position of the oxide edge. It is the region immediately below the oxide edge that is most markedly affected by the diminution of intensity, the metal's main edge remaining intact until oxidation is well advanced.

C. Titanium

General properties

The titanium target was prepared by evaporation of the metal on to a copper base. Analytically pure titanium was evaporated from a tungsten furnace. This provisional furnace was of 2 mm tungsten plate with small depressions ground into the surface to hold grains of titanium. Titanium melts at 1720° C, and evaporation took place just above the melting-point. There was considerable risk of alloying if the furnace was overheated. It is quite likely that the evaporated film contained some oxide, as it was not possible to degas the X-ray tube effectively for such a high furnace temperature.

Titanium crystallises in the hexagonal system, and the transition to the body-centred cubic form does not occur until 880° C.

The main K absorption edge for TiO_2 is 12,3 V above the corresponding edge for the pure element [SANNER 1941].

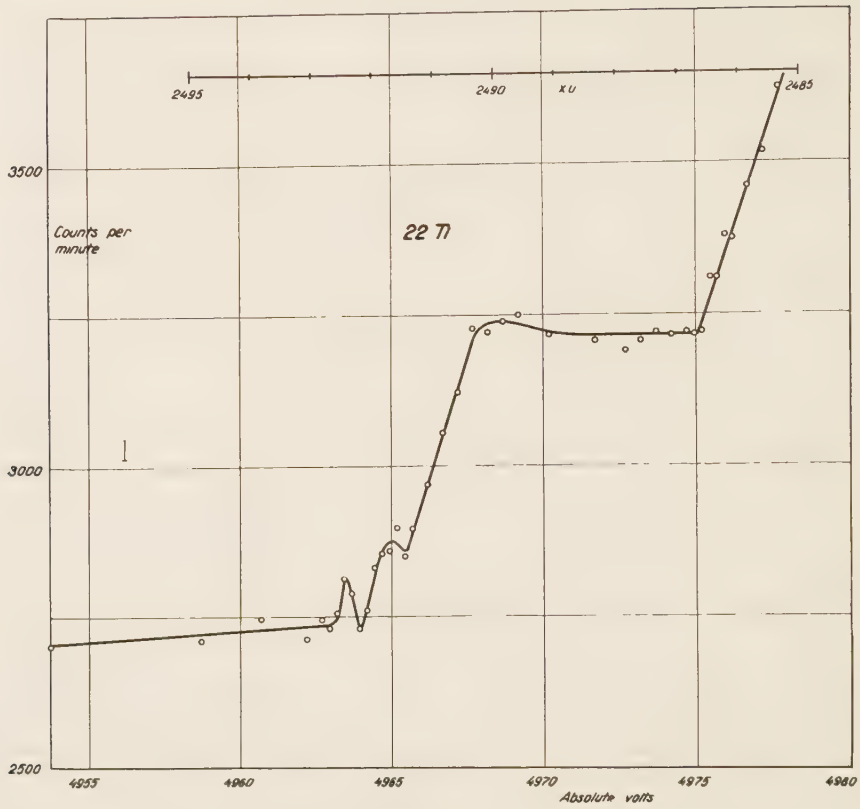

Fig. 27. Ti Kα_1. Evaporation deposit on copper. Nos. 1–3, Table 12.

Table 12. Ti Kα_1.

No.	E_{mean}	V_{R+r}	V_0	h	S	H	R	P
1	1.28206	4 938.1	4 943.8	4 963.3	4 964.5	4 966.0	4 967.5	—
2	1.28206	4 938.1	4 943.8	—	4 964.7	4 966.3	4 967.9	—
3	1.28206	4 938.1	4 943.8	—	4 964.7	4 966.2	4 967.7	4 975.1
4	1.28205	4 938.1	4 943.8	4 963.6	4 964.8	4 966.4	4 967.9	4 975.3
8	1.28201	4 937.9	4 943.6	4 963.7	4 964.8	4 966.1	4 967.3	4 974.7
9	1.28199	4 937.8	4 943.5	—	4 964.8	4 966.4	4 967.9	4 974.5
			Mean, abs. volts	4 963.5	4 964.7	4 966.2	4 967.7	4 974.9
			Mean without v_φ-correction	4 959.0	4 960.2	4 961.7	4 963.2	4 970.4

Anticathode: Titanium, evaporation deposit on copper (except no. 4, where a thin Ti layer was evaporated on to a beryllium target).

Cathode: Tungsten filament.

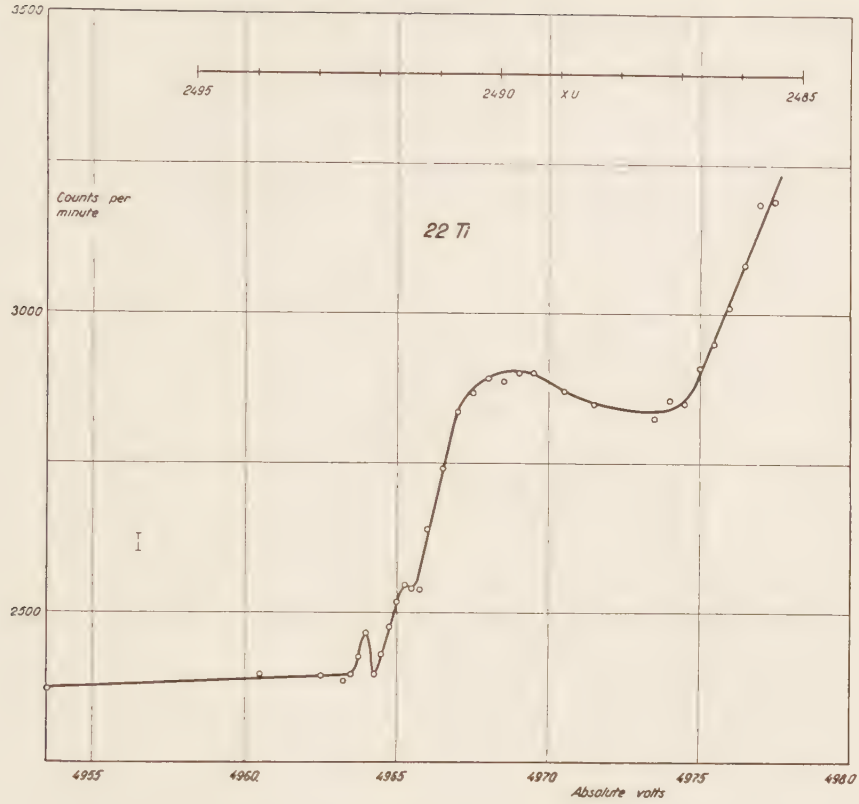

Fig. 28. Ti Kα_1. Evaporation deposit on copper. No. 8, Table 12.

Table 13. Ti Kα_1.

No.	E_{mean}	V_{R+r}	V_0^*	S	R	P
5	1.28204	4 938.0	4 938.0	4 963.4	4 966.7	4 972.9
6	1.28204	4 938.0	4 938.0	4 961.8	4 965.7	4 973.4
7	1.28204	4 938.0	4 938.0	—	—	4 973.6
10	1.28198	4 937.8	4 937.8	4 964.0	—	—
Mean, abs. volts (oxide cathode)				4 963.1	4 966.2	4 973.3
Mean, abs. volts (W-cathode, tab. 12)				4 960.2	4 963.2	4 970.4
$V_{\text{oxide}} - V_W$				2.9	3.0	2.9

Anticathode: Titanium, evaporation deposit on copper.
Cathode: Oxide-coated cathode (Nos. 5–7, 10).

The work function correction is omitted in this table.

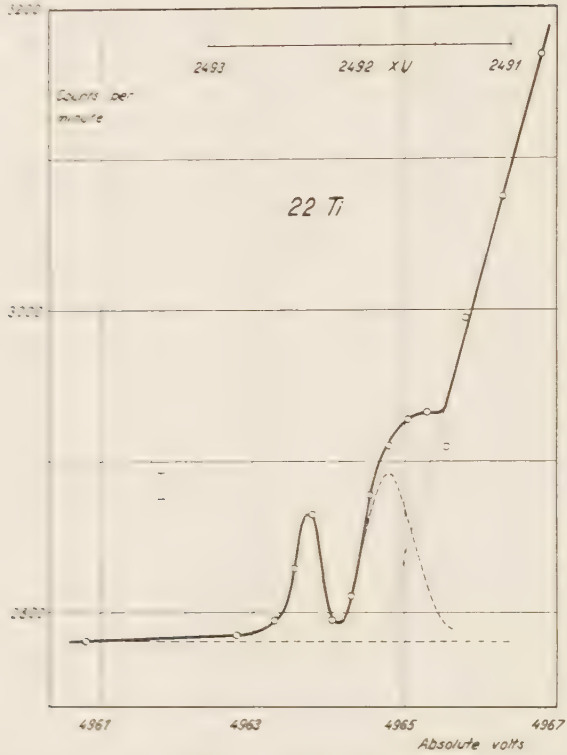

Fig. 29. The fine structure of the Ti $K\alpha_1$ excitation curve. Mean of three series of readings.

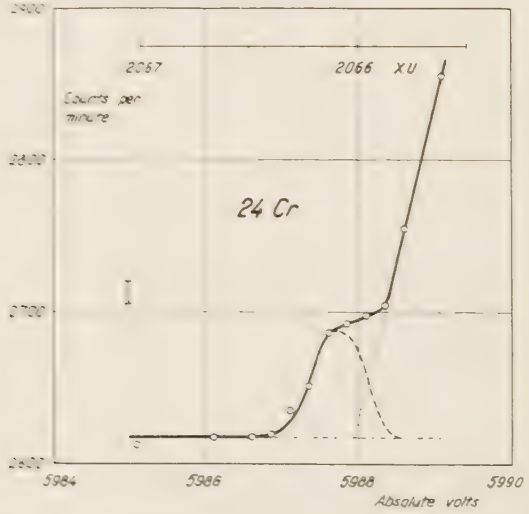

Fig. 30. The fine structure of the Cr $K\alpha_1$ excitation curve. Mean of four series of readings.

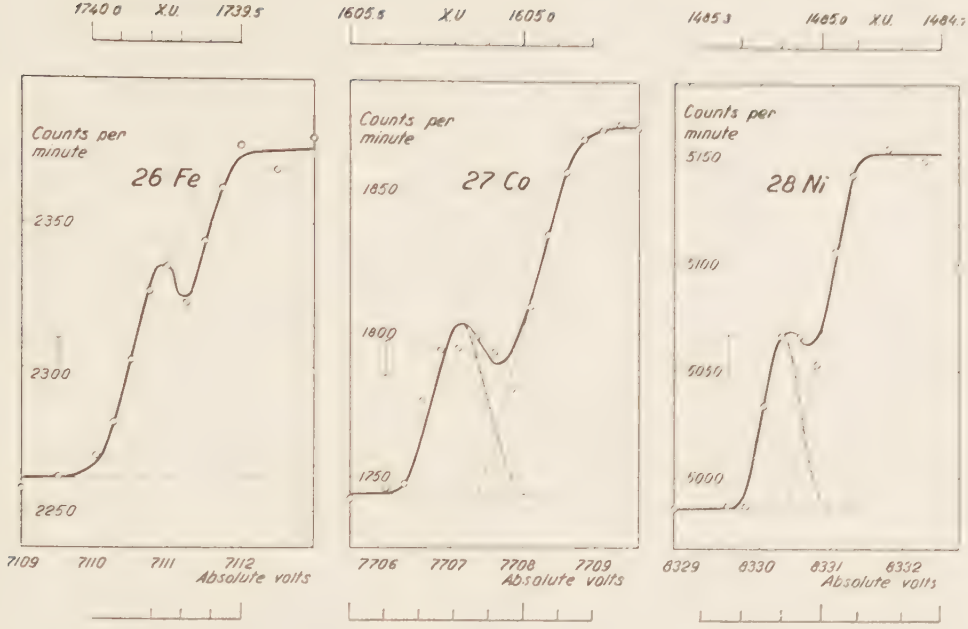

Fig. 31. The main edge and the fine structure of the $K\alpha_1$ excitation curves for Fe, Co and Ni.

The Fe curve is the mean of Nos. 2–5, Table 14, the Co curve of Nos. 4–5, Table 15, and the Ni curve of six series of readings, No. 4, Table 16.

Tables and curves

The excitation potentials from curves obtained with tungsten cathodes are given in Table 12. Voltage differences and intensity characteristics are given in Table 21. Figs. 27–29 show excitation curves. These exhibit considerable resemblances to the chromium curves. The *RP* plateau is horizontal for entirely uncontaminated targets. In contrast to the other metals, the *h* structure has a double peak, which may be due to oxidation. This explanation is supported by (1) the risk of oxidation during evaporation, and (2) the conspicuous similarity of the *h* structure of titanium and the type of oxide influence shown in Fig. 37 for Cu. Against the oxide explanation are (1) the absence of an absorption edge in this region, and (2) the "purity" of the curve in other respects.

D. Iron

General properties

The iron targets were prepared by evaporation either on to a solid copper base or on to a 1 mm iron plate inset in the copper base. The temperature of the target was regulated by the emission, which was lowered to a value at which incandescence ceased.

The material evaporated was a piece (diam. 2.5 mm) of spectroscopically pure iron in the tungsten crucible (Fig. 8).

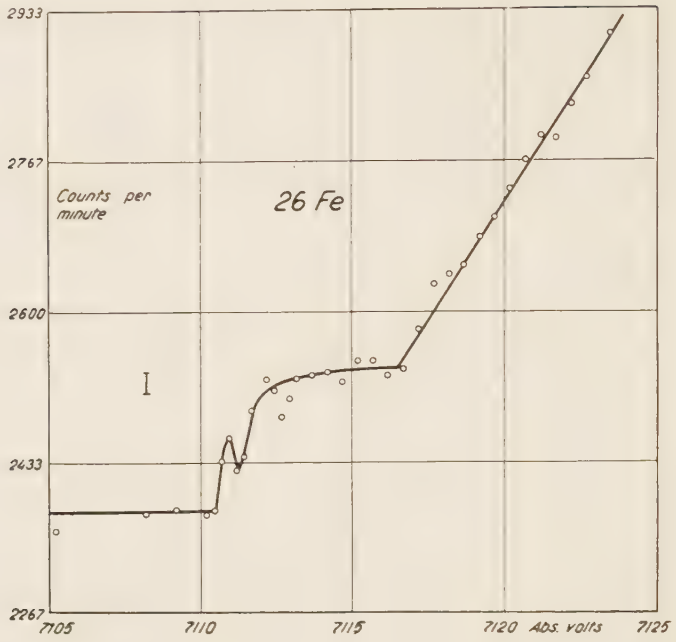

Fig. 32. Fe Kα_1. Evaporation deposit on 1 mm iron plate. No. 3, Table 14.

Table 14. Fe Kα_1.

No.	E_{mean}	V_{R+r}	V_0	h	S	H	H_0	R	P
1	1.28247	7 088.0	7 093.5	7 110.6	—	—	7 112.2	—	7 116.4
2	1.28245	7 087.9	7 093.4	7 110.8	(7 111.2)	(7 111.7)	7 111.8	(7 112.2)	7 116.6
3	1.28244	7 087.8	7 093.3	7 110.6	7 111.0	7 111.5	7 111.5	7 112.0	7 116.6
4	1.28233	7 087.2	7 092.7	7 110.4	(7 110.7)	(7 111.3)	7 111.6	(7 111.9)	7 116.2
5	1.28232	7 087.2	7 092.6	7 110.2	(7 110.4)	(7 111.0)	7 111.0	(7 111.6)	7 116.8
Mean, abs. volt (Nos. 2–5)				7 110.5	7 110.9	7 111.4	7 111.5	7 111.9	7 116.6

Anticathode: No. 1. Iron, evaporation deposit on copper.
Nos. 2–5. Iron, evaporation deposit on 1 mm iron plate.

Cathode: Tungsten filament.

The brackets indicate uncertainty in identifying the point in question. These voltages have been assigned a weight of $^1/_2$ in the calculation of the mean.

Iron melts at 1539° C. and evaporation took place just below the melting-point. There was no observable tendency to alloy with the tungsten.

Iron crystallises at normal temperatures in body-centred cubic crystals (α-Fe), and transformation to the paramagnetic form begins at 769° C without alteration of the crystal system. Iron adopts a face-centred cubic modification (γ-Fe) in the range 900–1400° C. Above 1400° C the stable form is again body-centred cubic.

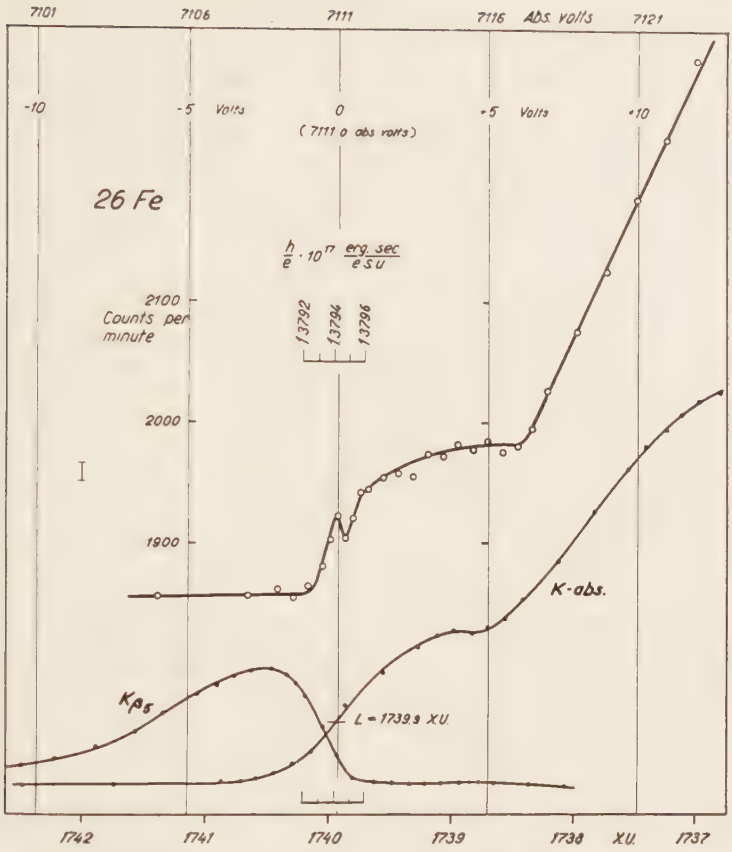

Fig. 33. $K\alpha_1$ excitation curve for Fe (No. 5, Table 14), and the K absorption edge for comparison.

(Fe target: — evaporation deposit on 1 mm iron plate.)

The excitation curve is moved + 0.4 V in order to bring the main edge into coincidence with the mean values in Table 14.

The K absorption edge and the $K\beta_5$ line in Figs. 33, 35, 36 and 38 are taken from BEEMAN and FRIEDMAN [1939], being redrawn with the same voltage dispersion as the corresponding excitation curve. The absolute-volt scale belongs to the excitation curve, and the wave-length scale to the absorption edge and the $K\beta_5$ line.

According to SANNER [1941], the main K absorption edge for FeO is 9.2 V higher than the corresponding edge for the pure element, and that for Fe_2O_3 12.1 V higher. BARNES [1933] observed, however, structural details in the Fe_2O_3 curve extending as far as to the main edge for the pure element.

Tables and curves

The excitation potentials are given in Table 14, and the voltage differences and intensity characteristics in Table 22. Figs. 31-33 show the excitation curves.

Uninterrupted determinations could not last more than about 20 mins. with cooled targets, owing to the rapid oxidation. Series of two or three times this duration could

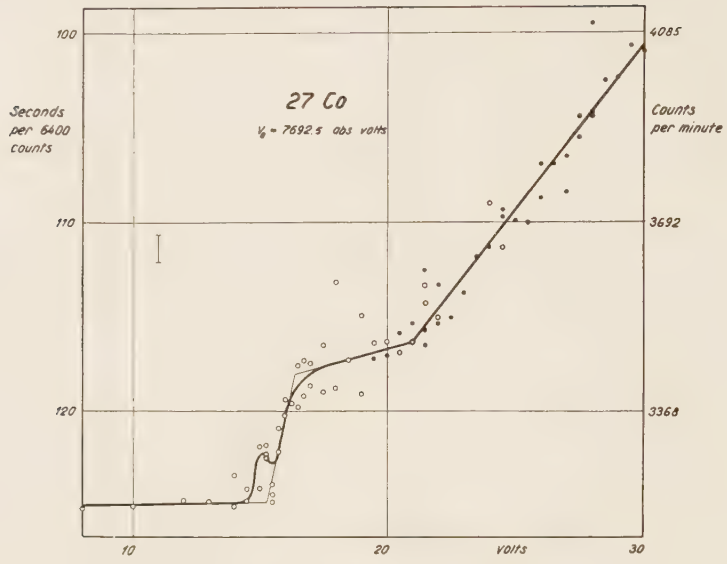

Fig. 34. Co $K\alpha_1$. Evaporation deposit on 1 mm cobalt plate, No. 1, Table 15. Original series of readings.

The horizontal axis gives the additional voltages as read form the Roller-Smith voltmeter. The curve was taken from right to left, and the different kinds of points marked indicate different cobalt evaporations. The voltages have to be corrected for a small drift in the Roller-Smith scale (here −0.1 V), and the intensity values for the dead time of the Geiger counter.

be obtained with the 1 mm iron plates (at about 500° C). This temperature is lower than the Curie temperature, where displacements of the excitation potential may be expected. The means in the table refer to the film evaporated on to the iron-plate target, while control determinations were made with an iron deposit on copper.

The *h* structure of iron is farther up on the main edge than in the case of Cr and Ti, but it is not really higher in counts/min. (32 c/m for Fe and 27 c/m for Cr, with the background reduced to 1000 c/m). For iron, the *RP* plateau represents only 6 % of the background, whereas it is 18 % for chromium and 22 % for titanium (Tables 20–22).

The identification of the points *S* and *R* is uncertain, as Figs. 32–33 indicate, so a new point, H_0, has been introduced. In determining this point, the curve is drawn as in Fig. 16, and H_0 is identified as the intersection point of the line *RS* and a horizontal line through the plateau of the *h* structure.

E. Cobalt

General properties

The targets were prepared by evaporation of spectroscopically pure cobalt from a tungsten crucible on to a 1 mm thick cobalt plate. (Cf. Fe.) Two curves were obtained with thin layers of cobalt on beryllium (Nos. 4, 5, Table 15), the Be layer on a cobalt plate for one of them and on copper target for the other. (Cf. Cr $K\beta_1$.)

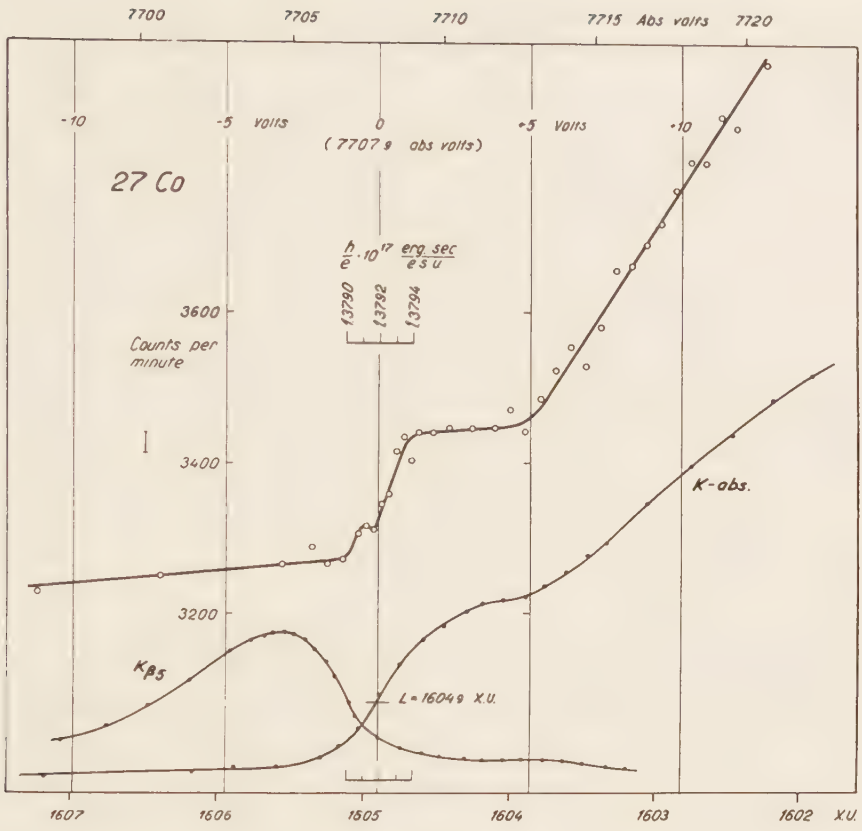

Fig. 35. $K\alpha_1$ excitation curve for Co (No. 3, Table 15), and the K absorption edge for comparison. (Co target: — evaporation deposit on 1 mm cobalt plate.)

Cobalt melts at 1495° C, and evaporation took place just below the melting-point. There were no observable signs of alloying with tungsten.

Cobalt crystallises in hexagonal crystals at normal temperatures (α-Co). The transition to the cubic modification (β-Co) occurs at a temperature between 450 and 800° C, depending on the size of the crystallites. Evaporation gives a fine-grained layer [LEVINSTEIN 1949], which retards the α-β transition. Both α- and β-cobalt are ferromagnetic; the Curie temperature is 1120° C.

According to BARNES [1933], the foot of the K absorption edge of Cr_2O_3 is only 1 V above that of the pure element.

Tables and curves

The excitation potentials are given in Table 15, voltage differences and intensity characteristics in Table 22. The excitation curves are shown in Figs. 31, 34 and 35.

The rapidity of oxidation under electron bombardment was about the same for cobalt as for iron.

Table 15. Co Kα_1.

No.	E_{mean}	V_{R+r}	V_0	h	S	H	H_0	R	P
1	1.28296	7 687.1	7 692.5	7 707.2	7 707.7	7 708.3	7 708.0	7 708.8	7 713.3
2	1.28266	7 685.3	7 690.7	7 706.7	7 707.2	7 708.2	7 707.8	7 709.2	7 713.6
3	1.28265	7 685.3	7 690.7	7 707.0	7 707.4	7 708.1	7 707.7	7 708.8	7 712.8
		Mean, abs. volts		7 707.0	7 707.4	7 708.2	7 707.8	7 708.9	7 713.2
4	1.28264	7 685.2	7 690.6	7 706.6	7 707.4	7 708.1	7 707.9	7 708.7	7 713.5
5	1.28258	7 684.8	7 690.2	7 706.6	7 707.5	7 708.2	7 708.0	7 708.9	—
		Mean, abs. volts		7 706.6	7 707.5	7 708.2	7 708.0	7 708.8	7 713.5
		Mean, Nos. 1–5, abs. volts		7 706.8	7 707.4	7 708.2	7 707.9	7 708.9	7 713.3

Anticathode: Nos. 1–3. Cobalt, evaporation deposit on 1 mm cobalt plate. Below red heat or just faintly glowing.
No. 4. Cobalt, evaporation deposit on Be–Co plate. Thin Co layer.
No. 5. Cobalt, evaporation deposit on copper. Thin Co layer.

Cathode: Tungsten filament.

The continuous background was repressed when thin cobalt films were used. There was no discernible voltage displacement for these films, nor for the different target temperatures.

It will be seen from Table 22 that there is a striking resemblance in shape between the Fe and Co curves.

F. Nickel

General properties

The targets are described in Table 16. Evaporation was performed with analytically pure nickel from a tungsten crucible (cf. Fe).

Nickel melts at 1453° C. The evaporation temperature chosen was just below the melting-point. Very slight overheating melted the nickel, which immediately formed an alloy with the tungsten of the crucible, making evaporation impossible.

Nickel crystallises in face-centred cubic crystals. The Curie point is about 380° C.

Nickel is resistant to oxidation under electron bombardment. A cooled target was tested for 10 hrs. continuous operation, and there was scarcely any visible contamination.

The foot of the K absorption edge for Ni_2O_3 is 5–6 V above the corresponding point for the pure element [BARNES 1933].

Tables and curves

The excitation potentials are given in Table 16, voltage differences and intensity characteristics in Table 22. An excitation curve is shown in Fig. 36.

Series Nos. 1–4 were all determined below the Curie point. With incandescent targets there was a displacement of about 1 V upwards. Similar observations regarding the L_{III} absorption were made by CAUCHOIS [1952].

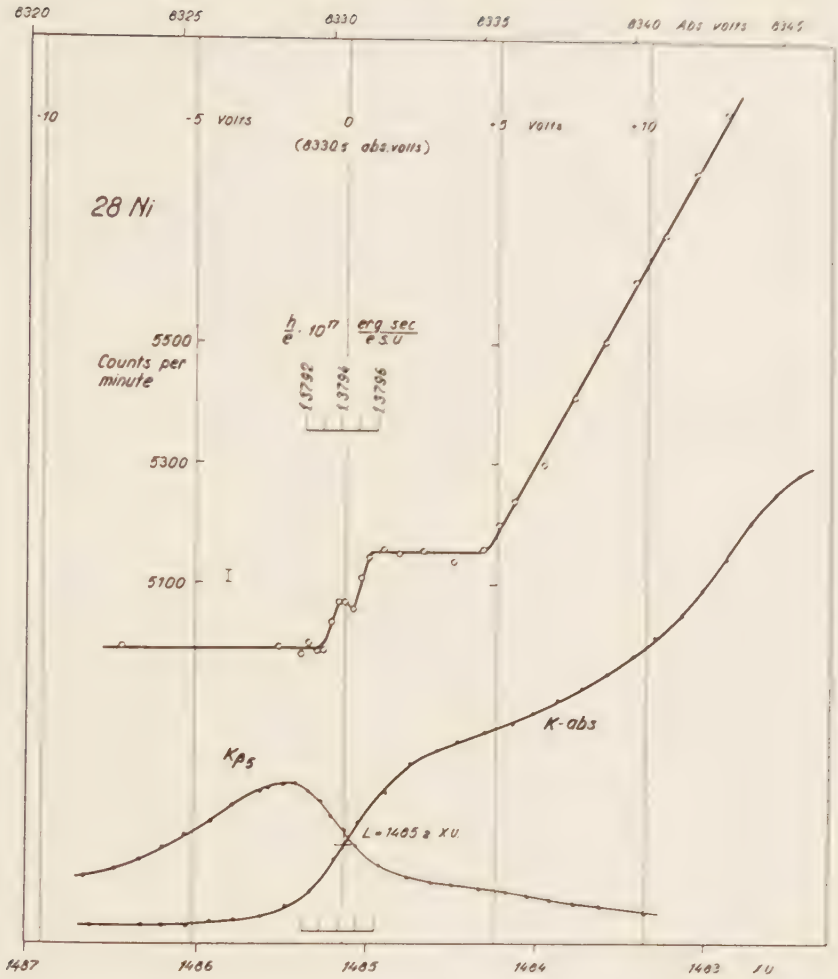

Fig. 36. $K\alpha_1$ excitation curve for Ni (No. 4, Table 16), and the K absorption edge for comparison. (Ni target: — evaporation deposit on copper.)

In nickel, the *h* structure has sunk in height and width. The height for chromium, iron and cobalt was about 30 counts/min. (I_{os} = 1000 c/m), but is only half as great in the case of nickel (16 c/m). The *RP* plateau for nickel is also only half the height of iron's and cobalt's (Table 22).

G. Copper

General properties

The targets were prepared by the evaporation of electrolytic copper on to a copper base. A molybdenum furnace was used for the evaporation. Molten copper does not wet molybdenum, and the molten metal in the furnace gathered in a globule at the bottom.

Table 16. Ni Kα_1.

No.	E_{mean}	V_{R+r}	V_0	h	S	H	H_0	R	P
1	1.28468	8 308.7	8 314.0	8 330.3	8 331.1	8 331.6	8 331.5	8 332.1	8 335.9
2	1.28226	8 308.0	8 313.3	(8 330.0)		—	—	—	8 335.2
3	1.28225	8 307.9	8 313.2	8 329.4	8 329.8	8 330.3	8 330.1	8 330.8	—
4	1.28224	8 307.9	8 313.2	8 330.0	8 330.4	8 330.9	8 330.8	8 331.3	8 335.2
Mean (weighted), abs. volts				8 329.8	8 330.3	8 330.8	8 330.6	8 331.2	8 335.3

Anticathode: No. 1. Nickel-electroplated copper.
Nos. 2, 4. Nickel, evaporation deposit on copper.
No. 3. Nickel, evaporation deposit on a nickel plate (below red heat).

Cathode: Tungsten filament.

The weights assigned to the different series of readings are proportional to the number of counts per point. See Table 22.

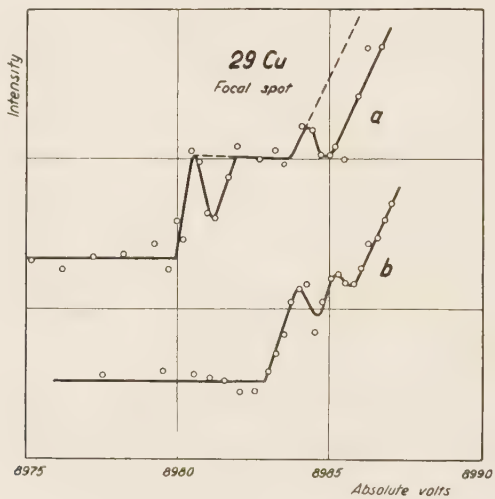

Fig. 37. Cu Kα_1 excitation curves.

a. Sligthly contaminated Cu target. The pure Cu curve is indicated by the dotted line.
b. Heavy contamination. The electron-bombarded Cu surface was left for some days in vacuum and further determination then carried out.

Copper melts at 1083° C. The evaporation temperature was above the melting-point.

Copper crystallises in face-centred cubic crystals.

The foot of the main K absorption edge of CuO is about 3 V above the corresponding point for the pure element [BARNES 1933].

Tables and curves

The excitation potentials are given in Table 17, voltage differences and intensity characteristics in Table 22. Excitation curves are shown in Fig. 38.

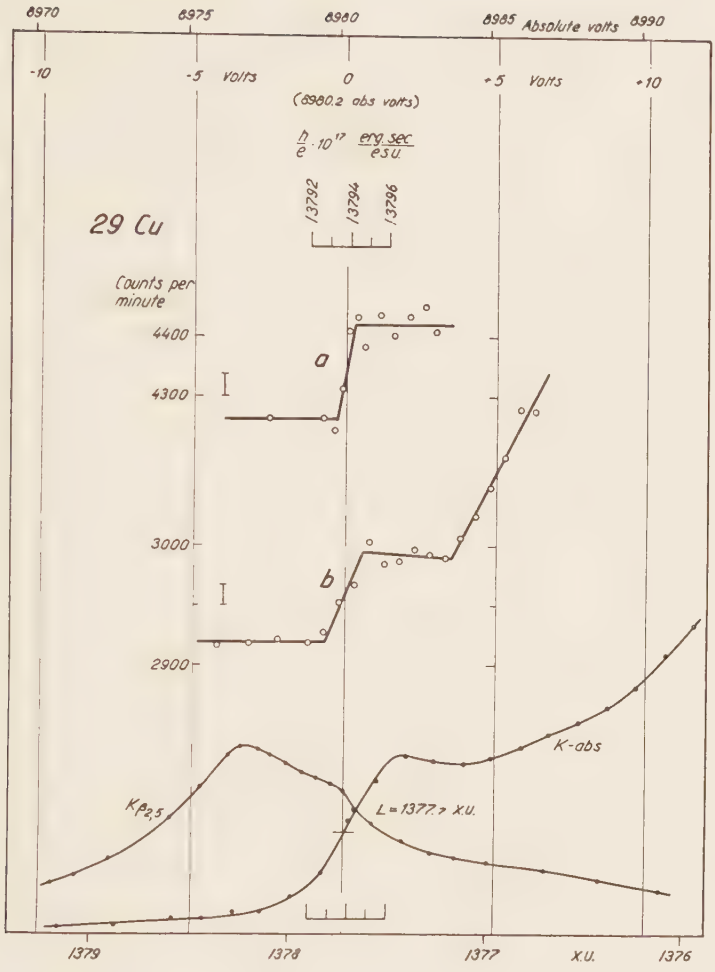

Fig. 38. $K\alpha_1$ excitation curves for Cu, and the K absorption edge for comparison.

Curve *a* corresponds to No. 5 and curve *b* to the mean of Nos. 1–3, Table 17, The anticathode was evaporated Cu on a copper base. The additional voltage was advanced in steps of $\frac{1}{2}$ V, except near the main edge of curve *a*, where the steps were $\frac{1}{4}$ V.

The excitation curves are slightly displaced in the voltage scale, to bring the main edge into coincidence with the means in Table 17: — curve *a* −0.3 V, curve *b* + 0.3 V.

The period of uninterrupted determinations was short (20–40 mins.), owing to the risk of target oxidation.

The *h* structure has completely disappeared in the copper curves. The *RP* plateau has the same low height as for nickel, and showed a tendency to negative slope in some series of determinations.

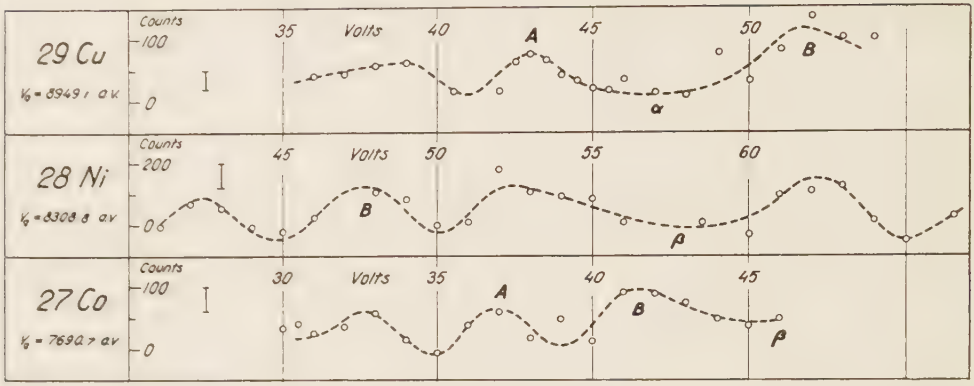

Fig. 39. The fine structure of the excitation curves for Co, Ni and Cu some tens of volts above the excitation potential.

The figure shows the intensity difference between the points determined and a straight line in the general direction of the excitation curve in the voltage range in question.

Table 17. Cu Kα_1.

No.	E_{mean}	V_{R+r}	V_0	S	H	R	P
1	1.28568	8 944.0	8 949.1	8 979.3	8 979.9	8 980.5	8 983.5
2	1.28545	8 942.4	8 947.6	8 978.5	8 978.9	8 979.3	8 982.6
3	1.28546	8 942.5	8 947.7	8 979.9	8 980.5	8 981.0	8 984.3
4	1.28505	8 939.6	8 944.7	8 980.6	8 981.0	8 981.4	8 984.6
5	1.28505	8 939.6	8 944.7	8 980.2	8 980.5	8 980.8	—
			Mean, abs. volts	8 979.7	8 980.2	8 980.6	8 983.8

Anticathode: Copper, evaporation deposit on copper.

Cathode: Tungsten filament.

Table 18. Summary in absolute volts.

	h	S	H	H_0	R	P
22 Ti	4 963.5	4 964.7	4 966.2	—	4 967.7	4 974.9
24 Cr	5 987.4	5 987.9	5 989.4	—	5 990.9	5 997.0
26 Fe	7 110.5	7 110.9	7 111.4	7 111.5	7 111.9	7 116.6
27 Co	7 706.8	7 707.4	7 708.2	7 707.9	7 708.9	7 713.3
28 Ni	8 329.8	8 330.3	8 330.8	8 330.6	8 331.2	8 335.3
29 Cu	—	8 979.7	8 980.2	—	8 980.6	8 983.8

For notation, see Fig. 16.

Table 19. Summary in int. volts.

	h	S	H	H_0	R	P
22 Ti	4 961.9	4 963.1	4 964.6	—	4 966.1	4 973.3
24 Cr	5 985.4	5 985.9	5 987.4	—	5 988.9	5 995.0
26 Fe	7 108.1	7 108.5	7 109.0	7 109.1	7 109.5	7 114.2
27 Co	7 704.2	7 704.8	7 705.6	7 705.3	7 706.3	7 710.7
28 Ni	8 327.0	8 327.5	8 328.0	8 327.8	8 328.4	8 332.5
29 Cu	—	8 976.7	8 977.2	—	8 977.6	8 980.8

Table 20 a. Voltage differences and intensity characteristics of the excitation curves for Cr Kα_1.

Nos.	counts/point	SR	RP	SP	ΔI	$\left(\frac{\Delta I}{\Delta V}\right)_{SR}$	$\left(\frac{\Delta I}{\Delta V}\right)_{PQ}$	Anticathode
		volts			counts	counts/volt		
1– 3	1 600	2.9	6.0	8.9	217	75	57	Chromium plate (Fig. 7 a) Temp. = 1 000° C
4– 5	2 560	2.8	6.2	9.0	229	82	45	
14–15	6 400	2.9	5.7	8.6	224	77	55	
	Mean	2.9	5.9	8.8	223	78	52	
7–12	6 400	2.9	6.4	9.3	(110)	(38)	(30)	Chromium-electro-plated copper
16–19	6 400	3.0	6.4	9.4	(135)	(45)	(38)	
	Mean	3.0	6.4	9.4	—	—	—	
20	3 200	3.0	6.8	9.8	181	60	49	Evaporation deposit on copper
21	19 200	3.1	6.1	9.2	193	62	69	
22	9 600	2.9	6.1	9.0	168	58	44	
	Mean	3.0	6.3	9.3	181	60	54	

The intensities correspond to a continuous background (I_{OS}) of 1 000 counts per minute. For notation, see Fig. 16. In the intensity columns of the Tabs. 20–22 the word "counts" stands for counts per minute.

Table 20 b. Voltage differences and intensity characteristics of the excitation curves for Cr Kα_1, Cr Kα_2 and Cr Kβ_1.

Nos.	counts/point	SR	RP	SP	ΔI	$\left(\frac{\Delta I}{\Delta V}\right)_{SR}$	$\left(\frac{\Delta I}{\Delta V}\right)_{PQ}$	Line
		volts			counts	counts/volt		
22	9 600	2.9	6.1	9.0	168	58	44	Cr Kα_1
23	9 600	2.9	5.7	8.6	80	28	24	Cr Kα_2
24	9 600	3.0	5.6	8.6	(34)	(11)	(15)	Cr Kβ_1

Table 21. Voltage differences and intensity characteristics of the excitation curves for Ti Kα_1.

Nos.	counts/point	*SR*	*RP*	*SP*	ΔI	$\left(\frac{\Delta I}{\Delta V}\right)_{SR}$	$\left(\frac{\Delta I}{\Delta V}\right)_{PQ}$
		volts			counts	counts/volts	
3	8 000	3.0	7.4	10.4	170	57	56
4	6 400	3.1	7.4	10.5	(301)	(97)	(66)
8, 9	8 000	2.8	7.0	9.8	212	76	54
5–7, 10	6 400	3.1	7.1	10.2	263	85	65
	Mean	3.0	7.2	10.2	215	73	58

The anticathode of No. 4 was a thin Ti layer on a beryllium target and is not included in the intensity means. (I_{OS} = 1 000 counts per minute.)

Table 22. Voltage differences and intensity characteristics of the excitation curves for 26 Fe–29 Cu.

	No.	counts/point	*SR*	*RP*	*SP*	*hP*	ΔI	$\left(\frac{\Delta I}{\Delta V}\right)_{PQ}$
							counts	counts/volt
Fe	1	8 000	—	—	—	5.8	62	31
	2	16 000	1.0	4.4	5.4	5.8	49	24
	3	12 000	1.0	4.6	5.6	6.0	65	22
	4	19 200	1.2	4.3	5.5	5.8	63	30
	5	12 000	1.2	5.2	6.4	6.6	62	28
		Mean	1.1	4.6	5.7	6.0	60	27
Co	1	12 800	1.1	4.5	5.6	6.1	63	21
	2	25 600	2.0	4.4	6.4	6.9	67	24
	3	16 000	1.4	4.0	5.4	5.8	54	19
	4	6 400	1.3	4.8	6.1	6.9	(68)	(16)
	5	12 800	1.4	—	—	—	(84)	—
		Mean	1.4	4.4	5.8	6.4	61	21
Ni	1	6 400	1.0	3.8	4.8	5.6	33	29
	2	12 800	—	—	—	5.2	33	17
	3	32 000	1.0	—	—	—	31	—
	4	64 000 (*OR*) 25 600 (*RQ*)	0.9	3.9	4.8	5.2	33	18
		Mean	1.0	3.8	4.8	5.3	33	21
Cu	1	12 800	1.2	3.0	4.2		25	16
	2	6 400	0.8	3.3	4.1		30	21
	3	12 800	1.1	3.3	4.4		32	17
	4	6 400	0.8	3.2	4.0		37	17
	5	12 800	0.6	—	—		37	—
		Mean	0.9	3.2	4.1		32	18

Nos. 4 and 5, cobalt, refer to thin Co layers and are omitted in the intensity means. (I_{OS} = 1 000 counts per minute.) For notation, see Fig. 16.

Chapter VII. Comparison of excitation curves and absorption edges

A. Electronic excitation

1. The K excitation curves

An excitation curve refers to the intensity of a single wavelength, and is therefore an isochromat. The photons associated with each point of the curve may be ascribed to two groups of electrons, both of which are spread over a certain energy band. The two groups correspond to the continuous and the characteristic radiation. Continuous radiation of wavelength λ may be emitted from any electron with kinetic energy in the interval eV to hc/λ, where λ is the wavelength of the line investigated and eV the maximum kinetic energy of the electrons striking the target. This energy band has here a breadth of 400–900 electron-volts. The characteristic radiation may be excited by electrons with energies between eV and eV_K, where V_K is the K excitation potential, — that is, within an interval small compared with that for the continuous radiation. The energy distribution within the intervals depends on the nature of the retardation mechanism exerted on the incident electrons by the target.

The continuous radiation forms a linear background of constant slope. The electrons which give rise to the K radiation are such a small proportion of the total, that the linearity established by Kulenkampff cannot be disturbed.

A knowledge of the electron energy distribution in the interval eV to eV_K is essential for the interpretation of the excitation curves. If the energy losses may be arbitrarily small, the existence of a horizontal section must be due to the occurrence of a forbidden energy band above the conduction band. A negative slope would be inexplicable [cf. DuMond 1947]. According to the electron theory of metals, no such forbidden band exists, as the unoccupied energy bands overlap. Hence the only way to explain the horizontal part of the curve is to assume the electron beam monochromatic. The negative slope discernible in Figs. 23, 37 may then be explained as a consequence of decreased level density due to the occurrence of oxide in the metal of the target.

2. The elementary process involved in the retardation of electrons by solids

The small energy losses of 5–8 kV electrons on passing through thin foils of various materials were determined experimentally by Ruthemann [1941, 1942, 1948] and Lang [1948] with a magnetic spectrometer of the semicircular type. Similar measurements at 25–40 kV were carried out by Möllenstedt [1949], using an electrostatic lens as velocity analyser. The foils used were a few hundred Ångström units thick. The energy distribution of the retarded electrons was given by Ruthemann and Lang in the form of photometer curves of the spectroscopic material. A maximum at zero energy decrement shows that some electrons passed through the foil without loss of energy. The retarded electrons are divided into a continuous band and one or a few strongly marked maxima. Where several maxima occur, they are equidistant. The existence of such maxima indicates that the electrons give up energy in discrete amounts at some kind of elementary retardation process. The continuous region may be interpreted as a statistical combination of several elementary processes. The zero maximum and the first retardation maximum in the distribution curve are well separated. The distance between them is 19–20 V for copper and 22–24 V for nickel. The discrete energy loss for

beryllium, 19.0 V, is nearly equal to the voltage difference between the short wavelength limit and the intensity minimum of the Ohlin structure in Fig. 25 [cf. NIJBOER 1946].

The investigations mentioned show that above the excitation potential, in a region corresponding to the discrete energy loss in the elementary process, the K radiation arises from a monochromatic electron beam, since each loss of energy renders the electron incapable of exciting a K level. This accords with the conclusions drawn in the preceding paragraph from the appearance of the excitation curves. The magnitude of the discrete energy decrement spans the whole structure around the RP plateau of the excitation curves.

The ratio of the area under the zero maximum to the total integrated area of the distribution curve shows that the non-retarded electrons are only a small fraction of the total number. From the foil thickness used we see that K quanta by direct electron impact at voltages near the excitation potential of a thick target are emitted from a surface layer some hundreds of Ångström thick. (Cf. Chapter I, A.)

3. $K\alpha_1$ emission from electron impacts

Let:

Φ_K = the cross section per atom for K excitation by electron impact.
n = the number of atoms per cm³.
x = depth below the target surface.
$m(x)$ = the number of electrons per cm² and sec., penetrating the layer x to $(x - \delta x)$ with energy $\geq eV_K$.
ω = the product of the K fluorescence yield and the ratio between the $K\alpha_1$ intensity and the total K emission.
V_K = the K excitation potential.
ε = the discrete energy decrement of electron retardation.
V = the maximum kinetic energy of the incident electrons.
C = an apparatus constant.

Then we have the following expression for the $K\alpha_1$ intensity δI per cm² of the layer x to $(x + \delta x)$, where δx is so small that the change in $m(x)$ may be neglected:

$$\delta I = \Phi_K \cdot n \delta x \cdot m(x) \cdot \omega C.$$

The radiation per cm² from a thick target is obtained by summation over all the emitting layers:

$$I = \Phi_K \cdot \omega C n \cdot \sum m(x) \delta x.$$

In accordance with the preceding section, the Σ-expression may be regarded as constant in the range V_K to $(V_K + \varepsilon)$. In this range the excitation curve therefore is a measure of the probability of K excitation.

If the voltage $V_K + \varepsilon$ is exceeded, a further term enters into the intensity expression, corresponding to excitation from electrons with energy $V - \varepsilon$.

K excitation may also occur indirectly by photo-absorption of bremsstrahlung quanta. Such fluorescence radiation cannot be neglected at higher values of V, V_K [STODDARD 1934 and 1935]. This contribution to the $K\alpha_1$ intensity is proportional to $(V - V_K)$ in the neighbourhood of the excitation potential. However, the

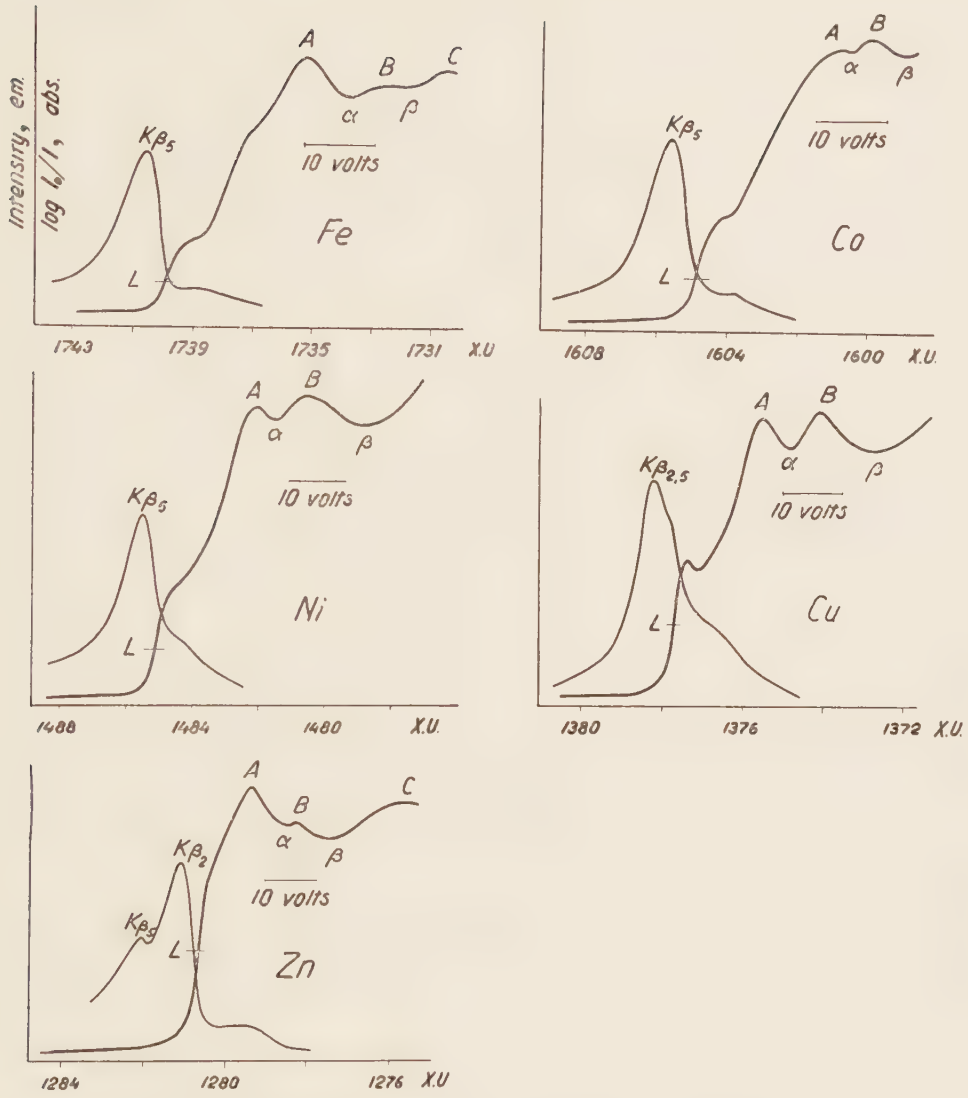

Fig. 40. X-ray absorption and emission curves for 26 Fe–30 Zn.
(After BEEMAN and FRIEDMAN 1939).

constant intensity on the RP plateau of the excitation curves indicates that the fluorescence radiation in this region is unimportant compared with the direct impact radiation.

B. The K absorption edge

The absorption edges in Figs. 33, 35, 36 and 38 are given with the same voltage dispersion as the excitation curves. Their relative positions are such that the vertical

zero line cuts both edges in corresponding points, — "corresponding points" here signifying points in the respective curves which represent the same energy value. The ordinate axis of the absorption curves is log I_0 I.

The absorption edges have been taken from BEEMAN & FRIEDMAN [1939]. Their curves were obtained with a double crystal spectrometer and GM counter. As may be seen from Fig. 40, the dispersion and resolution are sufficiently high for the double edges to be clearly apparent. The K_{β_5} emission bands from Fig. 40 have been inserted in Figs. 33, 35, 36 and 38 with a somewhat reduced scale of intensity.

The absorption coefficient may be expressed as a sum of terms

$$\mu = \tau_K + \tau_L + \cdots + \sigma$$

where τ refers to the photoelectric absorption at the different X-ray levels, and σ to the scattering, with and without change of wavelength. Within a small region near the K absorption edge all the terms may be regarded as constant, apart from τ_K. This term is zero on the long wavelength side of the edge; on the short wavelength side for the 3d elements it is about 10 times as large as the sum of the other terms. Each term in the expression for μ is proportional to the cross section of the corresponding process. If the cross section per atom for K excitation is called Θ_K, the coefficient μ in the neighbourhood of the absorption edge may be expressed in the following way:

$$\mu = n\Theta_K + \text{const.}$$

But μ is proportional to log I_0 I, so the absorption edges given in this scale are a direct expression for the cross section of the radiative K excitation.

What has been said in this and the preceding sections suggests that there is within limits an analogy between the two types of curve. They both represent K excitation cross sections, the absorption edges generally and the excitation curves in a region near the excitation potential. It will be seen from the figures that no considerable difference appears until higher energies are reached. Then the excitation curve continues to move upwards, while the absorption curve gradually assumes a constant value.

According to the electron theory of metals the cross section for K excitation is proportional to the density $N(E)$ of the unoccupied levels above the Fermi surface, and to the transition probability $p(E)$. [JONES, MOTT & SKINNER 1934, JONES & MOTT 1937]. E is here the energy relative to the bottom of the conduction band. Expressing this in symbols, we have

$$\Phi_K(E) = A \cdot N(E) \cdot p(E)$$
$$\Theta_K(E) = B \cdot N(E) \cdot p(E)$$
$$\text{and } \Phi_K = \Theta_K \cdot A/B.$$

It seems justifiable to consider A/B constant [cf. GRAF SODEN 1934], and full agreement may therefore be expected in the neighbourhood of the main edge between the two types of curves, not only as regards position but also in their shapes.

The existence of a retarded exciting electron in one of the excitation events can disturb the identity of the level density function $N(E)$ for the two cases. As this electron, however, must occupy a level in or above the Fermi surface and thus belong to the lattice, rather than to a single atom, the possible fine structure created is probably too small to be recorded with the present method.

C. The resolution of the structure

1. The voltage resolution

A comparison between the absorption edge and the excitation curves reveals a considerable difference in the resolution of the structure.

The resolution of the excitation curves depends only on the voltage and current circuits connected to the X-ray tube. The continuous background depends on the slit-width and focusing defects, that is true, but since it varies linearly, it has no effect on the resolution of the excitation curves. The main factors limiting the resolving power are the inhomogeneity of the electron beam and the ripples in the target voltage.

The size of the ripples is determined by the smoothing circuit used. The peak-to-peak voltage was measured as 0.08 V at 6 kV and 0.28 V at 10 kV. It seems correct to employ the double r.m.s. values, 0.06 and 0.2 V, when estimating the resolution.

The inhomogeneity of the electron beam is due to (1) uncertainty in the work function of the cathode arising from patch effects, (2) the thermal distribution of the electron velocities, and (3) the voltage drop across the cathode filament. The resolving power theoretically possible is determined by (1) and (2). The patch effects may be disregarded for a tungsten cathode. The uncertainty arising from the thermal distribution is about 0.2 V [KLEMPERER].

The voltage drop across the cathode introduces a maximum uncertainty of 0.3 V (cf. Chapter I). As the emission is mainly concentrated to the centre of the filament, we may ascribe a half-maximum width to this distribution. It can be taken as 0.2 V.

It is difficult to know how to combine the three main dispersive elements. Arithmetical addition certainly gives values which are too high. For the voltage dispersion of the electron beam we choose a quadratic addition and obtain the value 0.3 V, which we add arithmetically to double the r.m.s. value for the ripples. The total voltage dispersion is then 0.3–0.5 V and the resolving power, V/dV, about 20000.

This resolving power is twice as large as that attained by Beeman and Friedman for the absorption edges. They used calcite crystals, and obtained in the (1 + 1) position for Cu $K\alpha_1$, a half-maximum width of 39,5″ (= 2.9 volts). In the (1 − 1) position the width was 10.3″ (= 0.8 V). This value corresponds to a resolving power somewhat greater than 10000.

2. The width of the *K* level

The predominant limiting factor in the resolution of structural details in the excitation and absorption curves is the energy width of the X-ray levels. This is greater the deeper the atomic level. From the resolution point of view, it is therefore advantageous to select transitions from one of the outer X ray levels for the investigation of the level density in the conduction band. The existence of a detailed structure in the K excitation curves was therefore surprising. It indicated that the width of the K level of the 3d elements is smaller than the widths hitherto calculated from the spectral lines. The half-maximum width of an emission line is the sum of the widths of the initial and final levels between which the transition takes place. Hence it is possible to derive the width of all energy levels in an atom from the widths of the emission lines, if the width of one level is known.

RICHTMYER, BARNES & RAMBERG [1934] described a method of estimating the level widths on the basis of quantum mechanical radiation theory. Assuming the density distribution N(E) constant, the absorption edge has the form of an arctangent curve. The point of inflection of this curve corresponds to the Fermi surface, and the width of the X-ray level is obtainable from the energy difference in the absorption spectrum between 1/4 and 3/4 of the maximum value of the absorption coefficient. BEEMAN and FRIEDMAN used this method to determine the width of the K energy levels of some investigated elements. Point L in Fig. 40 indicates the position of the point of inflection of the appropriate arctangent curve. The wavelength given for the absorption edge refers to this point. The widths of the K levels for Fe, Co, Ni and Cu were determined to be 1.3 V, 1.9 V, 1.5 V and 1.8 V respectively. The value for copper is remarkably small compared with the value for the ferromagnetic metals. This difference can be explained by the occurrence of the *h* structure in the curves for Fe to Ni, and its absence in the Cu edge. The assumption of constant N(E) therefore applies strictly only to Cu. The arctangent curve is too flat for the other elements, leading to the higher values of the level widths.

BEARDEN & SHAW [1935] give the width of Cu $K\alpha_1$ as 2.7 V, from which the width of the L_{III} level is calculated to be 1.4 V. This value is suspiciously high, because the L_{III} level should be narrower than the K level. The fault could lie in an overestimation of the width of the $K\alpha_1$ line.

BROGREN has recently shown that the customary corrections applied to the measurement of line widths with double crystal spectrometer are probably too small [BROGREN, to be published]. This correction is usually obtained by subtracting the square of the half-maximum width of the rocking curve from the square of the width of the emission line. Measurements of the Cu $K\alpha_1$ width with different crystals and crystal planes have shown that the line widths corrected in this way are dependent on the resolving power of the crystal plane. If a linear subtraction is adopted, however, a line width independent of the resolving power is obtained. Such a correction is permissible, if the true line shape and the shape of the rocking curve are of the classical dispersion form [PARRATT 1934]. BROGREN obtained in this way values for the half-maximum width of Cu $K\alpha_1$ which lie between the limits 0.42 and 0.45 X.U. The average value gives a voltage width of 2.2 V. The width of the L_{III} level obtained from this value is 0.9 V, an acceptable figure in relation to a K level width of 1.3 V. [Cf. CAUCHOIS 1953, p. 180.] A similar correction applied to Fe $K\alpha_1$ gives a half-maximum width of 1.4 V, which must correspond to a K level width for Fe of about 1 volt. The K level width of 0.58 V for argon according to PARRATT [1939] agrees with these calculations.

The acceptance of the smaller line and level widths explains the high structure resolution in the excitation curves. The level width (b) and the voltage dispersion (w) are not additive. SKINNER [1946] gives a sum of the type $(b + \beta w)$, where the fraction β is equal to 1/3 when b and w are "roughly equal". A combination af w and b according to this formula shows that the resolution of the structure details is mainly limited by the finite width of the K level.

Chapter VIII. Determination of h/e

A. Comparison between the two X-ray methods

The X-ray determinations of h/e refer to the formula $eV = hc/\lambda$. Two methods can be used, one connected with the quantum limit of the continuous spectrum and the other with the excitation potential of characteristic X-ray lines.

The quantum limit method endeavours to find the smallest voltage of the X-ray tube that enables the electrons to produce continuous quanta of a frequency corresponding to the detector position, adjusted by means of a well defined emission line. The method with excitation potential involves a comparison between electronic and radiative excitation of convenient energy levels and is thus referred to wavelength data for absorption edges.

The determination of the wavelength to be put in the formula above involves two types of error, (1) error in the wavelength used as reference and (2) error in the adjustment of the spectrometer. In the latter group we include the focusing defects of the crystal. As regards the quantum limit method, error (1) is negligible to error (2). For the concave crystal spectrometer OHLIN [1941] calculated a mean square value, which amounted to 0.01 %, whereas the wavelength error of the reference line was taken to 0.001 %. For the excitation potential method, error (2) is zero and the inaccuracy is entirely caused by error (1).

The inaccuracy in the voltage determination is identical for the two methods.

The apparent advantage of the excitation method is, however, counterbalanced by a further important source of error, not existing in the quantum limit method: the error in the identification of corresponding points. For the identification we can start with a definite point in the excitation curve and try to find the corresponding point in the absorption edge. In such a case an identification error will appear in the wavelength determination. We can also enter the opposite way and introduce an identification error in the excitation potential.

B. The results

The determination of h/e in the present investigation is based on Figs. 33, 35, 36 and 38. The excitation curves shown in these figures have main edges which correspond to the mean values in the respective tables to within very small margins of error (0.1 – 0.2 V). The point L on the absorption curves is the point to which BEEMAN & FRIEDMAN's wavelength values refer. The inaccuracy in the wavelength determination is given to 0.02 X.U. The vertical zero line through L intersects the excitation curve in a point chosen as the point corresponding to L.

A scale with values of h/e is incorporated in the figures. This scale is calculated from the L value given and is fixed in relation to the volt scale and excitation curve. For different choices on this curve of voltage points corresponding to the wavelength point L, it indicates the resulting h/e value.

Copper and nickel give the most reliable determinations, and have been grouped by themselves. Copper has no h structure, so the corresponding points are easily fixed. The curve for nickel has a high degree of symmetry, which facilitates the determination of the point corresponding to L. Iron and cobalt give less accurate values, as will be seen from Fig. 33 and 35.

Table 23. Calculation of h/e from the excitation potentials.

X-ray line	λ_{abs} (X.U.)	V_{exc} (abs. volt)	$h/e \cdot 10^{17}$ erg · sec. / e.s.u.	Weight	Mean
Fe $K\alpha_1$	1 739.9	7 111.0	1.3794	1	
Co $K\alpha_1$	1 604.9	7 707.9	1.3792	1	1.3793 ± 0.0006
Ni $K\alpha_1$	1 485.2	8 330.5	1.3794	2	
Cu $K\alpha_1$	1 377.7	8 980.2	1.3794	2	1.3794 ± 0.0006
				Mean	1.3794 ± 0.0006

Table 24. Comparison of various recent values of h/e.

	Year	Method	$h/e \cdot 10^{17}$	Stated error	Notes
OHLIN	1941	Quantum limit	1.3799	± 0.0008	3–5 kV
SCHWARZ & BEARDEN	1941	Excitation potential	1.3795	0.0010	Ni & Co $K\alpha_1$, $WL\alpha_1$
PANOFSKY, GREEN & DUMOND	1942	Quantum limit	1.3786	0.0002	20 kV
BEARDEN & SCHWARZ	1950	Quantum limit	1.37926	0.00008*	8–10 & 20 kV Oxide cathode
BEARDEN, JOHNSON & WATTS	1951	Quantum limit	1.37928	0.00004*	6, 10 kV
NILSSON	1952	Excitation potential	1.3794	0.0006	Fe–Cu $K\alpha_1$

The OHLIN value given is recalculated from his original figures and corrected for the work function of the cathode.

Probable errors are indicated with an asterisk, the other ones are conservative maximum errors.

As identification error we may choose a fraction of the total main edge in the excitation curve. It is improbable that L falls outside a range 2 3 of the distance hR (See Fig. 16) in the iron and cobalt curves and for nickel and copper we can no doubt choose the smaller ranges $\frac{1}{2}hR$ and $\frac{1}{2}SR$ respectively. This introduces an identification error of ± 0.01 % for the former elements and ± 0.005 % for the latter. Table 23 summarises the values of h/e obtained.

For chromium and titanium there exist no measurements of the K absorption edge with a resolution and accuracy as high as in BEEMAN & FRIEDMAN's curves. As the h structure is small compared with the entire height of the main edge for these elements they are more convenient for h/e determination than the ferromagnetic group.

The K level determination of h/e may be compared with the quantum limit value $(1.3793 \pm 0.0006)10^{-17}$ erg · sec. e.s.u., given in Table 10. As previously mentioned, the value of c used in the calculation was $2.99790 \cdot 10^{10}$ cm sec., and of the conversion factor for kX units to Ångström, 1.00202.

In Table 10 a h/e value is also computed neglecting the work function correction. It is a remarkable fact that this value, $1.3783 \cdot 10^{-17}$ erg · sec. e.s.u., well agrees with OHLIN's values of h/e [1941] if these are recalculated with the constants used in this

investigation and with applied correction for the temperature effect in the resistors R. These recalculated OHLIN values are kept within the small range (1.3782 – 1.3784) 10^{-17} erg · sec./e.s.u.

Table 24 gives a summary of X-ray determinations of h/e from OHLIN and onwards. OHLIN's value was the first to bridge the gap between the X-ray values and those determined from the formula for the Rydberg constant [OHLIN 1942 b]. His recalculated value in Table 24 is corrected for the work function of the cathode.

SCHWARZ & BEARDEN's value from excitation potential determinations [1941] is averaged by the author, who has also corrected it according to a note in the paper of BEARDEN & SCHWARZ [1950, Tab. II]. All the h e values agree perfectly well with the value $1.3793 \cdot 10^{-17}$ erg · sec./e.s.u. computed from the Rydberg constant.

C. Error discussion

The use of the method of least squares for computing the so-called probable errors requires great statistical material. In the present investigation we prefer to perform a conservative maximum error estimation. In the calculation of the accuracy of the high voltage seven systematic errors are introduced. As all the errors probably do not act in the same direction we may add them by computing the square root of the sum of the squares. The accidental error, taken as the average deviation of the mean, is then added arithmetically.

A survey of the estimates of the relative errors is given below. The maximum errors are introduced in Table 23.

1. Errors in the determination of the voltage

a) The standard cells (Tab. 4)	8×10^{-5}
b) The Wolff precision potentiometer	10×10^{-5}
c) The resistors R (Chapter V, B)	10×10^{-5}
d) The resistors r (Chapter V, B)	10×10^{-5}
e) The correction factor for the bridge ratios (Chapter V, B)	5×10^{-5}
f) Zero point drift of the galvanometer	7×10^{-5}
g) Contact potentials and thermo-*emf* (arbitrary estimation)	10×10^{-5}
The square root of the sum of squares	23×10^{-5}
Average deviation from the mean (calc. for the S and P voltages)	5×10^{-5}
Sum:	$\pm 28 \times 10^{-5}$

2. Errors in the calculation of h/e

The excitation potential method.

a) Error in the wavelength determination [BEEMAN & FRIEDMAN 1939]	3×10^{-5}
b) Error in the voltage determination	28×10^{-5}
c) Error in the factor c^2 [acc. to BERGSTRAND, see BEARDEN & WATTS 1951]	2×10^{-5}
d) Error in the conversion factor kX to Å [BRAGG 1947]	3×10^{-5}
e) Identification error (Chapter VIII, B)	5×10^{-5}
Sum:	$\pm 41 \times 10^{-5}$

This sum refers to copper and nickel. For iron and cobolt the sum increases to 46×10^{-5} owing to the higher identification error.

The quantum limit method.

The identification error will be excluded, and the error in the wavelength determination changed to 10×10^{-5} in order to cover the errors due to the adjustment of the spectrometer [see OHLIN 1941]. The relative maximum error will then amount to 43×10^{-5}.

Chapter IX. The structure of the excitation curves and the electron theory of metals

A. Theoretical outline

1. The energy bands

According to the Sommerfeld theory of metals the energy states of the valence electrons form a continuum with a level density $N(E)$ proportional to the square root of the energy E. At the temperature of absolute zero the electrons occupy entirely the lowest states up to a discrete limit $E_{\max}$, above which the energy levels are completely empty. At finite temperatures electrons in the neighbourhood of the limit $E_{\max}$ (the Fermi level) are to a certain degree thermally excited. Generally, the density of occupied states will be expressed with the Fermi distribution function $f(E, T)$. Thus the number of electrons having energies between E and $E + dE$ is

$$2f(E, T) \cdot N(E)\, dE = \frac{2N(E)\, dE}{1 + e^{\Delta E / kT}},$$

where for ordinary temperatures approximately $\Delta E = E - E_{\max}$. The sharp jump in the density of occupied levels at zero temperature will be diffused over an energy range of the order of size kT (Cf. Chapter VI, A).

For the majority of metals the Sommerfeld theory gives only a very rough approximation and it has been necessary to develop the theory with more accurate assumptions to get satisfying descriptions of the properties of real metals.

The Sommerfeld theory assumes a constant potential distribution over the entire volume of the specimen. In a real metal the potential is a periodic function, varying with the period of the lattice. An advanced metal theory must take this into consideration. The complexity of the problem prevents an exact treatment, but approximation methods have been developed for various important cases.

One of these, the "nearly free electron" method, assumes the periodic variations of the potential function small compared with the kinetic energies of the electrons. Owing to the lattice field the electron wave will suffer Bragg reflections for certain energies and directions. As a consequence of that the continuum of energy states in the free electron theory is divided into allowed and forbidden bands, corresponding to separate zones (Brillouin zones) in the momentum space.

A theory along these lines applied to the fine structure of the absorption edges in X-ray spectra has been worked out by KRONIG [1931, 1932]. In an investigation of the K absorption edge of different iron compounds COSTER & KIESTRA [1950] have shown that the Kronig theory is valid for energies about 175 eV above the Fermi level, in agreement with the assumption of small potential variations in relation to the kinetic energies of the electrons. Below 70 eV the absorption coefficient was mainly a property of the atom in question.

An approximate treatment, relevant to the case of small electron energies, is the

method of "tight binding", which, contrary to the Brillouin theory, assumes the electrons strongly bound to the respective atoms. The influence from the surrounding atoms is introduced as a perturbation of the atomic field. As atoms are brought together from far apart, the discrete atomic energy levels will according to this treatment be broadened into energy bands with continually increasing widths. If the atomic distances are decreased to crystal lattice dimensions, higher energy bands with states of different symmetry overlap and form so-called hybridized states. For most metals the overlapping occurs already at the energy band, containing the conduction electrons.

A third approximation method, intermediate to the two other ones, the "cellular method", is worked out by WIGNER, SEITZ and SLATER. The majority of the existing numerical calculations for real metals are performed by this method.

For a detailed treatment of the different aspects of the electron theory of metals the reader is referred to MOTT & JONES 1936, CAUCHOIS 1948, RAYNOR 1952 and MOTT 1952.

2. Electronic transitions from X-ray levels

At the excitation of an X-ray level, with which case we are concerned here, an electron is raised from the discrete deeper level to one of the unfilled energy bands above the Fermi limit. As mentioned above these bands usually overlap and the energy states are hybridized. An exact theoretical treatment will be very complicated. For the special case of transition in which an X-ray level is involved, however, a simplified model can be used. According to JONES, MOTT and SKINNER [1934, JONES & MOTT 1937] the wave function for an energy state can, in the neighbourhood of the nucleus, be developed in a series of terms, each referring to a single symmetry $s, p, d, \ldots$. In the case of X-ray transitions we are therefore allowed to (1) regard the level densities $N(E)$ as a superposition of separate level densities with pure symmetry:

$$N(E) = N_s(E) + N_p(E) + N_d(E) + \cdots$$

and (2) apply the atomic selection rules to electronic transitions to or from the conduction band.

The selection rules for dipole radiation require a change in the l quantum number with $\Delta l = \pm 1$. This means that transitions to or from the K level can occur only to or from energy states with p character. Quadrupole radiation, with possible transitions for $\Delta l = 0$ or ± 2, could be taken into consideration, but the probability of such transitions is so small in relation to that of dipole transitions that they may be neglected.

Thus we can consider, according to Chapter VII, the partial absorption coefficient $\tau_K(E)$ proportional to the product of the density of unoccupied levels and the transition probability in the following way:

$$\tau_K(E) \propto N_p(E) \cdot p_{s\to p}(E).$$

The transition probability $p_{s\to p}(E)$ will be approximately constant in a small range. The absorption coefficient $\tau_K(E)$, the excitation cross section Φ_K and the radiated intensity $I_{K\alpha_1}$ (with the limitations metioned in Chapter VII), are therefore proportional to the density of energy states with p character:

$$I_{K\alpha_1}(E) \propto N_p(E).$$

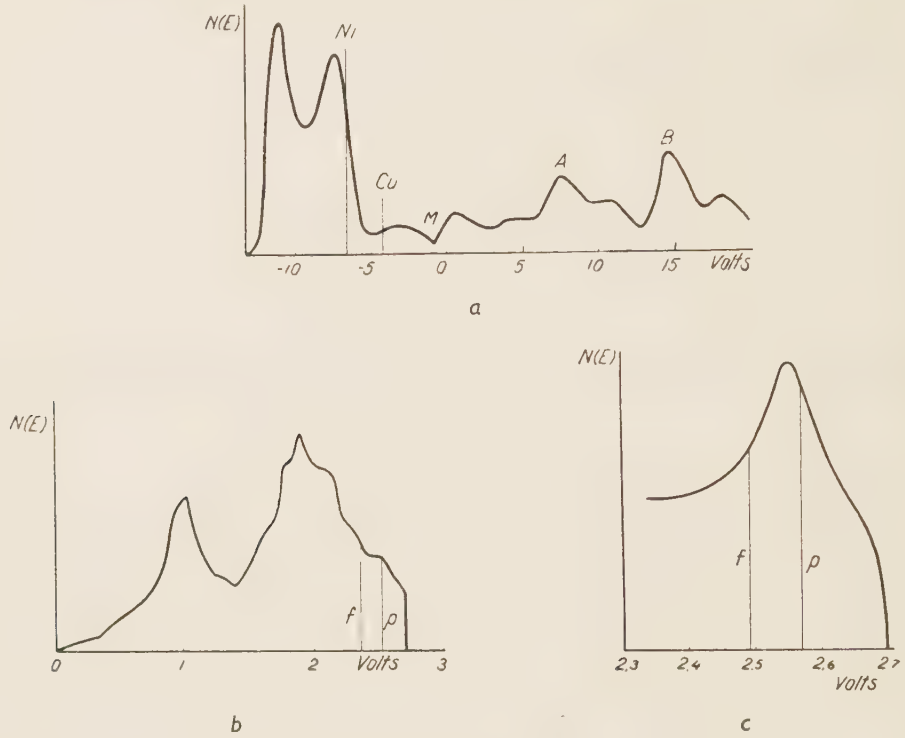

Fig. 41. Density of states as a function of energy.

a. Filled and unfilled energy bands of copper. After RUDBERG and SLATER 1936.
b. The 3d band of nickel. After FLETCHER and WOLFARTH 1951.
c. The higher energy maximum of the 3d band of nickel. FLETCHER 1952.

As a consequence of the theoretical considerations of JONES, MOTT and SKINNER we make use of the expressions "3d band", "4s band" and "4p band", according to the main symmetry, and identify these bands in the excitation curves. It must however be remembered that such a notation is mainly formal and that its correspondence to real properties is strongly limited.

3. The 3d elements

The 3d elements have the argon shell $1s^2\ 2s^2\ 2p^6\ 3s^2\ 3p^6$ completely filled. From the X-ray spectroscopy we know that the next higher states, 3d, 4s and 4p, are, because of the crystal formation, broadened into wide overlapping energy bands. The different energy levels around the Fermi limit must therefore exist in hybrid (spd) states. The investigated element with the lowest atomic number, 22 Ti, has 4 electrons outside the argon shell. These partly fill the 4s and partly the 3d band. The number of 4s electrons per atom is for the 3d elements nearly constant and as we proceed to higher atomic numbers the added electrons fall in the 3d band, which at 29 Cu contains 10 electrons, the maximum number for this band.

For a few of the 3d elements and the neighbouring metals the energy levels are calculated with some of the approximation methods mentioned in section A, 1.

The most extensive treatment has been applied to the band structure of copper and nickel. The cellular approximation method is applied to copper by KRUTTER and SLATER [KRUTTER 1935, SLATER 1936, RUDBERG & SLATER 1936]. The density curve for copper according to RUDBERG & SLATER is shown in Fig. 41 a. The states are occupied by electrons to the level marked Cu. The 3d band with its 10 electrons per atom has a remarkably high level density. It overlaps the 4s band which extends with low density from about the bottom of the 3d band to the trough M in the figure. The 3d band is split in two peaks, the lower containing two and the higher three sub-bands. According to Krutter the lower energy peak has no p admixture. [Cf. BEEMAN & FRIEDMAN 1939.] From the point M and above, the bands are mainly of p symmetry. Two sharp density maxima, A and B, occur.

The theoretical results for copper are extrapolated to nickel. The nickel bands contain one electron less than copper and the Fermi level is shifted to the level marked Ni in Fig. 41 a.

Recently FLETCHER and WOHLFARTH [1951] have recalculated the density of states for the 3d electrons in nickel with the method of tight binding. The general appearance of the resulting density curve is, as shown in Fig. 41 b, similar to the one calculated by RUDBERG & SLATER. An important difference exists, however. The tight binding method gives a total width of the 3d band of 2.7 volts, which is less than half the energy width according to RUDBERG & SLATER. The paramagnetic form of nickel is filled with electrons of both spins to the level marked p in the figure. For the ferromagnetic form the electrons of one spin fill the entire band, while the ones with the opposite spin have the upper limit marked f, thus having an empty range of 0.2 eV, which according to the improved calculations by FLETCHER [1952] includes the peak of the higher energy maximum (Fig. 41 c).

B. Discussion of the structure

1. The copper and nickel curves

The copper excitation curve (Fig. 38) and the corresponding absorption curve of BEEMAN & FRIEDMAN are similar in the main tracks. As is seen in Fig. 41 a the Fermi level lies in the 4s band, the p admixture of which determines the height ΔI of the RP ridge in the excitation curve. This ridge has a horizontal or slightly negative slope and is terminated by a sudden intensity increase at P, indicating the beginning of the 4p band with a high p level concentration. From P onwards the intensity curve rises almost linearly.

The SR edge is very sharp as is seen in Fig. 38 a, where the resolution is higher than in the curve b, because of the smaller intervals in the additional voltages v. The width SR of the edge corresponds to the breadth of the K level according to the discussion in Chapter VII, C. The Fermi limit is represented by the point H.

CAUCHOIS [1953] has measured copper's L_{III} absorption and found a second sharp increase in absorption about 3.5 eV from the main edge. This distance is in good agreement with the distance of 3.6 volts in the excitation curve between the points H and P, corresponding to the first and second intensity increase. In remarks on the work of CAUCHOIS, MOTT [1953] calls attention to the occurrence of s states of high density at the bottom of the 4p band (second Brillouin zone) but according to the sharp intensity increase in the excitation curve for about the same energy level the symmetry cannot be entirely of s character. The uncorrected width of the L_{III} edge

is given by CAUCHOIS to be 1.2 volt, slightly greater than the *SR* width for copper in Tab. 22.

Apart from the *h* structure the nickel excitation curve is very similar to the copper curve. The $N_p(E)$ function for copper and nickel is drawn in the reference MOTT 1953, where for the bottom of the 4s band a density distribution proportional to $E^{3/2}$ is suggested on account of the earlier paper by JONES, MOTT & SKINNER [1934]. The distribution function reaches a maximum a few volts from the 4p band and has then a negative slope. For copper the Fermi limit lies near the maximum of the distribution function, while for nickel it lies at a more levelled range with low densities. The change in slope should be noticed in the excitation curve of nickel but is screened by the existence of the *h* structure, which, as we shall see later, can be interpreted as transitions to the empty part of the 3d band. This, according to FLETCHER, has a width of 0.2 volts for ferromagnetic nickel, but in our case we must reckon with a blurring effect because of the width of the K level. A reconstruction of the 3d contribution to the intensity could therefore give an estimate of this width. Such an attempt is made in Fig. 31 with the rough approximation of a straight line for the 4s edge. The value obtained is 0.6 V (the same size as for the copper edge measured with the smaller voltage intervals).

Fig. 39 shows the fine structure higher up on the *PQ* part of the excitation curves for copper, nickel and cobalt. The letters in the figure indicate the position of the points similarly marked in the absorption curves of BEEMAN & FRIEDMAN and in the theoretical curve in Fig. 41a according to RUDBERG & SLATER. For copper a numerical comparison is performed in Tab. 25 between the positions of the points $L(=H)$, $M(=P)$, *A* and *B* in the experimental and theoretical curves. It is seen that these are in good agreement.

In the case of nickel and cobalt some maxima are to be found, in the excitation curves, which do not correspond to similar structures in the absorption edges. It is interesting to note that the beginning of the extra Ni maximum above the maximum *B* has a voltage distance from the sharp intensity increase at *P* equal to the discrete energy loss measured for Ni by LANG (See Chapter VII).

2. General remarks

The h structure

The assumption that the *h* structure (See Figs. 29–31) corresponds to a transition into the empty 3d band is supported by several observations:

(1) The *h* structure decreases in width and height from Ti to Ni and disappears entirely at copper. Such a behavior corresponds to the decrease of the unfilled upper

Table 25. Comparison of the calculated and observed structure of the copper curves.

Structure	Theory	Exc. curve	BEEMAN and FRIEDMAN
H–P (*L–M*)	3.4	3.6	4.0
P–A (*M–A*)	8.3	8.2	10.7
A–B	7.2	8.7	9.4

part of the 3d band. The measured h dimensions are about the same for the elements Cr, Fe and Co. (The cobalt curve in Fig. 31 is measured with a thin cobalt target and has a somewhat larger h structure than the curves with thick targets. See Figs. 34 and 35.) Titanium definitely gives, however, a wider and higher h structure and nickel a smaller and lower one than the intermediate elements.

(2) If the interpretation of the h structure as arising from the 3d band is correct, the Fermi level should correspond to the point h (Fig. 16). A calculation on such assumptions for the $M_{II,III}$ level has been made for nickel and chromium and the result compared with directly measured values (Tab. 26). The agreement between calculated and experimental values supports the 3d interpretation, especially in the case of chromium, where a choice could possibly be made between the points h and H as representing the Fermi level and where the distance between these points is large enough not to be overbridged by the inaccuracy in the voltage measurements.

In Tab. 26 the L_{III} and $M_{II,III}$ levels have been calculated for all the investigated elements from the determined voltage value of h (for copper H) and the precision measured emission lines $K\alpha_1$ and $K\beta_1$. Available earlier measurements of emission bands and absorption edges show generally good agreement with the calculated values. (The calculations were made with $h/e = 1.3793 \cdot 10^{-17}$ erg. sec./e.s.u.).

(3) As we can see from the Figs. 33, 35 and 36 the $K\beta_5$ edge and the inflection point L, corresponding to the Fermi level calculated by BEEMAN & FRIEDMAN, coincide for Ni but not for Co and Fe. The discrepancy is of the same order of magnitude as the width of the h structure. The absorption edges constitute a mean of the unresolved (3d, 4s) structure; the $K\beta_5$ edge, however, corresponds entirely to the 3d limit.

(4) The long wavelength side of the $K\beta_2\beta_5$ emission band of Zn (Fig. 40) shows a similar picture as the main edge of the excitation curves for Fe, Co and Ni. This emission band is a poorly resolved doublet, for which the lower energy maximum is identified as the $(K - M_{IV,V})$ transition and the higher energy maximum is ascribed to transitions from p states intermingled with the s states in the 4s band. A similar appearance can be expected for the edge in the excitation curves when the 3d band contains empty states as in the case of all the 3d elements.

Table 26. L_{III} and $M_{II,III}$ edges (in absolute volts), calculated from the K excitation potentials and compared with experimental data. (Wavelengths of $K\alpha_1$ and $K\beta_1$ from LANDOLT-BÖRNSTEIN, Zahlenwerte und Funktionen, 6. Auflage, 1950.)

	L_{III} edge		$M_{II,III}$ edge	
	Calc.	Exp.	Calc.	Exp.
22 Ti (h = 4 963.5)	453.1	(452.6) (em.)[1]	32.2	
24 Cr (h = 5 987.4)	573.3	(572.0) (em.)[1]	41.0	41.6 ± 0.3 (em.)[6]
26 Fe (h = 7 110.5)	707.4	(705.7) (em.)[1]	53.3	
27 Co (h = 7 706.8)	777.2	(776.3) (em.)[1]	58.1	
28 Ni (h = 8 329.8)	852.4	852 (em.)[2]	66.0	65.8 ± 0.1 (abs.)[4]
29 Cu (H = 8 980.2)	933.3	933 (abs.)[2] 932.4 (abs.)[3]	75.8	74.7 ± 0.5 (abs.)[5] 74.7 ± 0.3 (em.)[6]

[1] TYRÉN 1937. (These figures refer to the maximum of the Lα emission band.)
[2] CAUCHOIS 1953. [3] SØRUM 1946. [4] SKINNER and JOHNSTON 1937. [5] JOHNSTON 1939.
[6] GYORGY and HARVEY 1952.

Alternative explanations of the origin of the *h* structure could be taken into consideration: (1) Oxide influence of the type shown in Fig. 37, (2) creation of exciton levels [see however CAUCHOIS & MOTT 1949, MOTT 1949] and (3) fine structure due to the screening of the residual positive charge according to FRIEDEL [for references, see MOTT 1953]. These alternative explanations are however not free from objections and can hardly counterbalance the four favourable arguments given above.

The 4s band.

The 4s plateau arises to a height of about 20 % of the continuous background for the elements chromium and titanium. As is seen from Figs. 22 and 27 the *RP* ridge is very well marked. The intensity rises apparently linearly both at the primary and the secondary edges. Tabs. 20 21 show that the slope of *SR* is slightly steeper than the slope of *PQ*. According to this observation the density of states with p character at the bottom of the 4s bands must be somewhat higher than at the bottom of the 4p band.

The width of the primary edge for Cr and Ti, 3.0 V, is larger than the dispersion of the voltage due to the K level width and limited apparatus resolution, and must be ascribed to a continuous increase in the p character admixture. At the bottom of the first zone the density of p states should be proportional to $E^{3/2}$ according to JONES & MOTT [1937]. If this is the case here, it cannot be seen from the excitation curves because of the fine structure at the foot. From emission bands, expected to vary with $E^{3.2}$, it can easily be seen that if the lowest part of the band is cut off, the rest has an approximately linear appearance. Compare, for instance, the emission bands in the reference SKINNER 1938, p. 271.

In comparison with Ti and Cr the elements Fe to Cu have a remarkably lower 4s plateau, indicating a fall of the p admixture in the 4s band as the atomic number increases. In the same direction the length of the plateau decreases, partly because of change in the relative position of the Fermi level with added electrons and partly because of the general shrinking of entire structure. Data for length and height of the 4s plateau are given in Tab. 22.

The 4p band.

Here we can expect a strong intensity increase because of the favourable symmetry of the dominating states. From Fig. 15 it can be seen that the steep slope of the intensity curve is definite. Fine structure occurs but is difficult to measure. An attempt has been made in the earlier considered Fig. 39. The most evident variations refer to the lattice influence on the excited electrons. Towards higher voltages the excitation mechanism will be more and more complicated and a detailed analysis difficult. Retarded electrons will soon be able to excite the K level and the fluorescence excitation by continuous quanta will be increasingly important.

Summary

1. A concave crystal spectrometer is used to determine the intensity function of K emission lines in the neighbourhood of the excitation potential for some 3d elements.

2. A method has been worked out to obtain pure targets under vacuum conditions and to suppress the contamination velocity in order to get reproducible intensity measurements of the characteristic radiation. The X-ray tube is reconstructed and equipped according to this method.

3. A Geiger counter is constructed with high efficiency in the wavelength region 1.5–2.6 Å.

4. The intensity function is recorded and the K excitation potential determined for the following lines:

a) the $K\alpha_1$, $K\alpha_2$ and $K\beta_1$ lines of chromium and

b) the $K\alpha_1$ line of titanium, iron, cobalt, nickel and copper.

5. The intensity function is recorded for Cr $K\alpha_1$ at a target temperature of 1000° C.

6. An isochromat is recorded, containing the quantum limit of the continuous spectrum and the excitation curve for the Cr $K\beta_1$ line.

7. A proof is given for the necessity of work function correction in the determination of the excitation potential.

8. A summary in absolute and international volts is given in Tabs. 18 and 19 of the excitation potentials measured. Voltage differences and intensity characteristics for the structure of the excitation curves are given in Tabs. 20–22.

9. The electronic and radiative excitation is discussed. A comparison of the absorption edges and excitation curves is given in Figs. 33, 35, 36 and 38.

10. A value of h/e is obtained from the K excitation potentials and the K absorption edges for the elements 26 Fe to 29 Cu. The result is $(1.3794 \pm 0.0006) \cdot 10^{-17}$ erg · sec./e.s.u.

11. L_{III} and $M_{II,III}$ edges are calculated for the 3d elements investigated.

12. An attempt is made to explain the structure of the intensity curves from the band theory of metals.

REFERENCES

VAN ARKEL, A. E., Reine Metalle. Berlin 1939.
BARNES, A. H., Phys. Rev. *44*, 141 (1933).
BEARDEN, J. A., JOHNSON, F. T., WATTS, H. M., Phys. Rev. *81*, 70 (1951).
BEARDEN, J. A., and SCHWARZ, G., Phys. Rev. *59*, 934 (1941).
—— Phys. Rev. *79*, 674 (1950).
BEARDEN, J. A., and SHAW, C. H., Phys. Rev. *48*, 18 (1935).
BEARDEN, J. A., and WATTS, H. M., Phys. Rev. *81*, 73 (1951).
BEEMAN, W. W., and FRIEDMANN, H., Phys. Rev. *56*, 392 (1939).
BRAGG, W. L., Phys. Rev. *72*, 437 (1947).
BROGREN, G., Nova Acta Reg. Soc. Scient. Upsaliensis, Ser. IV, Vol. 14, No. 4 (1949).
BROGREN, G., and FRISKOPP, K. G., Arkiv f. Mat. Astr. o. Fysik *36 B*, No. 4 (1948).
CAUCHOIS, Y., Les spectres de rayons X et la structure électronique de la matière. Paris 1948.
—— Phil. Mag. *43*, 375 (1952).
—— Phil. Mag. *44*, 173 (1953).
CAUCHOIS, Y., and MOTT, N. F., Phil. Mag. *40*, 260 (1949).
COMPTON, A. H., and ALLISON, S. K., X-rays in theory and experiment. New York 1935.
COSTER, D., and KIESTRA, S., Phil. Mag. *41*, 144 (1950).
COSTER, D., and VAN ZUYLEN, J., Nature *129*, 942 (1932).
DUMOND, J. W. M., Phys. Rev. *72*, 276 (1947).
—— Phys. Rev. *74*, 1883 (1948).
DUMOND, J. W. M., and COHEN, E. R., Rev. Mod. Phys. *20*, 82 (1948).
EISENSTEIN, A. S., Oxide coated cathodes. Advances in Electronics I. New York 1948.
ESPE, W., and KNOLL, M., Werkstoffkunde der Hochvakuumtechnik. Berlin 1936.
FARMER, E. C., and BROWN, S. C., Phys. Rev. *74*, 902 (1948).
FLETCHER, G. C., Proc. Phys. Soc. *A 65*, 192 (1952).
FLETCHER, G. C., and WOHLFARTH, E. P., Phil. Mag. *42*, 106 (1951).
FRIEDENSTEIN, H., MARTIN, S. L., and MUNDAY, G. L., Rep. Progr. Phys. *11*, 298 (1946–47).
v. FRIESEN, S., Uppsala Universitets Årsskrift, No. 14 (1935).
GRAF SODEN, D., Ann. Physik *19*, 409 (1934).
GYORGY, E. M., and HARVEY, G. G., Phys. Rev. *87*, 861 (1952).
HAGLUND, PH., Arkiv f. Mat., Astr. o. Fysik *28 A*, No. 8 (1941).
HANAWALT, J. D., Z. Physik *70*, 293 (1931).

HERRMANN, G., and WAGENER, S., Die Oxydkathode. Leipzig 1943 (I) and 1944 (II).
HUBER, H., and WAGENER, S., Z techn. Physik *23*, 1 (1942).
INGELSTAM, E., Arkiv f. Mat., Astr. o. Fysik *27 B*, No. 4 (1939).
JNANANANDA, S., High Vacua. New York 1947.
JOHANN, H. H., Z. Physik *69*, 185 (1931).
JOHNSTON, J. E., Proc. Camb. Phil. Soc. *35*, 108 (1939).
JONES, H., and MOTT, N. F., Proc. Roy. Soc. *A 162*, 49 (1937).
JONES, H., MOTT, N. F., and SKINNER, H. W. G., Phys. Rev. *45*, 379 (1934).
KLEMPERER, O., Einführung in die Elektronik. Berlin 1933.
KRUTTER, H. M., Phys. Rev. *48*, 664 (1935).
KRONIG, R. DE L., Z. Physik *70*, 317 (1931) and *75*, 191 (1932).
KULENKAMPFF, H., Ann. Physik *69*, 548 (1922).
KURYLENKO, C., Thèse. Paris 1939.
KÖNIG, H., Naturwiss. *35*, 261 (1948).
LANG, W., Optik *3*, 233 (1948).
LAW, R. R., R. S. I. *19*, 920 (1948).
LEVINSTEIN, H., J. App. Phys. *20*, 306 (1949).
MORRISON, J. D., and NICHOLSON, A. J. C., J. Chem. Phys. *20*, 1021 (1952).
MOTT, N. F., Proc. Phys. Soc. *A 62*, 416 (1949).
—— Progr. in Met. Phys. *3*, 76 (1952).
—— Phil. Mag. *44*, 187 (1953).
MOTT, N. F., and JONES, H., The theory of the properties of metals and alloys. Oxford 1936.
MÖLLENSTEDT, G., Optik *5*, 499 (1949).
NEHER, H. V., and PICKERING, W. H., Phys. Rev. *53*, 316 (1938).
NIJBOER, B. R. A., Physica *12*, 461 (1946).
NILSSON, Å., and OHLIN, P., Arkiv f. Mat., Astr. o. Fysik *33 A*, No. 23 (1946).
OHLIN, P., Diss. Uppsala Universitets Årsskrift (1941).
—— Arkiv f. Mat., Astr. o. Fysik *29 A*, No. 3 (1942).
—— Arkiv f. Mat., Astr. o. Fysik *29 B*, No. 4 (1942).
PANOFSKY, W. K. H., GREEN, A. E. S., and DUMOND, J. W. M.. Phys. Rev. *62*, 214 (1942).
PARRATT, L. G., Phys. Rev. *46*, 749 (1934).
—— Phys. Rev. *49*, 132 and 502 (1936).
—— Phys. Rev. *56*, 295 (1939).
PARRATT, L. G., and JOSSEM, E. L., R. S. I. *23*, 188 (1952).
PIORE, E. R., HARVEY, G. G., GYORGY, E. M., and KINGSTON, R. H., R. S. I. *23*, 8 (1952).
RAYNOR, G. V., Rep. Progr. Phys. *15*, 173 (1952).
RICHTMYER, F. K., BARNES, S. W., RAMBERG, E., Phys. Rev. *46*, 843 (1934).
RUDBERG, E., and SLATER, J. C., Phys. Rev. *50*, 150 (1936).
RUTHEMANN, G., Naturwiss. *29*, 648 (1941) and *30*, 145 (1942).
—— Ann. Physik (6) *2*, 113 (1948).
SANDSTRÖM, A. E., Nova Acta Reg. Soc. Scient. Upsaliensis, Ser. IV, Vol. 9, No. 11 (1935).
SANNER, V. H., Diss. Uppsala 1941.
SIEGBAHN, M., Spektroskopie der Röntgenstrahlen. Berlin 1931.
SILFVERBERG, L., Arkiv f. Mat., Astr. o. Fysik *31 B*, No. 10 (1944).
SKINNER, H. W. B., Proc. Roy. Soc. *A 135*, 84 (1932) and *A 140*, 277 (1933).
—— Rep. Progr. Phys. *5*, 257 (1938).
—— Phil. Trans. Roy. Soc. *A 239*, 95 (1946).
SKINNER, H. W. B., and JOHNSTON, J. E., Proc. Roy. Soc. *161*, 420 (1937).
SLATER, J. C., Phys. Rev. *49*, 537 (1936).
STAHL, H. A., J. App. Phys. *20*, 1 and 8 (1949).
STODDARD, K. B., Phys. Rev. *46*, 837 (1934) and *48*, 43 (1935).
SZABÓ, Z. G., and LAKATOS, B., Naturwiss. *39*, 486 (1952).
SORUM, H., K. Norske Vidensk. Selsk. Forh. *19*, No. 13 (1946).
TERRILL, H. M., Phys. Rev. *22*, 101 (1923).
TYRÉN, F., Arkiv f. Mat., Astr. o. Fysik *25 A*, No. 32 (1937).
WILLIAMS, E. J., Proc. Roy. Soc. *A 130*, 310 (1930–31).
YARWOOD, J., High Vacuum Technique. New York 1946.

Tryckt den 5 maj 1953

Uppsala 1953. Almqvist & Wiksells Boktryckeri AB